Clean up of bleed air contamination

Sadaf Aftab

A thesis submitted for the degree of PhD
at the
University of St Andrews

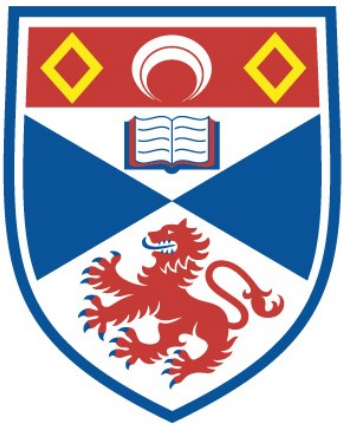

2020

Candidate's declaration

I, Sadaf Aftab, do hereby certify that this thesis, submitted for the degree of PhD, which is approximately 34,000 words in length, has been written by me, and that it is the record of work carried out by me, or principally by myself in collaboration with others as acknowledged, and that it has not been submitted in any previous application for any degree.

I was admitted as a research student at the University of St Andrews in September 2015.

I received funding from an organisation or institution and have acknowledged the funder(s) in the full text of my thesis.

Date 06.05.2020 Signature of candidate

Supervisor's declaration

I hereby certify that the candidate has fulfilled the conditions of the Resolution and Regulations appropriate for the degree of PhD in the University of St Andrews and that the candidate is qualified to submit this thesis in application for that degree.

Date 13.05.2020 Signature of supervisor

Permission for publication

In submitting this thesis to the University of St Andrews we understand that we are giving permission for it to be made available for use in accordance with the regulations of the University Library for the time being in force, subject to any copyright vested in the work not being affected thereby. We also understand, unless exempt by an award of an embargo as requested below, that the title and the abstract will be published, and that a copy of the work may be made and supplied to any bona fide library or research worker, that this thesis will be electronically accessible for personal or research use and that the library has the right to migrate this thesis into new electronic forms as required to ensure continued access to the thesis.

I, Sadaf Aftab, confirm that my thesis does not contain any third-party material that requires copyright clearance.

The following is an agreed request by candidate and supervisor regarding the publication of this thesis:

Printed copy

Embargo on all of print copy for a period of 1 year on the following ground(s):

- Publication would preclude future publication

Supporting statement for printed embargo request

I am currently in process of writing publications

Electronic copy

Embargo on all of electronic copy for a period of 1 year on the following ground(s):

- Publication would preclude future publication

Supporting statement for electronic embargo request

I am currently in process of writing publications

Title and Abstract

- I agree to the title and abstract being published.

Date 06.05.2020 Signature of candidate

Date 13.05.2020 Signature of supervisor

Professor John T S Irvine

Underpinning Research Data or Digital Outputs

Candidate's declaration

I, Sadaf Aftab, understand that by declaring that I have original research data or digital outputs, I should make every effort in meeting the University's and research funders' requirements on the deposit and sharing of research data or research digital outputs.

Date 06.05.2020 Signature of candidate

Permission for publication of underpinning research data or digital outputs

We understand that for any original research data or digital outputs which are deposited, we are giving permission for them to be made available for use in accordance with the requirements of the University and research funders, for the time being in force.

We also understand that the title and the description will be published, and that the underpinning research data or digital outputs will be electronically accessible for use in accordance with the license specified at the point of deposit, unless exempt by award of an embargo as requested below.

The following is an agreed request by candidate and supervisor regarding the publication of underpinning research data or digital outputs:

Embargo on all of electronic files for a period of 1 year on the following ground(s):

- Publication would preclude future publication

Supporting statement for embargo request

I am currently in process of writing publications

Date 06.05.2020 Signature of candidate

Date 13.05.2020 Signature of supervisor

Acknowledgments

I would like to thank my supervisor, Prof. John Irvine for his kind support and guidance throughout my time at St Andrews. I would also like to thank Dr Aida Fuente Cuesta and Dr Paul Connor for their time, support and guidance specifically in setting up mass spectrometer and for general discussion and suggestions. I would also like to extend my thanks to Mr Drew Anderson who has helped me with my rig assembly and Mr Ross Blackley for providing training for the SEM-EDS analysis.

I would like to dedicate my thesis to my father and mother, both of whom have made a lot of sacrifices to get me where I am today. My grandmother has been an integral part of my support, I have overcome problems with ease through her prayers. I would like to thank my husband who has been very understanding and supporting especially in the last few months. To the rest of my family and friends; thank you for the prayers, support and motivation. I could not have completed the work I have without the kind prayers of my father and mother in law and grandparents.

This work was funded by the Engineering and Physical Sciences Research Council and EPSRC Centre for Doctoral Training in Critical Resource Catalysis (Grant code: EP/L016419/1).

Abstract

To compensate for the low temperature and pressure at high altitude, the air provided to the cabin of the aircraft is drawn from the jet engine. This is known as bleed air which provides heat and pressurises the cabin and flight deck. As the air passes the engine, any minor mechanical faults can cause leakage of engine oil into the stream of air being fed into the cabin which can contaminate the air. There is growing evidence to suggest that this cabin air contamination in aircrafts is causing illness in passengers and this is accompanied by a concern that aviation safety regulators are not taking preventative actions.

The focus of this work was to develop a catalyst for bleed air contamination. For this, stainless steel 314 and 316 foams were modified and tested for the oxidation of known contaminants. The oxidised foam possessed had chemical composition of spinel oxides therefore, spinel oxides were also synthesised, reduced and etched during this work and were then tested. Stainless steel foam was an ideal candidate for this process as it can be used as a catalyst itself or act as a support to impregnate other catalytically active species on it. Spinel oxides also possess good catalytic capabilities. The main focus of the work was toluene as it is not only a contaminant in the cabin air but is also found in many industrial waste streams. It is also a model volatile organic compound therefore the catalytic system developed can be used in more than one application. Another contaminant studied was ethyl acetate which has been tested due to being present in the cabin air in the past.

Raw SS 314/316 foams were modified *via* oxidation and dip coating to be investigated for the oxidation of toluene/ethyl acetate in to CO_2 (g) and H_2O (v) in a lab scale rig at temperatures between 200 and 500 °C. $MnFeCrO_4$ and $MnNiCrO_4$ spinels were synthesised using solution combustion method and reduced at different temperatures. The reduced spinels were tested for oxidation of toluene. The results show that the impregnated SS 316 foams have higher selectivity towards production of CO_2 (g) at lower temperatures compared to SS 314 foams and spinels.

Contents

Table of figures

Introduction

1.1 Overview

Airplanes are becoming increasingly important in our daily lives and the conditions inside the cabin should be carefully controlled to fulfil the safety requirements for those travelling on board. The quality of cockpit and cabin air circulating during transportation in an aircraft is critically important to human health. The topic of cabin air quality has been of concern for over three decades now. Numerous studies have been published on this topic and the link between toxicity of bleed air and its effect on human health is still an open debate however, generally, concerns are constantly being raised to implement a safer cabin air system [1]. The purpose of this chapter is to give an overview of the bleed air system, the potential contaminants found in the cabin of the aircraft, the current filtration system and the possible catalytic systems that can be used to oxidise the contaminants found.

1.2 Bleed Air

Toxic contaminants can enter the cabin air through the bleed air system and cause sickness in the passengers and crew members. Since 1953, the air used to provide oxygen for the flight deck and the cabin of the aircrafts is often drawn from the engines as bleed air [2,3,4,5,6]. Figure 1.1 summarises the pathway of bleed air into the cabin.

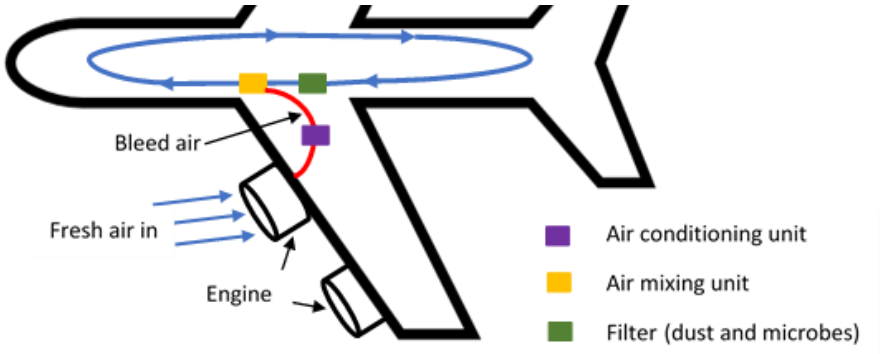

Figure 1.1. Schematic of bleed air pathway

The Environmental Control System (ECS) of the aircraft uses bleed air drawn from the engine to ventilate and pressurise the cabin, flight deck and to cool the avionics

of the aircraft [7,8,9,10]. Mostly, the ECS uses the air from the compressor stage of the engine where the temperatures of around 200-500 °C are found [11,12,13]. This air is then cooled by passing through air/air and air/water heat exchangers (air conditioning unit) followed by a water coalescer (air mixing unit) which mixes the bleed air with recirculated cabin air [10].

The cabin air contains 10-fold less bleed air whereas, the air provided to flight deck follows a different pathway. The flight deck has a continuous stream of air from outside through the engines to the cockpit [2]. As the bleed air is passed through the engine, occasionally it can get contaminated by the accumulation of engine oil or jet oil [2,8,14,15].

1.2.1 Causes of contamination

The contamination can occur due to various reasons mainly because of maintenance irregularities, faults in design or mechanical failures [9,13]. The toxic components of the engine oil can enter the cabin due to malfunctioning of the engine components; the more common error is found to be in the engine seals.

1.2.1.1 Engine seals

Engine seals used in flight operations known as wet seals comprise of a thin film of engine oil which prevent the rotating surfaces to come into contact with each other. Due to fluctuations in the pressure and temperature over the seal, the oil and vapours can be lost into the engine of the aircraft. These vapours can enter the inlet of the compressor and cause contamination in the bleed air system. The oil leaks can cause an odd smell to occur or could also cause smoke in the cabin making the journey unpleasant, such events are termed as fume events [2,8].

The bleed air has been previously found to be contaminated by volatile organics and/or organophosphates found in the jet engine oil, lubricating and hydraulic fluids of the aircraft [2,8,14,15]. The composition of the jet engine oil revealed presence of many mixtures of compounds.

1.3 Jet engine oil

Mobil Oil Jet II consists of a synthetic ester mixture of 95% C_5 to C_{10} fatty acid esters of dipentaerythritol and pentaerythritol, tricresyl phosphate (TCP) (3%), phenyl-alpha-naphthylamine (1%), benzamine, 4-octyl-*N*-(4-octylphenyl) and some "partially unknown" ingredients [16].

1.3.1 Organophosphates

Synthetic jet lubricants contain 1-10% triaryl phosphates and exposure of triaryl phosphates to the passengers and crew members has been recorded to be approximately 23% on the monitored flights [17]. Jet engine oils are also known to contain small amounts of organophosphates. The UK Health and Safety Executive states that the organophosphates block normal function of an enzyme called acetylcholinesterase at neuromuscular junction hence interfering with the normal nerve impulses transmission [18] which causes brain disorders. The after effects of such events have been notified for over 30 years now [19].

1.3.1.1 Aerotoxic Syndrome

Despite this, it wasn't until 1999 when a team of international scientists published the term "Aerotoxic syndrome" to describe symptoms and exposure conditions of fume events recorded by the aircraft crew members specifically in Australia, Europe, and US. This term can be divided into two components where the aerotoxic refers to the toxic compounds found in the air and aircraft and the effects of the associated exposures of these compounds form a syndrome [20,8]. These symptoms vary from short term unwell feeling to mental impairment in those travelling on board specifically the crew members depending upon the exposure time and concentration.

The main reason behind aerotoxic syndrome has not been pinned down to a cause yet and it is still debatable due to a lack of interest from the airline companies and hence evidence collected during flights. Furthermore, the toxicological aspects of human body are extremely complex therefore scientists are actively trying to understand the mechanisms behind the interaction between chemicals and nervous system. However, due to the speed at which new chemicals are being introduced in

the market and the evolution of human body, it has been proven difficult to establish a cause between the symptoms experienced by those on board to the toxic chemicals present in the cabin air [21]. A lot of contradictions in this area of research can be found in the news or literature publications, however, toxicity of organophosphates is agreed upon by both the airline companies and private researches looking in to this field [2,8]. The neurotoxicity of phosphate esters dates back to late 1880s. In 1899 the first case of neurotoxicity related to aromatic phosphate esters was reported after patients with tuberculosis were treated with phosphocreosote- a mixture of esters derived from phosphoric acid and coal-tar phenols [22,23,24 25,26].

According to the list of hazardous substances in the Hazardous Substances Regulation, the two main toxic components of the jet engine oil are found to be TCP and phenyl-alpha-naphthylamine. Volatile organic compounds (VOCs) are also an area of concern as they can potentially cause risk to the health of crew members and passengers. Most compounds i.e. benzene, toluene, xylenes and esters are listed as toxic [27]. Amongst all the other VOCs, limonene and toluene are found to be in highest concentrations in the cabin air system [17].

1.3.2.1 Tricresyl phosphate

Phosphoric acid, tris(methylphenyl) ester more commonly known as TCP (Figure 1.2 is commonly industrially produced from the reaction between a mixture of phenols, mainly cresols and phosphorus oxychloride. More specifically, one molecule of TCP contains three cresyl(methylphenyl) groups all linked by a phosphate group [28].

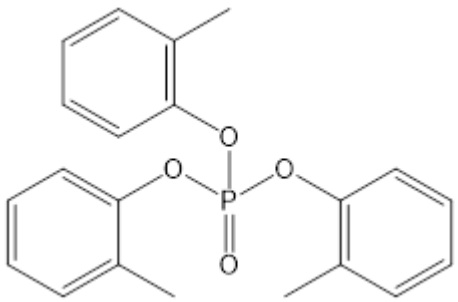

Figure 1.2. Tricresyl phosphate

Cresol (Figure 1.3) contains a hydroxyl and methyl group attached to a benzene ring. The industrial cresol is a mixture of all three ortho-, meta- and para- isomers. The prefixes arise based on the position of the methyl group relative to the hydroxyl group found in cresol.

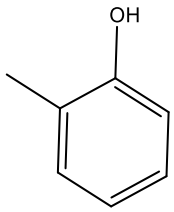

Figure 1.3. O-cresol

TCP is also commercially found to comprise a mixture of isomers; it exists in more than 10 isomeric forms however the ortho- substituted ring is known to be a neurotoxin [16, 29].

1.3.2.2 Metabolism of TCP

Inside the human body, the o-TCP is oxidized by the cytochrome P450 at the benzylic positions, this reaction releases o-cresol and is catalysed by serum albumin. The product formed is an irreversible inhibitor of human acetylcholinesterase which is thought to be the cause of neurotoxicity (Figure 1.4) [30,31].

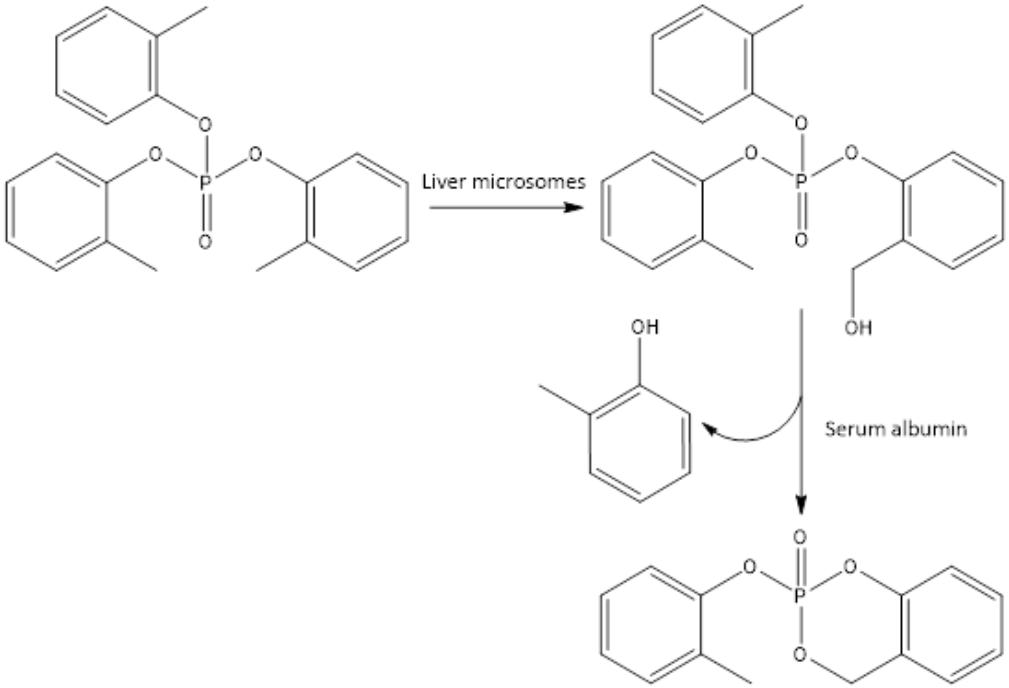

Figure 1.4. Schematic of metabolism of TCP in human body

Initially, industrial TCP contained a high concentration of all isomers. However, due to concerns related to the neurotoxicity of tri ortho-cresyl phosphate (ToCP or o-TCP), lower concentrations of the o-cresol were introduced in TCP manufacturing process [32].

Extremely toxic Torpedo oil used in World War II was found to contain approximately 25-40% o-cresol as a main source of toxicity [33]. This meant that the toxicity of TCP is not the only factor that should be considered, the presence of other ortho containing molecules also needed to be considered.

After this, manufacturers started using lower levels of ortho- isomers to avoid the risk of neurotoxicity. Around 1950s, o-cresol isomer present within the manufactured TCP had dropped to only 3-5% of the overall concentration. Further work in this field led to further decrease in the ortho-cresol content between 1980 and 1990s. As it was difficult to establish the exact amount of the ortho- isomer causing the toxicity to emerge, toxicity was still being observed in the commercially available products even in 1988 [34].

Even to this date, it is still hard to determine the exact ortho-cresol content in TCP containing products world-wide. However, an estimation of 0.1-1 % is thought to

be close to the actual concentration. This means that a product containing 3 % TCP would contain 0.003-0.03 % ToCP [34].

TCP has been used commercially in many products such as lubricants, plasticisers, hydraulic fluids, and dust suppressants. Although most commercial uses have now been ceased, it is still used in jet oil [16,35].

1.3.2.3 TCP as an anti-wear additive

Although TCP was known to have detrimental health effects, it has been used as an anti-wear additive in the lubricants and engine oils. Lubricants when mixed with additives reduce friction and wear [36,37]. TCP has been used since the early 1940s, the time when synthetic neopentyl polyol ester base stocks were more readily used as lubricants and it was found that the addition of TCP in to the lubricant not only produced a critical phosphate film needed for the anti-wear mechanism, it also decreased reactivity of the base stock [38,39]. In most cases the wear reduction mechanisms are not fully known. Various studies have tried to understand the anti-wear mechanism of TCP. It is generally concluded that a reactive phosphate film is produced on the surface of the metals which is crucial to prevent wear of the metal. Back in 1968, Bieber and co-workers studied the effect of increasing load in the presence of TCP on the wear improvement behaviour in ester base fluids and stated that the TCP forms polar impurities which become responsible for the anti-wear behaviour of TCP [40]. Later in the 1970, the anti-wear protection was shown to be due to the formation of phosphate layer [41]. This idea was agreed upon by another group of researchers who found that there was an interaction between the sliding metal surfaces and the additives which caused the formation of a phosphite layer or a film of phosphates by adsorption mechanism, according to their study this film reduced wear [42].

More recent possible mechanisms for the film formation causing anti-wear properties observed under the presence of metal oxide is thought to involve adsorption of the phosphate ester on the oxide surface followed by displacement of the alkyl group by breaking P-O bond to yield a phosphate which reacts with the metal as well as toluene and cresol as by products [38,43].

1.3.2.4 Quantification of TCP

TCP is found at the concentration of around 3%, of which the ortho isomers concentration is approximately 0.03 %. Since TCP is found in such small quantities; not only is it hard to detect, it is also not easy to link the symptoms experienced by those on board with TCP contamination alone.

There have been many studies that have been unable to detect TCP following complaints of crew members or passengers. An investigation was carried out in 1998 by the University of British Colombia after ill effects of oil odour were recorded by the crew members working on British Aerospace BAe 146-200 aircraft. All components of cabin air including the concentration of TCP were measured and the study was not able to detect any TCP during in-flight measurements and could not associate the observed health effects with TCP or the oil odour [19,44]. Another study published by Harvard University also looked at cabin air quality of Boeing aircraft and could not detect any TCP during in-flight measurements [12,45]. Furthermore, according to the British Airways Health Services, the TCP poisoning is caused due to swallowing the food or drink contaminated with toxins rather than through occupational exposure. Moreover, they also claimed that the stages at which the exposure could occur more frequently are the manufacturing, packaging and storage of the consumables rather than the point at which they have been consumed and stated that the intoxication reports are very rare [19].

Although the claims made in the above studies seem to have reasonable argument, the toxicity of TCP however cannot be ignored.

In the 1930, the cause of Ginger Jake paralysis was investigated as this affected between 10,000 to 50, 000 individuals who had consumed ginger contaminated with TCP extracts. The ToCP was concluded to have been the paralytic agent in this case [46,47]. In the 1959 Moroccan poisoning caused by contaminated ToCP in cooking oil paralysed 10,000 people [48,49]. In the late 1950s, it was reported that the metabolism of ToCP in liver generates toxic metabolites that could cause the poisoning [15,50,51].

Since then there have been many cases where the epidemic poisonings have been associated with the consumption of food contaminated with TCPs [52, 53, 54, 55].

An investigation published in the 1987 by the Environmental Control System (ECS) of an Automatic Direction Finding (ADF) aircraft showed the presence of TCP in the water coalescer bags of the engine bleed air indicating possibility of flight deck contamination by the TCP [36].

After this, several cabin air contamination cases in the passenger aircraft BAe 146 operating in Australia and the UK were published in the 1990s. The contamination source was thought to have been caused by the engine oil fumes of the jet engine turbine compressor fitted to provide cabin air to the people on board [20].

Three types of ADF crafts were investigated in 2011 for the contamination of TCP and the study confirmed presence of TCP in the cockpit air [10]. Before this, the investigators failed to quantify TCP contamination in the cabin air of commercial aircrafts [20].

Looking at the lack of evidence present for a correlation between the amount of TCP present in the cabin air and the aero toxicity experienced by the cabin crew members, it is hard to say if TCP is solely responsible for the illness experienced. Instead, it makes more sense to look into other known hazardous substances which have been found in the cabin air and also are a potential hazard in other places as well. Further to this, as mentioned earlier, TCP is known to form a phosphate ester film on the surface of the engine seals for lubrication purposes therefore, the concerning components of bleed air would be the by products of TCP breakdown or other chemicals present in the jet engine oil. Other VOCs which are present in higher concentrations with well-known health effects could instead be causing the problem.

1.4 Volatile Organic Compounds

VOCs by definition are carbon-based chemicals that evaporate readily at room temperature due to possessing a Reid vapour pressure (10.3 Pa at 293.15 K) [56,57,58]. Alongside being problematic in the cabin air, VOCs are major contributors to air pollution [59,60,61]. Research states that presence of VOCs such as esters (e.g. ethyl acetate), alcohols, aromatics (such as toluene and benzene), alkenes and alkanes are common in buildings as well as the cabin of the aircraft [62]. This suggests that the

VOCs are not only problematic in the cabin but also in other places. Emission of VOCs can be due to many sources; inside the aircraft, VOCs are by products of the combustion that is carried out in the engine and can be bled into the cabin *via* bleed air system. Other sources include; petroleum refineries, chemical industries and transportation and [63,64,65,66]. The effects of VOCs are dependent upon the concentrations and emission sources. However, generally, they have been recognised to be responsible for carcinogenic and neurotoxic effects in humans [67]. Two of the VOCs discussed in this thesis are toluene and ethyl acetate.

1.4.1 Toluene

Toluene ($C_6H_5CH_3$) is a monosubstituted benzene derived VOC which has intensively been studied as a model VOC. It is widely used in many applications such as combustion engines, disinfectants and paint thinners *etc* due to its high stability, non-corrosiveness and low flammability. It is being used so intensively that the global demand for toluene is expected to reach ~ 31.8 billion USD in the next coming years which is ~7 billion more than in 2015. Concerningly, however, 86 % of toluene gets released into the troposphere due its high volatility and insolubility in water. Main sources of this release include chemical spills, industrial processes and emissions from aircraft exhausts [68]. Presence of toluene in air has detrimental impact on human health. Toluene is harmful *via* oral, dermal or inhalation routes. Amongst there, the inhalation route has the highest hazard profile. According to exposure limit guidelines published for toluene by World Health Organisation (WHO), an estimated 1800-2000 parts per million (ppm) exposure of toluene over 1-hour could be fatal. For an 8-hours of work, occupational exposure limit is only 46 ppm in the European Union [69]. The acuteness of toluene requires for economically viable and greener techniques to be used to decompose/decrease its release into the atmosphere or the cabin air environment. Though toluene is rather problematic, this isn't the only VOC that is known to cause issues. Ethyl acetate is also known to have harmful effects on human health.

1.4.2 Ethyl acetate

Ethyl acetate is also a volatile organic solvent with significant uses in industrial processes. It is also found in many products such as paints and varnishes. The exposure limit for ethyl acetate is 400 ppm for an 8-hours work shift. It has a depressant effect on the Central Nervous System (CNS) and therefore causes sickness [70]. Though ethyl acetate has low toxicity, however, severe exposure to high concentration can cause drowsiness and unconsciousness which can be very drastic specifically for crew members travelling on board.

Ethyl acetate and toluene are both problematic if inhaled over a long period of time. As aircrafts are a closed environment, any contamination that makes its way into the cabin stays there for the rest of the trip. Therefore, abatement of VOCs such as these becomes essential.

1.5 High Efficiency Particulate Air filter

Even though there is a genuine need for a correct filter system for destruction of VOCs to be implemented, to date, there are no specific filtration systems applied to overcome the issue of bleed air contamination found in the cabin of the aircrafts. Instead, most aircrafts contain high efficiency particulate air (HEPA) filters which are designed to remove bacteria and airborne particles that could lead to viruses [14]. In order to overcome the issue of contaminants entering cabin air; a catalytic filter system which is able to withstand high temperatures and pressures needs to be implemented in the aircrafts.

1.6 Techniques for abatement for VOCs

VOC emission can be controlled using approaches based on destruction and recovery. The recovery can be carried out *via* adsorption, absorption, condensation and separation membrane [71]. Adsorption using suitable adsorbents such as activated carbon can be used to selectively adsorb the VOCs. This technique is economically viable when the fluent gas stream is contaminated with a very diluted concentration of VOCs. The cost of adsorbents and the requirement of regenerating the adsorbents are major drawbacks of this process [72]. Absorption is particularly useful for VOCs that are water soluble as these can be removed from contaminated gas stream by

absorption using solvents. However, the main problem arises when the solvent used must be disposed off which causes more environmental and economical issues. Condensation technique is based on increasing/decreasing the pressure at given temperature or vice versa. The disposal of the coolants used in this process is one of the main limitation of this technique [73].

Silicon rubber membranes are most commonly used in membrane separation for removal of VOCs. This is a bio-filtration process where the VOC contaminated air is fed in to a solid phase reactor where the contaminants diffuse on to the surface of the biofilm which acts as an enzyme to degrade VOCs in to carbon dioxide, water and other microbial by products [74]. The biofiltration process and membranes are expensive to operate and maintain.

The destruction method can be based on thermal, biological or catalytic oxidation. Thermal oxidation is useful for high flow rate and high concentration of VOCs contaminated gas stream. It requires temperatures >1000 °C which make this economically less viable. Incomplete combustion can produce rather harmful substances therefore, making this a less environmentally friendly method [75]. Comparatively, the catalytic oxidation is thought to be the most effective and economically viable technique to convert VOCs into carbon dioxide, water and/or other lesser toxic by products. In catalytic oxidation, the presence of catalyst causes the oxidation to occur at lower temperatures due to catalyst being able to lower the activation energy required for oxidation to occur [76,77,78].

Catalytic oxidation is a more thermal efficient method as it requires lower operating temperatures and thus, cheaper to convert moderate amount of contaminated air in to less toxic products [79, 80]. The most critical part of catalytic oxidation is choosing the correct type of catalyst, which is effective, cheap and durable [81].

1.6.1 Types of oxidation catalysts

Type of oxidation catalysts can be divided in to three main categories: i. Noble metal catalysts, ii. Non metal oxides catalysts and iii. Mixed- metal /-oxides catalysts. Noble metals such as Pd, Au and Pt impregnated on different supports have been successfully used for oxidation toluene [82,83,84]. The cost, however, is the

main drawback, using such precious metals for the application of bleed air contamination will not be cost effective. Comparatively, non noble metal/-oxide-based catalysts are economically more viable and less prone to poisoning.

Metal oxides are used as non- noble metal catalysts due to their higher availability and low costs. Though the non- noble metal oxides are relatively less active than noble-metal catalysts, they are used for VOCs oxidation due to their low costs, capability of regeneration and higher tolerance towards coking [85, 86,87, 88].

Different metal oxides have been studied in the past as active/support for oxidation catalysts for toluene and ethyl acetate. Table 1.1 summarises different oxidation catalysts.

Table 1.1. Catalysts used for toluene/ethyl acetate oxidation at temperatures between 200-500 °C

Catalyst	VOC	Conditions	Conversion (%)
Au on CuO	Ethyl acetate (500 ppm)	150-350°C, fixed bed micro reactor, 60,000 mL/h g^{-1}	100 at 311 °C [89]
Mn-Ce	Ethyl acetate (7525 ppm)	50-300 °C. micro reactor	90 at 180 °C [90]
Ce-Co	Toluene (1500 ppm)	250°C, fixed bed reactor,3600 mL/h g	100 at 250°C [89]
Mn-Cu	Toluene (1000 ppm)	100-500°C, flow reactor, 30,000 h^{-1}	100 at 350 °C [91]
Au on Fe_2O_3	Toluene (1000 ppm)	40-400°C, flow reactor	90 at 300 °C [83]
Mn-Ce	Toluene (900 ppm)	160-400°C, fixed bed flow reactor	90 at 245 °C [90]
Pd on Nb_2O_5	Toluene (0.1 % vol)	200-450 °C, stainless steel reactor 20,000 h^{-1}	90 at 440 °C [82]

There are various other metal oxides that have been successfully used for oxidation of VOCs. The metal oxides mentioned in Table 1.1 would be useful for the temperature range of 200-500 °C for the application of bleed air contamination. The metal oxides mentioned in Table 1.1 have shown some promising results at relatively lower temperatures. The metal oxides can be impregnated upon support materials such as such as metallic/ ceramic foams, spinel oxides (Al_2O, Fe_2O_3) and zeolites. Based on this, the next part of the thesis will look at metallic stainless steel (SS) foams and spinel oxides as support/ catalysts for oxidation of VOCs.

1.7 Potential candidate materials for catalytic oxidation

Powder and structured catalysts could both be used in filtration systems [92,93,94,95]. Structured catalysts such as SS foams and powder catalysts such as spinels have been investigated to be used as support/active catalysts for oxidation of toluene and ethyl acetate.

1.7.1 Spinel oxides

Spinels are group of minerals with the basic formula of AB_2X_4 (where A = +2, B = +3/A = +4 and B = +2 and X = -2, the number refers to the charge on the ion). A and B can be a mixture of di- or tri- valent cations and X is an anion. A and B can also be the same metal with different valences, e.g. in the case of Fe_3O_4 where Fe is found in both, 2+ and 3+ oxidation states [96]. Spinels can be normal or inverse depending on the cation distribution. Normal spinel oxides such as AB_2O_4 shown in Figure 1.5 have cubic close-packed cubic structure with four octahedral and eight tetrahedral sites. Octahedral spaces are generally larger than the tetrahedral sites. A^{2+} ions (blue in figure) occupy $1/8^{th}$ of the tetrahedral holes whereas the B^{3+} (green in figure) ions occupy 1/2 of the octahedral holes.

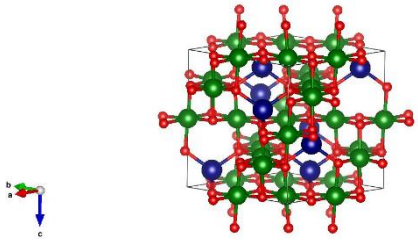

Figure 1.5. Normal spinel structure

There is a different cation distribution in the inverse spinel. In this, all the A^{2+} cations and half of the B^{3+} cations occupy the octahedral sites where the other half of the B^{3+} occupy tetrahedral sites. The position of the cation in the spinel structure is dependent upon the crystal field stabilisation energies of the transition metals. The preference to occupy octahedral sites comes from the d-electron count of the metal. If the A ions have a stronger preference towards the octahedral sites, they will displace half of the B ions from octahedral to tetrahedral sites. If the B ions have a low octahedral site stabilization energy, they will occupy the tetrahedral sites more readily making space for A ions on the octahedral sites. The occupancy is also dependant upon the radius of the ion, the smaller ions preferably occupy the A site [96,97,98,99]. Substitution of one/two of the cations is a way to improve the activity of the oxide catalysts. Spinel oxides exhibit good catalytic performance due to the presence of active metal ion pairs, high surface area and improved stability [100].

1.7.1.1 Synthesis of spinel

There are various possible synthetic routes to obtain a spinel structure. Hydrothermal, co-precipitation and sol-gel and combustion methods have all been used in the past to synthesise spinels. The choice of synthesis route depends upon the required properties of the final product.

1.7.1.1.1 Hydrothermal method

This is one of the most commonly used method for preparation of nanomaterials with a wide range of morphologies. In this synthetic method, the reactants are placed in an autoclave with water under high pressure and temperature [101]. For this process, a careful consideration of autoclave is required therefore, Teflon-lined containers are generally preferred due to their strong resistant to hydrofluoric acid. Hydrothermal synthesis firstly facilitates reaction to occur amongst the reactant, promotes hydrolysis and then crystal growth which results in formation of nanomaterials in solutions. The size, structure and morphology of the materials can be tailored by varying pH, temperature, pressure and concentrations of the reactants. One of the main disadvantages of this approach is that the crystal growth can not be monitored as it is carried out in a closed vessel. The cost of expensive autoclaves is another drawback of this technique [102].

1.7.1.1.2 Co-precipitation method

Co-precipitation reaction involves the nucleation, growth and agglomeration processes to take place simultaneously. The products are found in an insoluble species under supersaturation conditions. The nucleation process allows for small nanomaterial growth to occur. This process requires cheap reactants, does not generate solid waste and can easily be amended in the glovebox. This process requires trained personnel for maintenance and regeneration and also generates highly toxic liquid waste thus making it less feasible [103].

1.7.1.1.3 Combustion method

Combustion synthesis is proven to be a highly advantageous method for obtaining nano powders. It is a simple, rapid and versatile method of synthesising a variety of nanosized materials. This method is a self sustained exothermic reaction in which a homogeneous solution of different oxidising salts (metal nitrates) and fuel (urea, citric acid, glycine, tartaric acid etc) is mixed at a relatively low temperature (below 100 °C), followed by evaporation of the solvent (approximately 200 °C). The use of fuel causes intimate mixing of the reactants and thus, combustion results in formation of fine homogeneous nanosized powder which can then be calcined and sintered to form the desired spinel structure [104]. Compared to other synthetic routes, there are a few advantages of combustion synthesis:

The exothermic nature of this reaction eliminates the requirement for expensive equipment and facilities making this an economically friendly reaction.

High temperatures are reached during the combustion process which means that the low boiling point impurities get removed resulting in the formation of products with high purity.

The reactions can be carried out at relatively low temperatures and due to the exothermic nature of this reaction, the overall reaction time is reduced resulting in a lower overall operating cost.

Inorganic materials can easily be synthesised in one step reaction by making use of the chemical energy of the reactants [105].

Combustion synthesis can easily be carried out in lab and therefore, is more suitable for the synthesis of spinel oxides for the chosen application. The ease of synthesis,

good magnetic properties and simple chemical compositions make spinels interesting for waste water treatment reactions, catalysis and electronic devices [106]. Although powder catalysts have been used previously for catalytic applications, the use of structured catalysts is also becoming increasingly interesting in the field of catalysis. Compared to powder catalysts, a thin layer of catalyst that can be placed on a solid support is preferred, due to the ease of implementation and being more economically viable [107]. One such solid support system is metallic/ceramic foams which could consist of open or closed pores.

1.8 Open and closed pores foams

Generally, foams can be divided in two types: foams with open pores [108,109] and foams with closed pores [110]. The former is useful in catalytic activities as it allows for catalytic coating to be placed on the foam due to its 3D interconnected structure [111]. The 3D open-cell network structure of steel based foams have great anti-corrosive porosity, specific stiffness and high melting points therefore are becoming increasingly important in research specifically in the catalysis field [112, 113, 94, 114, 115]. The open cell structure also offers a high interface area between the gases and the catalyst therefore can be used in purifying exhaust gasses. Compared to open cell foams, close cell foams have closed pores which can be filled with any gas and although these have greater dimensional stability and show better mechanical properties, these are generally more expensive to produce [116,94,117,118]. The closed pores do not allow for gasses to pass through hence are limited to reactions not involving flow of gasses.

1.8.1 Ceramic vs. metal foams

Compared to ceramic foams, using metallic foams have several advantages, due to turbulent flow regime; mixing of reagents is better [111]. As well as having high permeability, metallic foams also have large surface area to volume ratio which make them applicable to many applications such as filters, catalytic reactors, heat exchangers, lightweight high-strength structural applications and many more [119,120]. Metal foams have large number of pores that are filled with air, the open cell structures have thin metal ligaments that form a 3D network which connect these

pores. Metallic foams can be made from single metals such as aluminium, copper or nickel or of alloys or stainless steel [121].

1.8.2 Stainless steel

Stainless steel is a steel alloy with a minimum Cr content of 11 %. The are four main types of stainless steels which possess different properties:

1. Austenitic stainless steels: These non-magnetic stainless steels contain high levels of Cr and Ni. These are known to have high resistance against corrosion and generally have a face centered cubic (FCC) crystal structure. Austenitic stainless steels are the most widely used grade of stainless steel.
2. Ferritic stainless steels: These magnetic stainless steels are high in Cr and have a very low carbon content. Good resistance to corrosion and cracking makes this grade of stainless steel being widely used in kitchenware and industrial equipment.
3. Martensitic stainless steels: These are magnetic and are similar to ferritic stainless steel grade but contain higher carbon content. Due to moderate resistance to corrosion, these are used in sheets or plate forms.
4. Duplex stainless steels: These are a mixture of austenitic and ferritic grade of stainless steel which gives them greatest strength compared to any other type of stainless steel. Duplex SS have lower Ni content compared to the austenitic SS grade but have similar resistance to corrosion. The most common uses of duplex stainless steel grade are in oil and gas refining, chemical processes, storage and transportation industries.

For applications involving gasses, stainless steel foams possess good catalytic characteristics.

1.8.2.1 Stainless steel foams

Stainless steel foams are metallic materials which posses several chemical and physical properties which make them useful in various application. The synthesis of SS foams can be carried out *via* the powder metallurgy route or the liquid metal route [122]. Production *via* sintering the metal powders in the presence of volatile cellulating agents results in formation of an ununiform pore structure and skeleton. The latter approach consists of using polymeric sponge structure, which is coated with the metal powder slurry, the excess slurry is removed from the sponge which

causes pore formation, after drying, the sponge structure is removed through pyrolysis. This process results in formation of more uniformed and open pores to be embedded on the structure of the foam. Properties such as high porosity, low density and high surface to volume ratio make these foams useful in various applications [123,124,125].

The foams are mostly used in applications where low weight, improved fuel efficiency and rigidity is required [126]. SS foams can also be used in heat exchangers due to high energy-absorption properties. These foams can particularly be useful as catalytic filters due to their capability of dealing with high gas flow rates without increasing the pressure drop however, the filtration efficiency is dependent upon the number of pores per inch (ppi), this ppi is generally a compromise between pressure drop and good filtration [76]. The morphology and composition of metallic foams can be modified by thermal or chemical treatments depending upon the application required. Oxidation and impregnation studies have been carried out on SS foams in the past to make them better candidates for catalytic applications.

1.8.3 Pre-treatments of stainless steel foams

1.8.3.1 Oxidation

Oxidation is the process by which an oxide layer is formed at the surface of the foam when submitted to different temperatures under air. The changes on the surface occur due to the movement of elements present in the metallic core to the pore surface forming an oxide layer. The new oxide layer prevents metallic segregation and creates roughness on the surface which has a positive impact on the quality of catalytic coating [127]. While the latter favours catalytic coating progress, the former is helpful in avoiding interaction between the catalyst being coated and the metallic components of the foam [128,129].

1.8.3.2 Impregnation

The surface area of the foam is generally low therefore a coat of appropriate metal oxides could enhance this surface area which improves the distribution of active metals and avoids segregation that can cause catalytic coking [76,130]. The applications of coated metallic foam vary from methane catalytic oxidation [131],

engine gas purification [132], methanol partial oxidation [133] and Fisher-Tropsch synthesis [134].

Sol-gel, powder plasma spraying or suspension methods can be used to place a coat on the support however impregnation via dip coating is more widely used in order to coat the metal foam as it strongly adheres the layer on to metallic support and is an easy process to carry out [116].

1.8.3.2.1 Sol-gel

The sol-gel process consists of "sol" which is a suspension of nanoparticles in liquid and "gel" which consists of a porous solid network surrounding a liquid phase. The sol-gel process is a wet-chemical technique which involves 5 main steps: 1. Hydrolysis and poly-condensation; 2. Gelation; 3. Aging; 4. Drying and 5. Crystallisation. This technique is preferred over other conventional thin film deposition processes as it allows for better control of chemical composition, uses simple equipment and overall the process can be carried out at low costs [135].

1.8.3.2.2 Plasma spraying

Plasma spray process consists of spraying molten material on to a surface in order to provide a coating. The material in form of powder is injected into a high temperature plasma flame where it is heated rapidly to be accelerated to high velocity. The hot material upon spraying comes in to contact with the surface of the substrate and cools down forming a coating [136].

1.8.3.2.3 Dip coating

Dip coating is the oldest commercially applied coating process which was first introduced in 1939. The process is generally divided in to three main technical stages:

1. Immersion and dwell time: The substrate is immersed in to a precursor solution at a constant speed and it is left in the solution to dwell for a certain amount of time in order to allow the substrate to interact with the coating solution to be completely wet.

2. Deposition and drainage: The substrate gets pulled upwards at a constant speed and in doing so, a thin film is deposited from the precursor solution on to the surface of the substrate. The excess liquid is also drained from the surface of the substrate during this process.

It is clear that the morphology of the foams can be modified with ease using one/combinations of the treatments described earlier. For the bleed air contamination application, it is also important to dwell into the potential impregnations of metal oxides that have been mentioned in section types of oxidation catalysts earlier, based on previous literature on destruction of VOCs from gas stream. Though the SS foam can potentially be used as a support/ catalyst for oxidation of toluene and ethyl acetate. Spinel oxides also have good potential to be used as catalytic support/ catalyst. This thesis will provide information on the catalytic activity, selectivity and morphology of the SS foams used and the synthesised spinel oxides.

1.9 Aim and objectives

The aim of this work is to reduce the potential health hazards associated with breathing contaminated cabin air by exploring suitable catalysts to oxidise the known toxic contaminants.

The following objectives will achieve this aim:

Review of literature on how the cabin air can be contaminated, health risks associated with such contamination and the potential catalytic materials which can be employed to deal with this issue

Synthesis of nanomaterials

Modification of materials to enhance their catalytic activity

Characterisation of modified/synthesised catalysts using techniques such as; Scanning Electron Microscopy (SEM) with Elemental Dispersive X rays (EDS), X ray Diffraction (XRD) and Mass spectrometry (MS)

Catalytic testing of materials on lab scale rig

Analytical techniques

2.1 Overview

This chapter will give an insight of the theory behind the techniques used in this thesis. SEM-EDS, XRD and MS have all been employed to characterise the synthesised/modified materials. ICP-MS was used to determine the metallic content of the foam after being purchased and was compared with the EDS. BET was employed to measure the surface area, the value, however, was too low to be reported.

2.2 Scanning Electron Microscopy

Scanning electron microscopy (SEM) works on the basic principle of using electrons to produce images which provide surface morphology information of the sample. SEM uses a focused beam of electrons which interact with the sample and produce signals that give information on the surface topography, morphology and composition.

Figure 2.1 shows schematic of the main components of SEM which are:

1. Electron gun as a source of electrons
2. Column consisting of electron lenses to focus the beam on to the specimen
3. Sample chamber
4. Detectors
5. Data output devices/ display monitor

SEM also requires a source of vacuum and a cooling system.

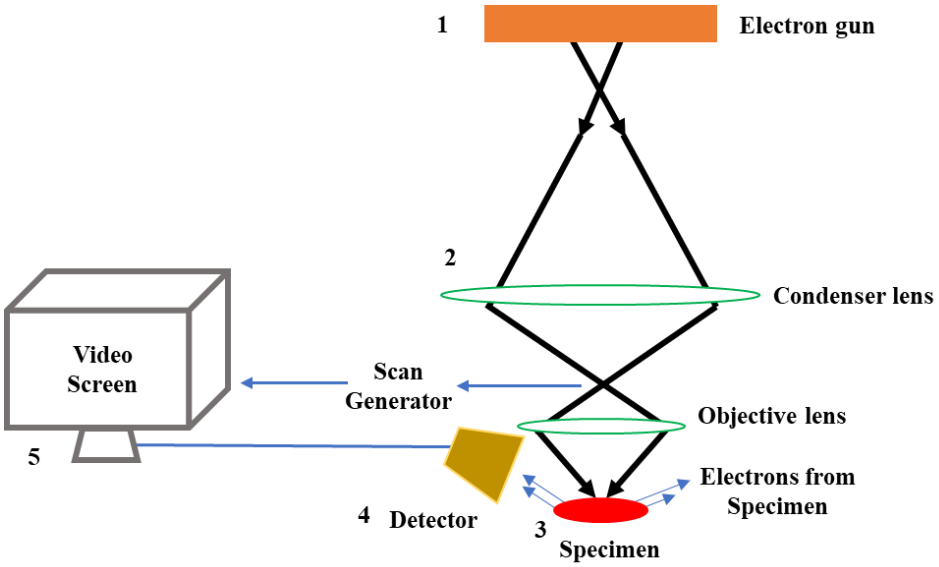

Figure 2.1. Schematic of SEM, redrawn from [137]

High kinetic energy electrons are produced at the top of the column and are accelerated down the column to interact with the solid sample mounted on the stage of the chamber area. There are three main electron sources in an SEM; thermionic tungsten filament, Lanthanum hexaboride filament and field emission gun. The two more common sources are thermionic emitter, and field emission gun. In thermionic emission, the filament is heated at high temperature to enable the electrons to overcome the energy barrier and interact with the specimen. Field emission gun applies a very high electric field to the tip which causes tunnelling of electrons to occur. This technique lowers the working distance between the specimen and the tip of the electron source causing a bright beam with small deviation in electron energy. The thermionic guns require vacuum of 10^{-6} Torr, the field emission gun require 10^{-10} Torr which is an additional cost in maintaining the instrument. The electrons coming down the chamber, come in to contact with different electromagnetic lenses which de-magnify the electron beam into a fine probe which is scanned across the selected surface of the specimen. The electron penetration occurs in a teardrop shaped volume, the dimensions of which are dependant upon the energy of the electron beam, the elemental atomic masses and the angle at which the electron beam interacts with the sample. The higher the electron beam energy, incidence angle and lighter the atomic mass, the more penetration depth there will be. The electron-sample interaction results in formation of different types of signals.

This interaction could lead to production of; secondary electrons, back scattered electrons, diffracted back scattered electrons, x-rays and occasionally light that can be collected by various detectors found in the specimen chamber. The secondary electrons and backscattered electrons are responsible for the image of the solid specimen. The X-rays are useful to obtain elemental composition information of the sample. The image magnification is the ratio of the side length of the display monitor to the length of the scanned pattern on the specimen.

The incident beam hits the outer orbital of the atom which causes the secondary electrons leave the specimen with energies >50 eV. These come from near surface layer of the specimen and the signal escapes from a very small area (size of the electron probe) which therefore results in forming the highest spatial resolution images. Secondary electrons give morphological and topographical information and the back scattered electrons are useful for showing contrast in composition of samples.

Back scattered electrons are incident electrons which come into close contact with the nucleus of an atom to be scattered. These have much higher energies and the images have slightly less resolution than secondary electron images as these electrons go deeper into the specimen. These are mostly used for compositional analysis, where the higher atomic mass element gives brighter contrast. The area causing the signal to appear in this case is larger than the size of the probe.

2.3 Energy-dispersive X-ray spectroscopy

In order to obtain quantitative/qualitative elemental information of the specimen being investigated under SEM, EDS is generally used as a common tool. To generate X-rays, an incident beam of electrons is focused on to the specimen. This incident beam causes excitation in the electrons found in the inner shell which causes the electron to leave the shell, leaving a hole behind. In order to fill this hole, the electron in the outer shell falls into the inner shell and in doing so, releases an X-ray. The energy and number of the X-rays being generated from the specimen are measured by an energy-dispersive spectrometer. The elemental composition of the specimen can be measured because the energies of X-rays being emitted correlate to the difference in energy between the two energy levels and in turn gives

information on the atomic structure of the emitting element. The penetration depth of specimen from which the X-rays are generated shown in Figure 4.2 is dependent upon the accelerating voltage of the incident beam, the atomic number and atomic weight and density of the specimen and can be calculated using Kanaya-Okayama principle given in equation 2.1.

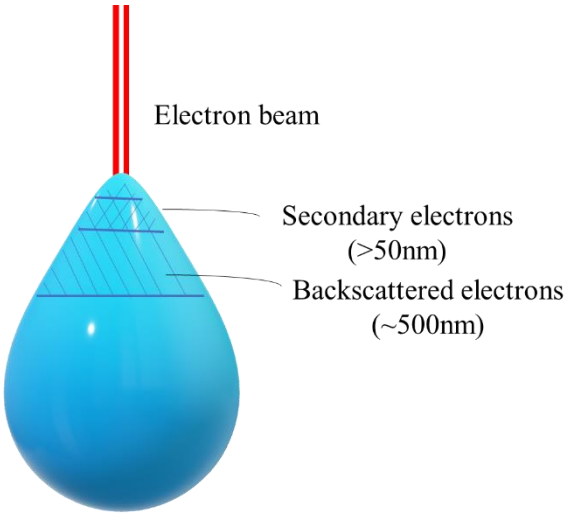

Figure 2.2. Schematic of the interaction volume of a specimen and the signals generated by the electron beam-specimen interaction, redrawn from [138]

$$d_P = 0.0276 \frac{A\,E^{1.67}}{Z^{0.89}\rho}\ \mu m \quad \textbf{(Equation 2.1)}$$

The d_P is the penetration depth, A is the atomic weight, E is the applied voltage (kV), Z is the atomic number and ρ is the density (g/cm^3).

SEM gives important information on sample morphology and is a very useful technique for qualitative and quantitative analysis of solid samples. Conducting samples do not require any additional preparations. It is also a non-destructive technique as the signals generated by electron-sample interactions do not cause volume loss therefore, the samples can be re-analysed or used further without the need to be sacrificed [139, 140].

2.3 X-ray diffraction

Powder XRD is mainly used for investigating phase identification of a finely ground crystalline solid material. This technique is useful in finding information on unit cell dimensions. XRD is based on interference between X-rays and the crystalline specimen.

X-ray diffractometers have three main components: a sample holder, an X-ray tube and an X-ray detector. X-rays are generated inside a cathode ray tube and are directed towards the sample. The interaction between the incident rays and the sample produce constructive interference and diffraction when the Bragg's Law shown in Figure 2.3 and Equation 2.2 conditions are satisfied.

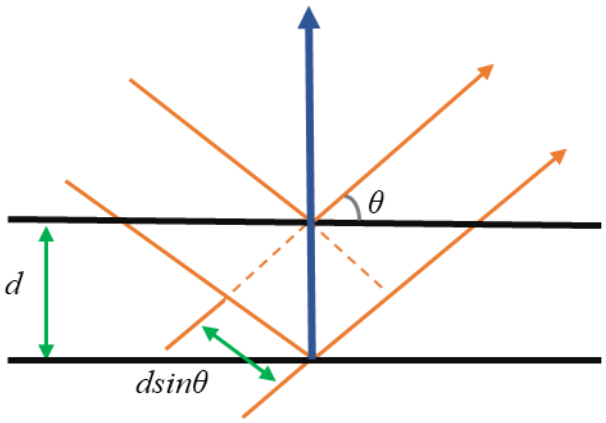

Figure 2.3. Schematic of diffracted X rays from atomic planes, redrawn from [141]

$$Braggs\ law:\ n\lambda = 2d\ sin\ \theta \quad \textbf{(Equation 2.2)}$$

where n is a positive integer, λ is the wavelength, d is the distance between the parallel planes (lattice spacing) and θ is the scattering angle on a set of parallel planes.

Braggs law correlates the lattice spacing and diffraction angle of a crystalline sample to wavelength of the incident electromagnetic radiation. The diffracted X-rays are detected and added up to present an XRD spectrum. The samples are scanned on a range of 2 θ angles so that all the diffraction directions within the powdered sample are attained. Each mineral has its own unique d spacing, therefore, conversion of the diffracted peaks into the d-spacings results in

identification of the material. Comparison of known d-spacings with reference standard reference patterns aid the phase identification process of the sample.

An XRD pattern is created by plotting the intensities of the diffracted peaks against the 2 θ Bragg's angle. This g

ives information on the crystal structure of the material and generally, there is a database that can be used to identify the crystal structures of the powders being investigated [142,143].

2.4 Mass spectrometry

Mass spectrometry is a quantitative analytical technique that is useful to know identity of unknown compounds within the sample. Generally, the process consists of converting the sample into gaseous ions which are characterised by their relative abundances against mass to charge (m/z) ratios.

Mass spectrometer is used to generate ions from a given sample, the ions are separated according to their mass-to-charge ratio (m/z) and the relative abundance of each ion type is recorded.

When the sample is first introduced into the mass spectrometer, it produces gas phase ions by electron ionisation. The main fragment is the total mass (M) -1 peak. Alongside the main peak, the initial ionisation results in formation of various other small fragments of the initial compound. The ions are separated according to their m/z ratios and are plotted against their relative abundance. Ions are useful in providing information regarding different components present within the structure of the compound being analysed.

Figure 2.4 shows the different stages inside the mass spectrometer which are:

Ionisation: An ion source produces the gaseous ions from the stream of products that is introduced into the mass spectrometer from the outlet of a reactor.
Acceleration: This enables the ions to be accelerated with same kinetic energy.

Deflection: A strong magnetic field is applied to deflect the generated ions. The lighter ions deflect more readily. This is also dependent upon the positive charge created on the ions after being ionised. Highly charged ions deflect more readily.

Analyser: This resolves the ions according to their m/z ratio

Detector: This detects the ions being produced and records the relative intensity of each one against the respective ion

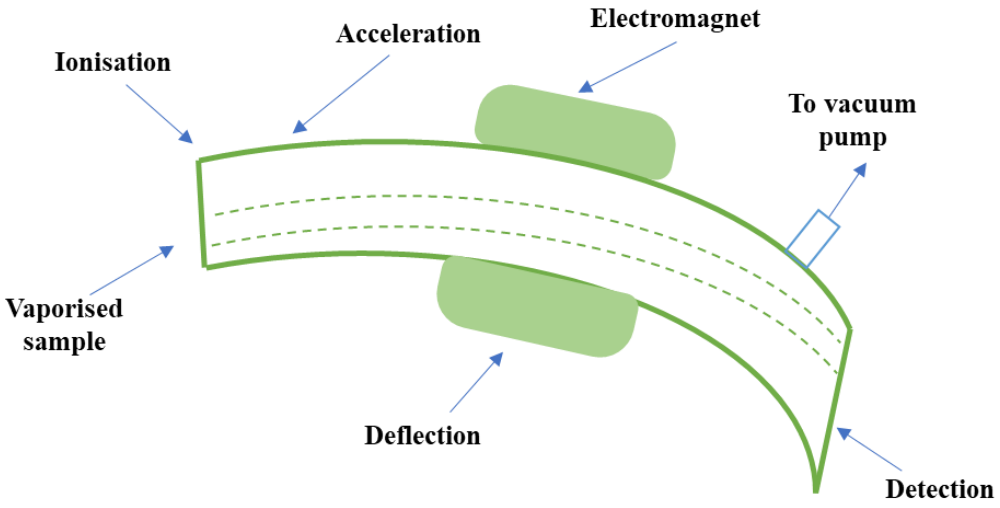

Figure 2.4. Schematic of mass spectrometer, redrawn from [144]

Experimental Procedures

3.1 Overview

This chapter describes the methods used in the modification and synthesis of catalysts and the parameters used for the techniques used. Any modifications made in the experimental procedures have been explained in the respective results chapters separately.

3.2 Stainless steel foams studies

3.2.1 Materials and reagents used for stainless steel foams studies

SS 314 foams (20 ppi, 4.5 % density) with a chemical composition of Iron (Balance), Chromium (23-26 %), Nickel (19-22 %), Manganese (2 %), Si (1.5-3 %), Carbon (03.25 %), Sulfur (0.03 %), Phosphorus (0.04%) were provided by Porvair plc. SS 316 foams (40 ppi, 0.55 g bulk density, 93 % porosity) with chemical composition of Iron (Balance), Chromium (16-18 %), Nickel (10-14 %), Molybdenum (2-3 %), Manganese (2 %), Si (0.75 %), Carbon (0.08 %), Sulfur (0.03 %), Phosphorus (0.04%) were brought from Good fellows.

The following reagents: Iron (III) nitrate nonahydrate (CAS no. 7782-61-8, ≥99.95 %), Copper (II) nitrate trihydrate (CAS no. 10031-43-3, 99 %), Cerium (III) nitrate hexahydrate (CAS no. 10294-41-4, 99.1 %), ethanol (CAS no. 64-17-5), terpineol (CAS no. 8000-41-7, 95 %) and Dodecyltrimethylammonium bromide (CAS no. 1119-94-4, 99%) and Polyvinyl butaryl were bought from Sigma Aldrich. Nickel (II) nitrate hexahydrate (CAS no. 13478-00-7, 99 %) was brought from Acros organics and the Manganese (II) nitrate hexahydrate (CAS no. 17141-63-8, 98+ %) was purchased from Alfa aeser. These were used for impregnation of active material on the surface of the foams.

3.2.2 General experimental procedure for SS foams modification

The summary of experimental procedure used to activate SS foams has been summarised in Figure 3.1. This was adapted from previous work with the SS foams [121,129].

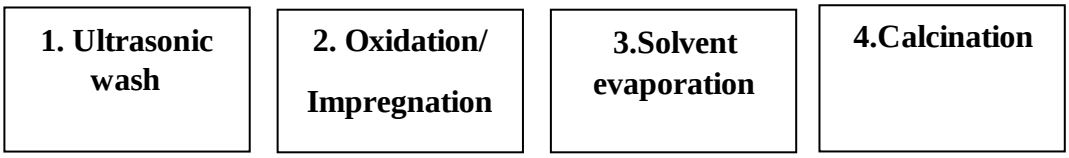

Figure 3.1. Schematic of modifications made to activate SS foams

1. SS foams were cut into cylindrical pieces of 13 mm diameters. The foams were spray washed with deionised water and then with acetone. The acetone wash was carried out in an ultrasonic water bath where the foams were left for sonication for 30 mins. The foams were then dried at 100 °C for 1 hour in a conventional oven. Washed foams were modified *via* two different pathways; oxidation and impregnation.

2. Oxidation step in the case of SS 314 was carried out to form a rough oxide layer on the surface of the foams in which the total metal oxide % increase had to be 5 wt. %. This increased roughness was to improve the impregnation of metal nitrates on the surface of the foam. For SS 316, the aim of oxidation was just to increase surface roughness for better impregnation, there was no set target for wt. % increase. The oxidation step was carried out in a tube furnace under static air. Different oxidation temperatures (300 – 900 °C) were tested in the course of the work. The furnace temperature was increased at the ramp rate of 5 °C/min, different dwell times were investigating at different temperatures, the cooling ramp rate of 5 °C/min was used in all cases.

The impregnation of metal nitrates on SS 314 and SS 316 foams were carried out *via* dip coating method. The 314 foams were impregnated in 0.5 M solutions whereas the 316 were impregnated with 0.1 M solutions. For the dip coating process, a set volume (40 ml) of solvent solution was placed in a beaker. The foam was slowly introduced into the solution and left to reach the bottom of the beaker at the speed of 5 ml/min. The foam was left in the beaker for 2 mins and it was then

pulled out at the same constant speed. Different solutions were made to find an optimal coating of the foams. The following parameters were tested for optimisation:

- Influence of substrate
- Influence of solution composition
- Influence of re-coating
- Influence of concentration of solution

3. After being impregnated with metal nitrates, the wet foams were dried at 100 °C in a conventional oven.

4.Once dried, the impregnated foams were calcined in a muffle furnace at different temperatures to obtain the respective metal oxides. Table 3.1 summarises the calcination temperatures used for their respective nitrates. The ramp rate of 5 °C/min and dwell time of 4 hours was used as a general calcination procedure.

Table 3.1. Calcination temperatures required for respective metal nitrates [145].

Metal nitrate	Calcination temperature (°C)
Ce (III) nitrate hexahydrate	350
Mn (II) nitrate hexahydrate	350
Ni (II) nitrate hexahydrate	380
Cu (II) nitrate trihydrate	400
Fe (III) nitrate nonahydrate	450

3.3 Spinel oxides synthesis

3.3.1 Materials and reagents used for spinel oxides synthesis

Iron (III) nitrate nonahydrate (CAS no. 7782-61-8, ≥99.95 %) and Chromium (III) nitrate nonahydrate (CAS no. 7789-02-8, ≥99.99 % trace metals basis) were bought from Sigma Aldrich. Manganese (II) nitrate hexahydrate (CAS no. 17141-63-8, 98+ %) was purchased from Alfa aeser. Nickel (II) nitrate hexahydrate (CAS no. 13478-00-7, 99 %) was brought from Acros organics. Citric acid CAS no. 77-92-9, ≥99.5 %) was bought from Sigma Aldrich.

3.3.2 Combustion synthesis

Combustion synthesis is a self sustained exothermic reaction which is simple, cheap and very beneficial for synthesising nano powders. $FeMnCrO_4$ and $MnNiCrO_4$ spinels were synthesised using this method which was adapted by previous work in the group [146].

For the general spinel oxide synthesis, the metal nitrate salts, all in 1:1 ratio was placed in a beaker with deionised water. The solution was placed on a hot plate and stirred until the salts had dissolved completely. Citric acid was used as a fuel and a chelating agent and was added into the solution. After stirring the solution to enable mixing, the temperature of hot plate was gradually increased to 100 °C. The solution was left at 100 °C for 1-2 hours in order to evaporate the water. This resulted in a formation of a gel so in order to allow for complete combustion to occur, the hot plate temperature was increased to 250 °C. Once hot enough, the slurry gradually started to dry and eventually resulted in the formation of very fine nano powders. The powder was placed in a muffle furnace where it was first calcined at 1000 °C for 10 hours, followed by sintering at 1500 °C for 10 hours. This process allowed the formation of spinel oxide structure to be synthesised. After this, the oxides were reduced under different temperatures, atmospheres and dwell times which will be discussed in chapter 4. General reduction was either carried out in a tube furnace equipped with 5 % H_2 and Ar or in a vacuum furnace with vacuum. The powders were analysed with XRD for phase identification and SEM was used for morphological changed. The prepared materials were tested in a lab scale rig.

3.4 Lab scale rig for catalytic tests

Figure 3.2 shows the lab scale rig assembly used for testing SS foams or synthesised spinels for toluene as a contaminant.

1. Compressed air from a cylinder was fed into a mass flow controller (MFC) where the flow of air was set to 200 ml/min for the purpose of keeping the flow rate as close to the real-life bleed air rate as possible. This air was fed into a two neck round bottomed flask which contained the contaminant. In order to get a homogenous formation of bubbles, a sparger was moulded into the inlet of the flask. A thermometer was kept just above the solvent to measure the temperature throughout the reaction in the 2nd neck of the round bottomed flask. Though the ideal flow rate for experiments was 200 ml/min, lower flow rates of 100 and 150 ml/min were also tested. Various flow rates were tested to make sure that the air entering the reactor was fully saturated with the contaminant. As 200 ml/min is a very high flow rate, there was a possibility that the air was not picking up the contaminant completely therefore, it was essential to test lower flow rates. At each flow rate tested, same toluene signal was observed which indicated that the saturation had occurred even when a very high flow rate was used.

2. 841 and 7275 ppm of toluene and ethyl acetate respectively were used for the purpose of this thesis. The toluene was kept at -33 °C in order to obtain the 841 ppm concentration of it [147]. Acetonitrile and dry ice were used to create the ice-solvent bath in a dewar flask. A thermometer was placed inside the bath as well as the round bottom flask to make sure that temperature inside the round bottom flask was correct and consistent. For ethyl acetate, in order to obtain the desired concentration, the rig was modified which will be discussed later in the section.

3. The air saturated with toluene ended up in the fixed bed quartz reactor which was placed vertically in a temperature-controlled furnace. A thermocouple was placed inside the furnace and outside the reactor, it sat parallel to the hot zone of the furnace which was the middle area. In the quartz reactor,

quartz wool was placed with the aid of a stainless steel rod first followed by the catalyst. The foam catalyst required a slight push to enter the reactor whereas powder was slowly poured into the reactor. Finally, quartz wool was placed on top of the catalyst. Quartz wool was used in blank experiment as well as with catalysts both cases for consistency. The temperature for the furnace was increased at 10 °C/min from 25 to 500 °C. After 25, 200 °C was tested. The temperature was increased at 50 °C step, i.e. 250, 300 *etc*. The furnace was left to settle at each temperature for 10 mins prior to taking any measurements. An average time of 30 mins dwell time was used at each temperature. 5°C/min ramp rate was tested, and the results obtained were the same as 10 °C/min therefore 10 °C/min ramp rate was used throughout. One-hour dwell time was also tested initially however, as the signals remained constant throughout, 30 mins average was chosen.

4. The outlet of the reactor was connected to a T-piece where one end was connected to the Cirrus mass spectrometer for analysis and the other was connected to a bubbler to dilute any resulting contaminants before being vented off to the air. The main quantified product was CO_2 as a complete oxidation product of toluene.

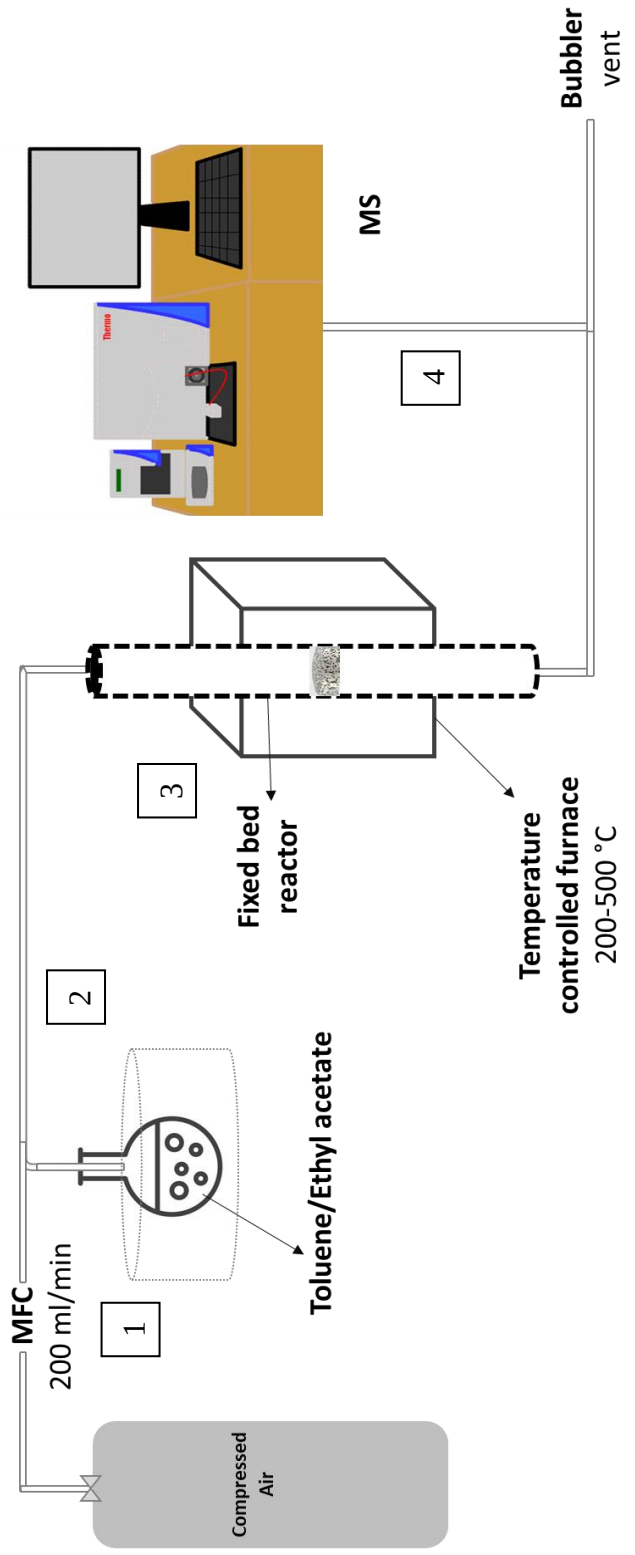

Figure 3.2. Schematic of lab scale rig used for catalytic testing of toluene

For ethyl acetate, the rig was modified slightly as vapor pressure data at different temperatures was not available. Instead of keeping it at lower temperatures, the saturated air was diluted with the aid of rotameters which is shown in Figure 3.3. The initial concentration of ethyl acetate at 25 °C was obtained by Sigma Aldrich as it was bought from there. A mixture of warm and cold water was used for water bath to maintain temperature of 25 °C. Compressed air was fed in to the round bottom flask containing ethyl acetate at 200 ml/min, the outlet was connected to Rotameter 1 (R_1) where the flow was reduced to 8 ml/min. This was diluted with 192 ml/min of compressed air coming in through Rotameter 2 (R_2).

Both the rotameters were separately continuously calibrated before every test. The calibration set up consisted of the outlet of the R_1 being connected to the inlet of a pipette, a mixture of soap and water were placed at the bottom of the pipette and the speed at which it travelled 10 ml was taken. The measurements were repeated 5 times and an average was taken to calculate the flow rate. Consistent readings were observed during calibrations therefore further confirming the consistency of rotameters. MFC were also used once to confirm the flow rates as rotameters readings can potentially fluctuate. There were no fluctuations in the measurements which indicated that the flow rates were constant.

Apart from the addition of rotameters, heating tape was wrapped around all lines which contained air with ethyl acetate. This was to avoid condensation of ethyl acetate in lines. The heating tape were kept at 60 °C as this was the lowest operating temperature. Flow rate of a 100 ml/min was also used for ethyl acetate to ensure the signal does not change with an increase of flow rate. Consistent signal was observed at all times in this case. Finally, a few different concentrations of ethyl acetate were calibrated however, the total concentration of 7275 ppm was used for catalytic testing.

The rest of the rig system was the same as toluene. The ethyl acetate contaminated air entered the quartz reactor. Blank experiment with and without quartz wool were first carried out followed by using stainless steel foams as catalysts. The ramp rate of 10 °C/min was used and 50 °C increase was used from 25 °C. In this case, the temperature was firstly increased to 50 °C from 25 °C and then to 100 °C, 150 °C

etc until 400 °C. The highest temperature of 400 °C was chosen because ethyl acetate has an autoignition temperature of 427 °C. The catalytic activity was monitored using mass spectrometer. CO_2 was the main oxidation product which was quantified.

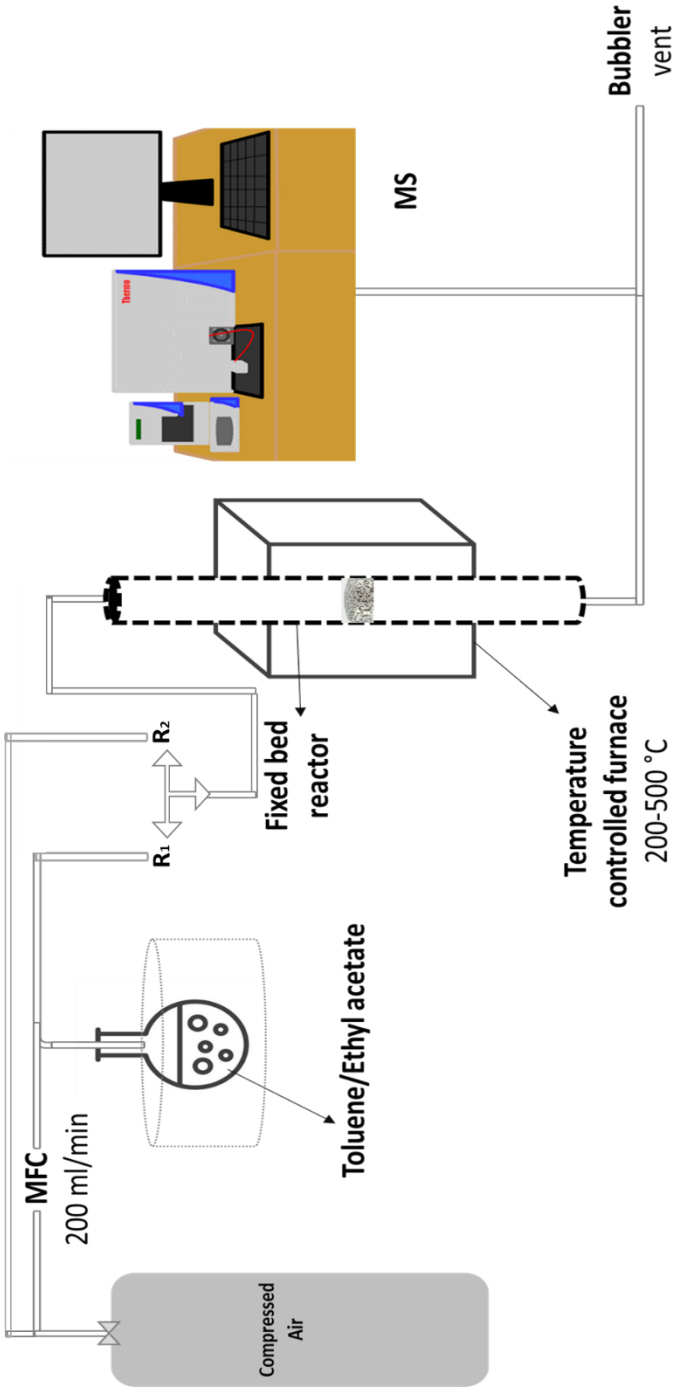

Figure 3.3. Schematic of lab scale rig used for catalytic testing of ethyl acetate

3.5 Scanning Electron Microscopy

After being calcined, the resulting metal oxide layer formed on the surface was analysed using SEM analysis and the elemental composition of the foams was characterised using EDS.

The morphological and chemical characterisation of the foams have been carried out via microscopy analysis using a SEM (Jeol JSM-5600), coupled with Energy Dispersive X-Ray detector. For this work, the SEM-EDS analysis was carried out with JSM 5600 for analysis of the SS foams. For EDS, the working distance of ~20 mm, 20 kV accelerating voltage and different image magnifications were used. The penetration depth was 1.6 µm for 20 kV accelerating voltage. The FEG SEM JSM 6700F was used for the purpose of monitoring morphological changes in spinel oxides. Generally, the working distance of 8 mm and 5 kV accelerating voltage were used for imaging. The foam/powder was placed on a carbon tape stuck on a stub which was placed in the specimen holder of SEM. No prior sample preparation was required for any of the samples.

3.6 Sessile drop technique

Contact angles between the solid substrate and the liquid solution are a good way of determining the extent of wetting of the solution on the substrate. This experiment is useful in calculating the interaction between the substrate and the solution which, in case of porous materials is very useful. The experiment can not be conducted on the porous medium therefore, SS disks were used. Due to the unavailability of the SS 314 disks, SS 316 disks were used instead. Both the SS 314 and SS 316 have a very similar elemental composition therefore, the results obtained would be representative of the SS 314. Solutions of different metal nitrates mentioned earlier in section 3.2.2 were prepared. Both raw and pre-oxidised samples were compared to see which one has the lower contact angle and thus, subsequently, better wetting of the substrate. The contact angles measured using a basic set up consisting of a substrate on a flat surface, a pipette to place the liquid drop on the substrate and a camera, to capture the angle as the liquid droplet sits on the surface. The measured angles were analysed using Image J software.

3.7 X-ray diffraction

For the course of this project, XRD analysis was carried out on PANalytical Empyrean diffractometer at room temperature with Cu $K\alpha_1$ radiation. 2θ range of 10-100 ° was used for scanning with dwell time of 1 hour.

3.8 Mass spectrometry

Cirrus mass spectrometer equipped with a quadrupole detector was used monitor the catalytic performance of the catalysts. The scan rate of 500 ms was kept constant throughout all experiments. In order to obtain quantitative analysis, the mass spectrometer was calibrated against known amount of concentrations to find the relative abundance which can then be used to monitor reaction quantitatively. For the catalytic testing, Cirrus mass spectrometer was calibrated with the main oxidation product, CO_2 (g). The calibration was carried out by introducing various different concentrations of CO_2 into the mass spectrometer, each known concentration gave a respective signal. The concentration was plotted against the signal of mass spectrometer, the straight-line equation (3.1)

$$y=mx+c \quad \textbf{(Equation 3.1)}$$

was used to work out the amount of CO_2 produced depending on the signal obtained from the test reactions. This calibration was repeated after every test to make sure that the results obtained were still representative and nothing had changed inside the mass spectrometer to cause a change in signals. The mass spectrometer was also baked in inert gas after every test to that any residuals from previous tests were not present in the next experiment.

Each material was tested at the temperature range of 200-500 °C for toluene and 50-400 °C for ethyl acetate. 10 °C/min was used as a standard ramp rate, 30 mins dwell time was kept consistent and 50 °C step rate was used for all experiments conducted. An average of the data obtained for the 30 mins dwell time from mass spectrometer was used to calculate catalytic activity and selectivity.

Characterisation and catalytic testing of SS 314 foams

4.1 Overview

In this chapter, stainless steel 314 foams have been modified *via* oxidation and/or impregnation treatments. The raw, oxidised or impregnated foams were tested for the conversion and oxidation of toluene at temperatures up to 500 °C in a lab scale rig with a fixed bed reactor. The gaseous products from the catalytic testing were monitored using a MS. The as prepared and post-testing foams were characterised using SEM analysis and EDS analysis to evaluate changes in morphology and elemental composition. EDS instrumental error was of +/- 2-3 %. For the elemental composition, O content will not be considered for quantification purposes as it is well known that O content in SEM-EDS analysis is not accurate. The error due to the presence of oxygen on the surface has been calculated using equation 4.1. The error was added in to the initial metallic atomic % which has been discussed.

*(Metal atomic % / Total of metallic content) * Oxygen atomic %*

(**Equation 4.1**)

4.2 Characterisation of SS 314 raw foam

Figure 4.1a show a low magnification SEM micrograph of the raw SS 314 foam. This foam consists of polyhedral open cells which are interconnected with solid struts and windows. The cell size of the foam investigated was 20 ppi linearly and there was no measurable surface area. The raw SS 314 has ~95 % porosity which makes it a highly porous material. According to the metallic EDS analysis in Figure 4.1b, the foam was rich in Fe (54 %), Cr (26 %) and Ni (20 %). This was the expected composition according to the theoretical composition of the 314 stainless steel and was also confirmed by the ICP-MS analysis.

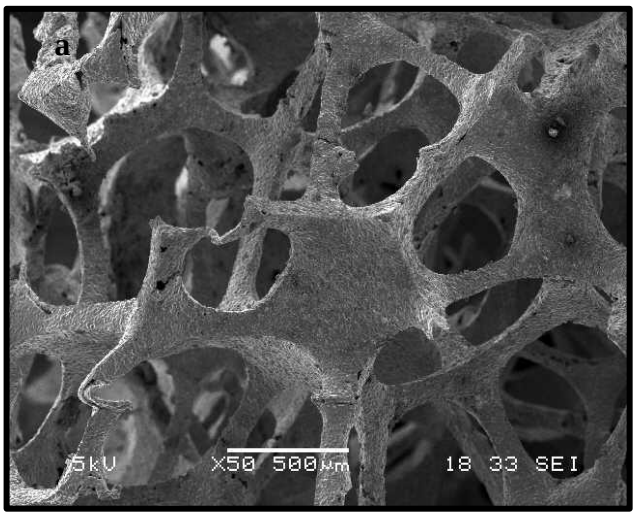

b

Element	Atomic %
Cr K	26
Fe K	54
Ni K	20
Total	100

Figure 4.1. SEM micrograph of (a) Raw SS 314 foam and (b) Elemental composition of this foam

Figure 4.2 reveals a closer look at the foam with the elemental mapping. It can be seen that the SS 314 raw foam being investigated had a very smooth surface with large grain sizes and well define grain boundaries. According to the metallic EDS mapping, Fe, Cr and Ni were present throughout the foam.

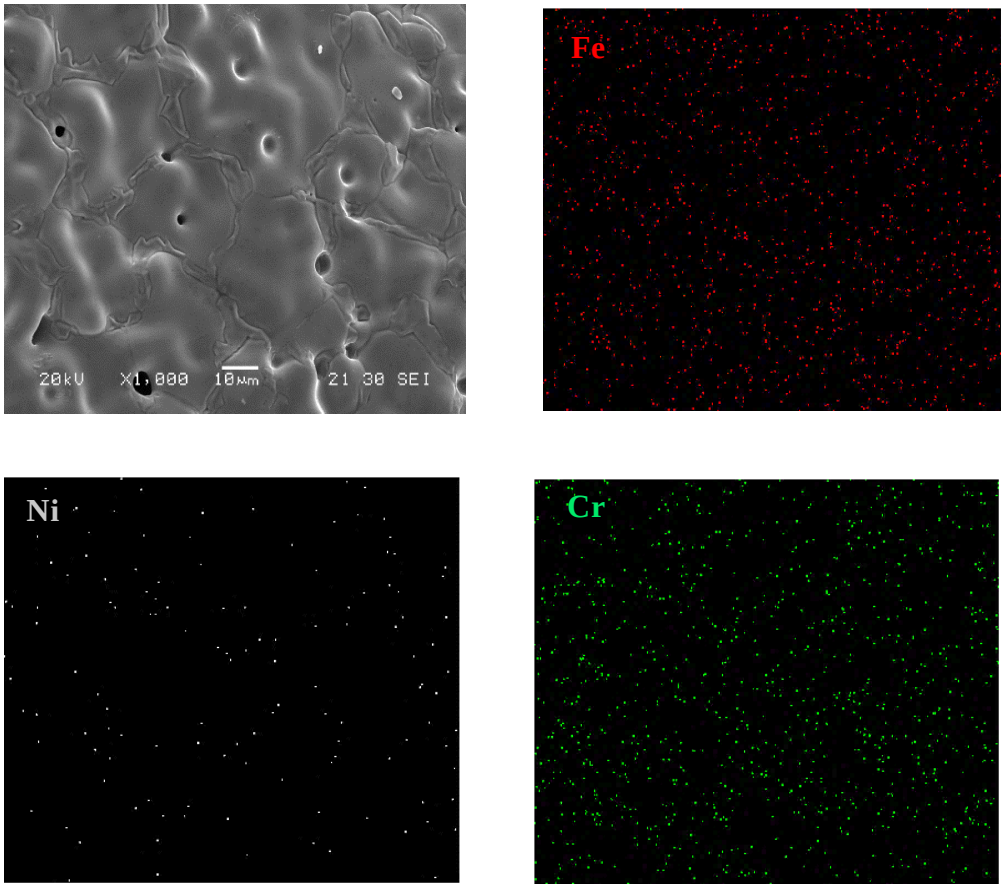

Figure 4.2. Raw SS 314 at high magnification with its EDS mapping of Fe, Ni and Cr

Previous work on this foam suggested that due to its smooth surface, the raw SS 314 foam lacks ability for metal nitrate impregnation. It was suggested that an increase in surface roughness can be obtained when the foam is oxidised in static air [121]. The oxidation step is more likely to create defects on the surface which result in better impregnation. Keeping this mind, the foams were first oxidised and then studied for the impregnation. The oxidation treatment to create defects has been summarised in the next section.

4.3 Modification on SS 314 foams

4.3.1 Oxidation treatment of SS 314 foam

In this work, a series of oxidation temperatures and dwell times were tested for their effects on the morphology and composition of the SS 314 foam. The first oxidation temperature and dwell rate tested was obtained from previous work with SS 314 [121,129]. Previous work on this foam suggested that the optimal surface morphology for SS 314 is obtained when the weight increase after oxidation of the raw foam is approximately 5 weight (wt.) % and a mixed metal oxide rich layer is formed at the surface of the foam. Previously, the oxidation step was carried out in order to increase surface roughness of the foam so that it became easier for it to be impregnated. This has been achieved in the past by oxidising the sample at 900 °C for 20 hours [121]. SS 314 was therefore oxidised at 900 °C for 20 h, the weight gain (34 %) in this case was seen to be a lot higher than the one previously reported. The foam also became very brittle after being treated at 900 °C for 20 hours. A high temperature can cause stainless steel foam to turn brittle as oxidising the foam creates defects to occur within the SS structure. These defects reduce the metal strength resulting in embrittlement [148].

In an attempt to keep the foam intact and still obtain an oxide rich layer on the surface, the raw SS 314 was oxidised at 600, 750 and 900 °C at different dwell rates. Table 4.1 summarises the increase in weight % obtained at respective dwell time and temperatures.

Table 4.1. Total weight increase (%) obtained with oxidation pre-treatment at different temperatures and dwell times evaluated

	Weight Increase (%)		
Dwell time (h)	**600 °C**	**750 °C**	**900 °C**
0		2	9
1	0.1	5	11
2	0.1	8	11
20	-	-	34

The first assumption of the brittle nature was attributed to the dwell time of 20 hours rather than the temperature. Much lower dwell rates of 0, 1 and 2 hours were then tested. Figure 4.3a shows that although the morphology of the foam showed an increase in surface roughness specifically when treated at 900 °C for 1 hour, the core smooth structure of the foam appeared to have been lost. According to the EDS analysis (Figure 4.3b), an oxide layer had formed on the surface of the foam. The O content had increased compared to the raw SS 314 sample, and the layer formed was rich in Fe mainly. At higher temperatures, the most common oxide of Fe is Fe_2O_3. Presence of Cr and Ni was also observed. The foams were treated at no dwell time at 900 °C in a final attempt to have an intact SS 314 structure at 900 °C however, the foams were still brittle making them unideal to be used for any application.

a

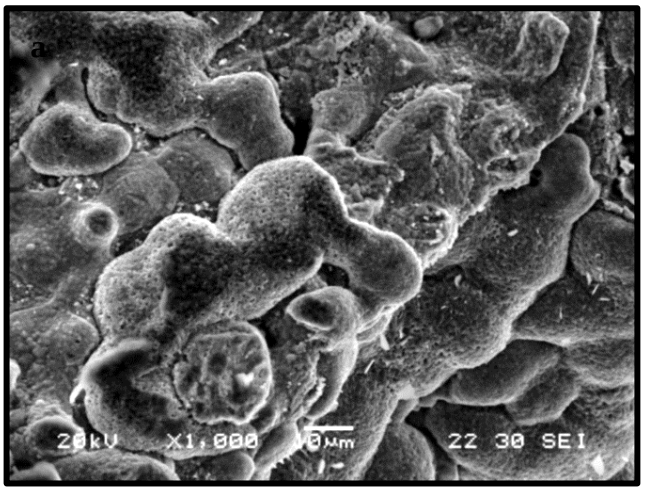

b

Element	Atomic %
Cr K	17
Fe K	76
Ni K	7
Total	100

Figure 4.3. SEM micrograph of (a) oxidised SS 314 foam at 900 °C for 1h and (b) the elemental composition of this foam

After looking at the different dwell times at 900 °C, it was established that the lack of mechanical of stability of the foam was not only because of the long dwell time but also, because of the temperature. The oxidation temperature was causing the core structure to breakdown making it brittle which decreased the durability of the foam and therefore makes it inadequate for catalytic applications.

Therefore, a lower oxidation temperature of 600 °C was chosen with 1-hour dwell time as a starting point. The weight increase in this case was too low hence, 2 hours dwell time was tested which gave the same result (Table 4.1). Figure 4.4a represents

the surface morphology of the foam oxidised at 600 °C for 1 h which was very similar to that of the raw SS 314 foam (Figure 4.2). Upon oxidation, an increase in presence of O could be seen however, oxidising at 600 °C had not caused a thorough rough oxide layer to be formed at the surface. EDS mapping was used to see elemental distribution of the foam. Figure 4.5 reveals that the SS 314 oxidised at 600 °C had a similar trend to that of the observed in the case of raw foam (Figure 4.2). Fe, Cr, Ni and O were seen to be evenly distributed throughout the foam.

a

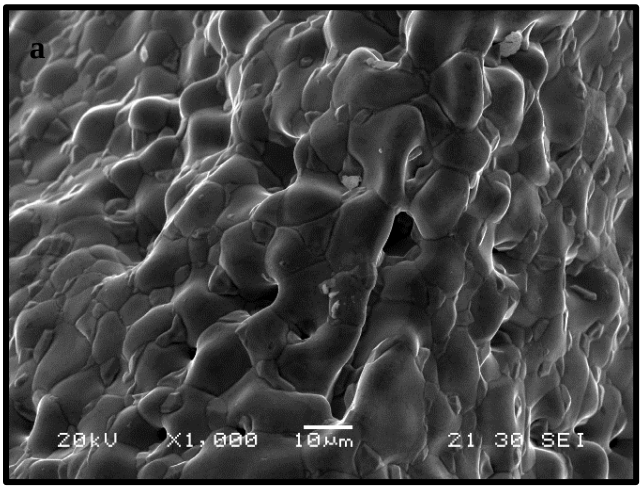

b

Element	Atomic %
Cr K	15
Fe K	71
Ni K	14
Total	100

Figure 4.4. SEM micrograph of (a) SS 314 oxidised at 600 °C for 1 h and (b) the elemental composition of this foam

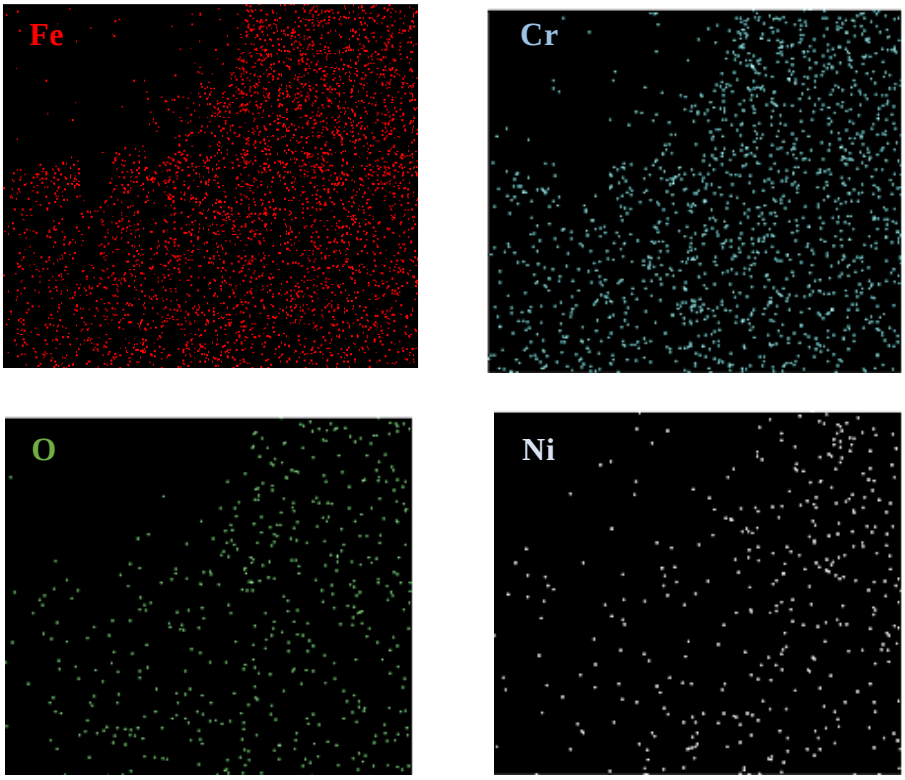

Figure 4.5. EDS mapping of Fe, Cr, O and Ni for SS 314 oxidised at 600 °C for 1h

According to the previous work on SS 314, the mixed oxide formed with 5 wt. % increase gives enough surface roughness for impregnation of metal nitrates [121, 129]. The composition of the oxide layer is dependent upon temperature, if the temperature or dwell times are too high then instead of having a mixed oxide layer on the surface, the oxide layer would be selective towards certain elements therefore, it was important to keep the 5 wt. % loading in mind in selecting the potential SS 314 substrate for impregnation. The increase in dwell time at 600 °C did not show any positive outcome, instead of increasing dwell time at 600°C, an intermediate temperature of 750 °C was chosen to be tested to form a rougher surface. Dwell time of 2 hours was first tested, in this case, the weight % increase (8 %) was somewhat closer but higher than the expected range (Table 4.1) and the foam remained intact. Keeping 750 °C as the temperature, the foams were studied further at 0- and 1-hour dwell times. Weight increase was lower (2 %) with no dwell. Finally, a 5 weight % increase was obtained when the SS 314 was oxidised

at 750 °C for 1 hour. Alongside the required increase in wt. %, the foam oxidised at 750 °C also had an increased roughness on the surface. Figure 4.6a represents the morphology of the SS 314 ox_750 °C, the foam still had smoothness however, most of it was covered with a rough layer in some regions. EDS analysis revealed presence of Fe, Cr and O mainly, similar to that of the SS 314 ox_600 °C (Figure 4.4b**)**. Lower content of Ni was observed in this case, Ni, at this temperature was being masked by Fe and Cr forming the oxide layer. The elemental composition except oxygen content, this sample was closer to that of the sample oxidised at 900 °C (Figure 4.3b). The foam oxidised at 750 °C for 1 h gave an optimal surface roughness for it to be used as a substrate for impregnation.

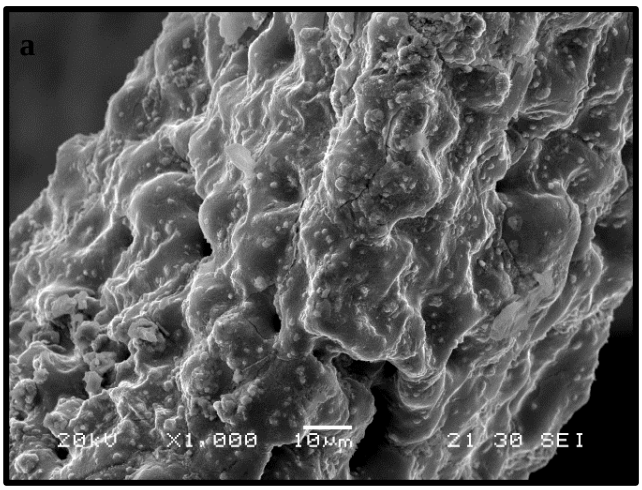

b

Element	Atomic%
Cr K	15
Fe K	82
Ni K	3
Totals	100

Figure 4.6. SEM micrograph of (a) SS 314 oxidised at 750 °C for 1 h and (b) the elemental composition of this foam

Figure 4.7 summarises the elemental analysis of Fe, Cr and Ni only (without O) on the raw and oxidised and samples discussed earlier, it can be concluded that the foam oxidised at 750 °C had the highest concentration of Fe (Figure 4.4) on the surface. The oxide layer formed on the surface after the foam was oxidised at 750 °C for 1 hour was high in rich in Fe and Cr only compared to other oxide layers which were rich in Fe, Cr and Ni when oxidised at 600 or 900 °C.

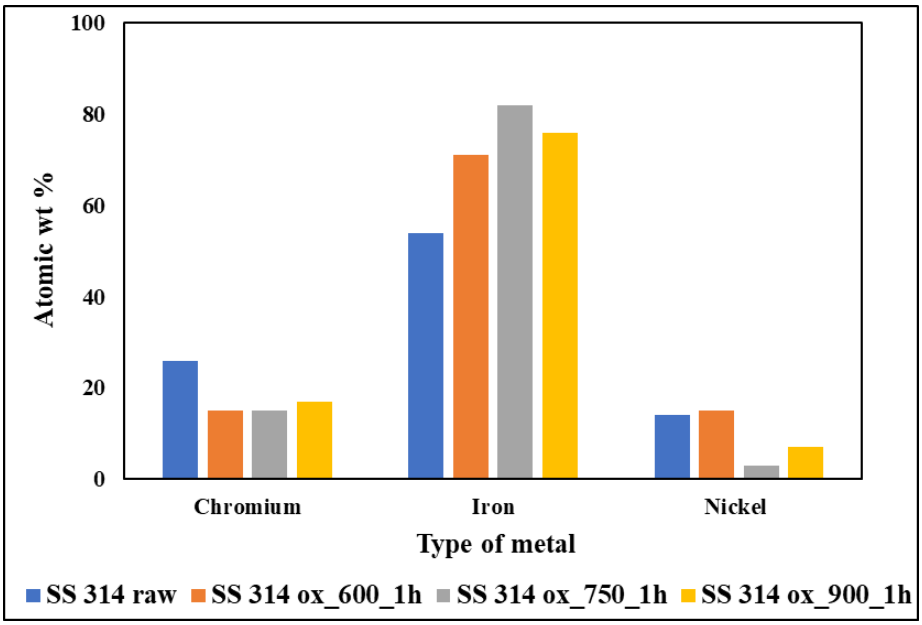

Figure 4.7. Comparison of elemental analysis of raw and oxidised foams

Overall, the oxidation process had been successful in forming an oxide layer on the surface of the SS foams. The rough surface obtained with the oxidation treatment should allow for a better metal loading *via* impregnation which will be discussed in the next section. Alongside being used as a substrate for impregnation, SS 314 oxidised at 750 °C for 1h could also be tested for catalytic process itself which would also be discussed in the later sections. The chosen impregnations were based on previous work which has been discussed in the Introduction chapter, section 1.6.1. To summarise, metal oxides have been known to be good oxidation catalysts, amongst the rest of them; Fe, Cr, Ni, Mn, Cu, Ce oxide are cheap and effective oxidation catalysts [149]. Fe and Mn oxides were chosen to be impregnated on SS 314 foams.

4.3.2 Impregnation of metal nitrates on SS 314 foams

The SS 314 foams were impregnated with different metal nitrates *via* dip coating to form a metal oxide rich layer on the surface of the foam. The following experimental parameters were modified during the process of dip coating:

- Type of substrate
- Solution composition
- Number of coatings
- Metal nitrate concentrations

4.3.2.1 Influence of substrate

In order to find the best substrate for impregnation, three types of foams, SS 314 raw, ox_600_1h and ox_750_1h were initially dip coated with 0.1 M iron (III) nitrate solution in ethanol only. Samples treated at 900 °C were not used for further testing as the foams became very brittle upon oxidation.

The metal loading (wt. %) after calcination has been summarised in Table 4.2**.** As it can be seen, the metal loading was lower than 1 wt. % regardless of the substrate used. The SS 314 ox_600_1h and SS 314 ox_750_1h samples slightly had more metal oxide loading (%) compared to the SS 314 raw sample. The pre-oxidised samples were expected to load better due to their surface being rougher than the raw foam, the increased roughness increases the surface area hence resulting in slightly more loading.

Table 4.2. Metal oxide loading (wt. %) on different SS 314 foams impregnated with Fe nitrate (0.1 M) in ethanol after calcination

Substrate	Metal oxide loading
Raw SS314	0.24 wt. %
SS314 ox_600_1h	0.31 wt. %
SS314 ox_750_1h	0.43 wt. %

Figure 4.8a shows a representative micrograph of SS 314 raw impregnated with 0.1M Fe nitrate solution (SS 314 raw 0.1M_E). Some areas of the foam remained

smooth whilst others were seen to be breaking into flakes. The small pores embedded within the raw structure had formation of cracks. Overall, a very small amount (0.24 %, Table 4.2) of increase was obtained therefore a very small change in the morphology was observed. There were two different regions which were separately chosen for EDS point analysis. Both regions had a similar elemental composition, both regions were rich in Fe and Cr (Figure 4.8b and 4.8c). Raw SS 314 foam had 54 % Fe content and after impregnation, this had increased to 76 %. The Cr content of 26 % had slightly decreased to 24 % which was still within the instrumental error of SEM. After being impregnated, Ni was not detected by the SEM. The increase in Fe and O content indicated that the SS 314 raw_0.1M_E sample was successful in coating small amount of Fe oxide on the surface. Though there was a very slight increase in the metal oxide wt. % loading (Table 4.2), there was still a change in the morphology and the overall metallic composition of the foam.

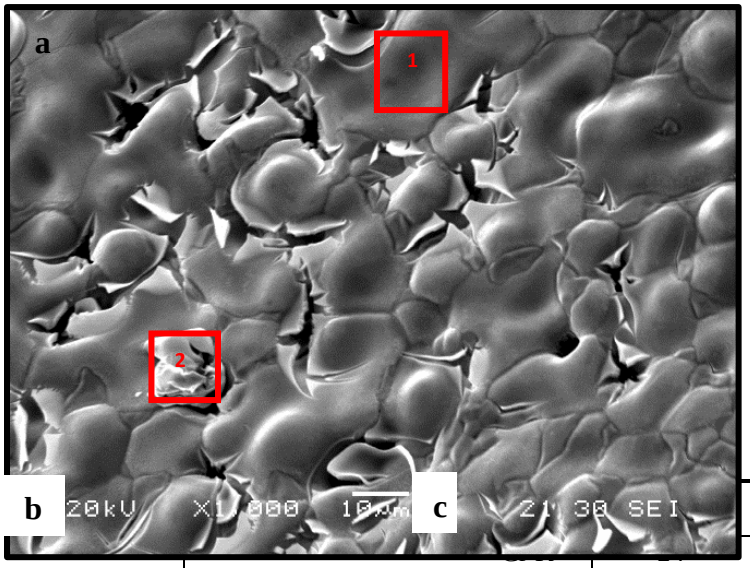

Figure 4.8. SEM micrograph of (a) SS 314 raw 0.1M_E sample and (b) EDS of point 1 and (c) EDS of point 2 of this sample

Figure 4.9a represents the morphology of SS 314 oxidised at 600 °C for 1h impregnated and calcined with 0.1M Fe nitrate solution (SS 314 ox_600_0.1M_E). This foam had an interesting morphology, again two different regions were chosen for EDS point analysis. The bottom layer of this sample was smooth, and the impregnated layer had been formed in form of chunks, the impregnation was scattered on the surface rather than being evenly distributed. The smooth surface (Figure 4.9b) had a similar metallic composition to that of the SS 314 ox_600 sample (Figure 4.3b) in terms of the presence of Fe, Cr and Ni. The Cr (17 %) content had remained the similar after impregnation however, Ni (3 %) had decreased and an increase in the Fe content to 80 % compared to 73 % was observed. The bottom layer had similar morphology and elemental composition to that of the substrate (SS 314 oxidised for 1h). The impregnation resulted in the formation of top layer which had an increased amount of Fe (83 %) and decreased amount of Cr (15 %) Figure 4.9c). Ni was not observed in the top layer.

a

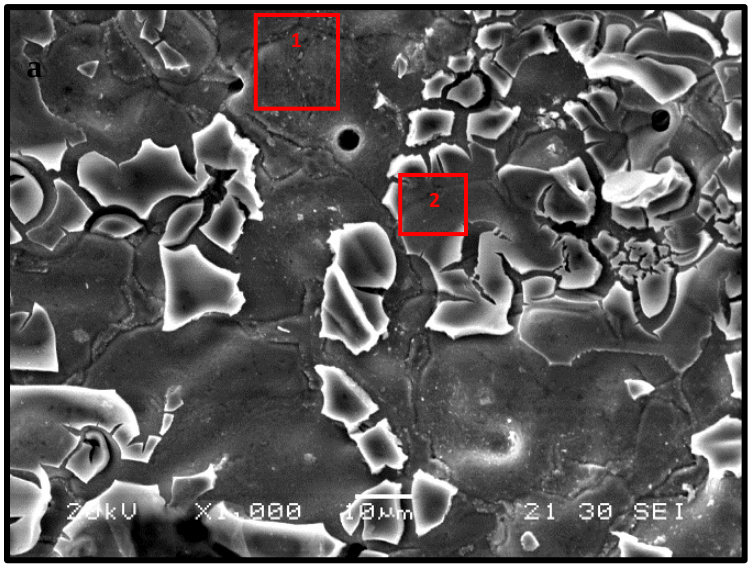

b

Element	Atomic %
Cr K	17
Fe K	80
Ni K	3
Total	100

c

Element	Atomic %
Cr K	15
Fe K	85
Total	100

Figure 4.9. SEM micrograph of (a) SS 314 ox_600_1h_0.1M_E sample, (b) EDS of point 1 and (c) EDS of point 2 of this foam

Figure 4.10 represents SS 314 oxidised at 750 °C for 1h followed by impregnation with 0.1M iron nitrate solution (SS 314 ox_750_1h_0.1M_E). It can be seen in Table 4.2; this sample had a higher loading of wt. % compared to previously tested substrates. The impregnation had worked better with the SS 314 ox_750_1h sample as more coverage on the surface was observed. The morphology was somewhat similar to that of the SS 314 ox_600_0.1M_E sample (Figure 4.9a) as the top layer observed under SEM consisted of chunks of impregnated material however, in this case the top layer was more evenly distributed than the previous sample so the coverage was better. Some of the pre-oxidised substrate was observed after the impregnation which indicated that the substrate was successful in anchoring metal nitrates on itself. The substrate and the impregnated regions were chosen for EDS point analysis and are shown in Figure 4.10b and 4.10c respectively. The EDS metallic composition (Figure 4.10b) of the substrate was similar to that of the SS 314 ox_750 sample (Figure 4.4) in terms of its Fe (81 %), Cr (15 %) and Ni (4 %) content. The impregnated layer was heavily rich in Fe (91 %) indicating a successful impregnation of Fe oxide on the surface had occurred.

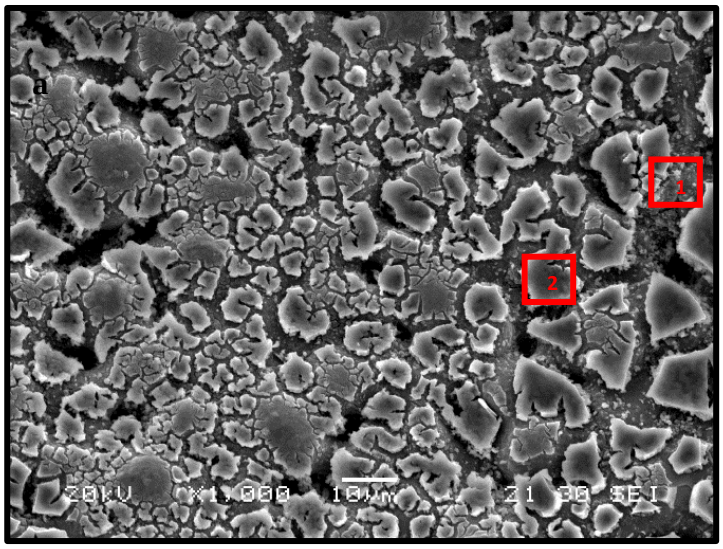

b

Element	Atomic %
Cr K	15
Fe K	81
Ni K	4
Total	100

c

Element	Atomic %
Cr K	9
Fe K	91
Total	100

Figure 4.10. SEM micrograph of (a) SS 314 ox_750_1h_0.1M_E sample, (b) EDS of point 1 and (c) EDS of point 2 of the sample

After doing some initial changes in type of substrates used, it was clear that the peroxidised sample, specifically the sample oxidised at 750 °C for 1h was a better substrate for impregnation as compared to the one oxidised at 600 °C for 1h or the raw sample. The SS 314 ox_750_1h sample had increased metal wt. % loading (Table 4.2) and had better surface coverage (Figure 4.10a). Though the morphology of the foam showed positive outcome, the overall wt. % loading was lower than the target therefore further modifications were required. Prior to making any further modifications, wetting experiment was conducted to investigate whether the difference of morphology or loading observed on unoxidised or oxidised samples could be explained using contact angles. For this, only the unoxidised (raw) and sample oxidised at 750 °C_1h were chosen, oxidation at 600 °C was not investigated any further as it was decided to use the best and worst sample for wetting experiments.

4.3.3 Wetting experiment

Wetting experiments were chosen as a mean to calculate the interaction between the substrate and the solution. Information obtained from this experiment can be useful in explaining why certain substrates have better coverage than others. For the purpose of this project, SS disks were used as substrate representatives as foams were not suitable to be used due to their high porosity. Due to the unavailability of the SS 314 disks, SS 316 disks were used instead. Both the SS 314 and 316 have very similar chemical composition therefore, the results obtained were representative of the SS 314. Contact angle was used as a measure of explaining the spread of solution on substrate. The contact angle between a substrate and a solution gives an indication of how a liquid will spread over a surface. In the case of porous materials, wetting experiment conducted on a non-porous medium representative of it is a useful indication of how well the solution will spread through the pores of the materials rather than agglomerate at one spot. The lower the contact angle, the better the solution will spread and therefore the higher the wettability of the material. Keeping this in mind, contact angles were measured using sessile drop technique. Water was used as a starting point to test contact angles. Figure 4.11a shows that the SS 316 raw disk has a higher contact angle compared to the oxidised sample. This meant that the oxidised material had better wettability compared to

the unoxidised/raw material. Lower contact angle suggested better wetting which meant that the solution was more likely to spread through the pores of oxidised material compared to the raw material.

An attempt was made to measure contact angles between the SS 316 disks and the 0.1M iron nitrate solution. Figure 4.11b shows that the raw SS 316 disk had a higher contact angle compared to the oxidised disk confirming that the raw SS 316 disk obtained a poorer wetting compared to the oxidised material. In the previous section, it was found that the impregnation was better on the pre-oxidised sample and the reason behind this was due to the contact angle being lower when the sample is oxidised.

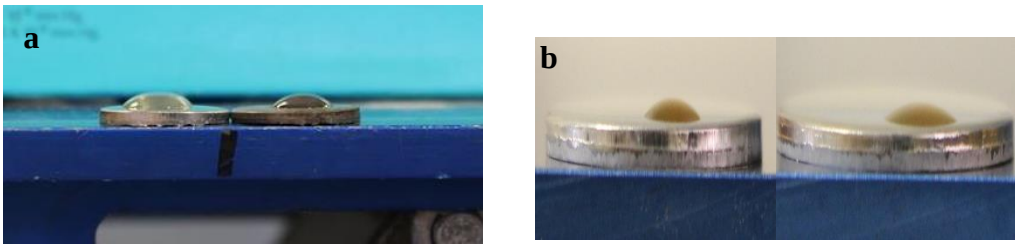

Figure 4.11. Measurement of contact angle using sessile drop technique with (a) water on raw SS 316 disk on the left and oxidised SS 316 disk on the right and (b) 0.1M iron nitrate solution used for impregnation on raw (left) and oxidised (right) SS 316 disks

The wetting experiment was useful in knowing that the pre-oxidised sample were more likely to have homogeneous surface coverage compared to the raw surface. After looking at the wetting behaviour of the substrates, further modifications were carried out in an attempt to increase homogeneity on the oxide layer and to improve the overall metal oxide wt. % loading. For this, solution composition was modified next.

4.3.4. Influence of solution composition

The next set of experiments were carried out on SS 314 raw and SS 314 pre-oxidised at 750 °C for 1 hour. The previous surface morphological investigation of the SS 314 foams showed that the foams lacked homogeneity regardless of the pre-treatment. The metal oxide wt. % loading with ethanol only as a solvent was not high enough therefore further modifications were made to increase metal oxide wt. % loading and improve surface coverage of the foams. In this attempt, both raw and pre-oxidised sample were dipped in an ethanol and terpineol (3:1 by volume) based solution. It was expected that the addition of terpineol would increase the viscosity of the solution which in turn would increase the metal oxide loading. Table 4.3 summarises the impact of the addition of terpineol. This addition increased the metal oxide loading on both the raw SS 314 and SS 314 ox_750_1h samples achieving values of 0.91 and 1.2 wt. % respectively.

Table 4.3. Metal oxide loading achieved on SS 314 raw and SS 314 ox_750_1h samples when using an ethanol: terpineol based solution

Substrate	Metal oxide loading
SS 314 raw	0.91 wt. %
SS 314 ox_750_1h	1.2 wt. %

Figure 4.12a shows representative micrograph of SS 314 raw sample impregnated with ethanol: terpineol 0.1M iron nitrate solution (SS 314 raw 0.1M_ET). With the loading being still low, it was expected that this sample would not have an even surface coverage. SEM revealed that addition of terpineol had resulted in formation of agglomerated chunks on the surface of the foam rather than a layer. The smooth surface of the SS 314 raw (Figure 1a) was still observable. Point id analysis of point 1 (Figure 4.12b) revealed that the metallic composition was similar to that of the SS 314 ox_750_1h sample (Figure 4.6b) as it consisted of Fe (73 %), Cr (15 %) and Ni (12 %). In the impregnated layer found at the top of the foam, only Fe and O were detected by EDS point id analysis as shown in Figure 4.12c, this denoted that

the impregnation was successful in producing an iron oxide rich layer on the surface.

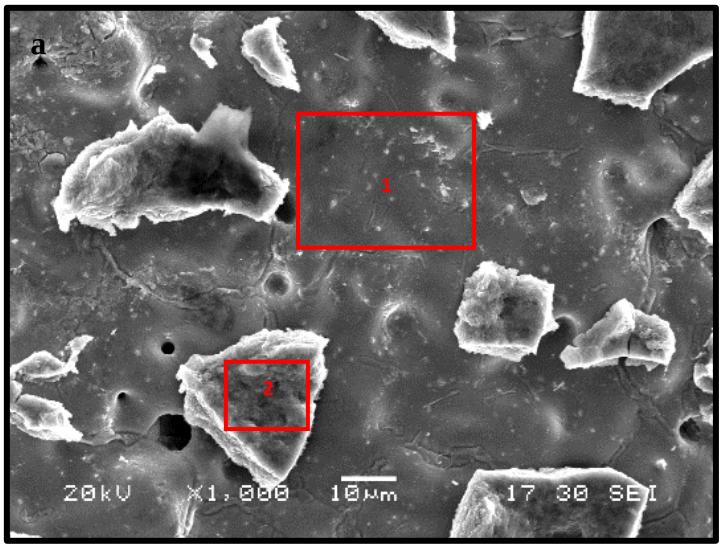

b

Element	Atomic %
Cr K	15
Fe K	73
Ni K	12
Total	100

c

Element	Atomic %
Fe K	100
Total	100

Figure 4.12. SEM micrograph of (a) SS 314 raw 0.1_ET sample, (b) EDS of point 1 and (c) EDS of point 2 if this sample

Figure 4.13a shows a representative SEM micrograph of the SS 314 oxidised at 750 for 1h coated with 0.1M iron nitrate solution with ethanol: terpineol sample (SS 314 ox_750_1h_0.1M_ET). The micrograph shows a drastic change in morphology compared to any other sample discussed earlier. The surface showed large agglomeration of particles with needle like structures deposited on the surface.

Interestingly in the smoother region **(**Figure 4.13b), the metallic composition was different to that of the SS 314 ox_750 as the Fe content of 78 % had now changed to 95 % and the Cr content of 19 % had decreased to only 2 % and Ni had dropped from 3 % to 1 %. As the EDS analysis revealed that the smoother region was also different to that of the substrate used, it meant that the results obtained were due to

a coverage of the impregnated layer. The needle like structures were high in O and Fe indicating presence of Fe oxide.

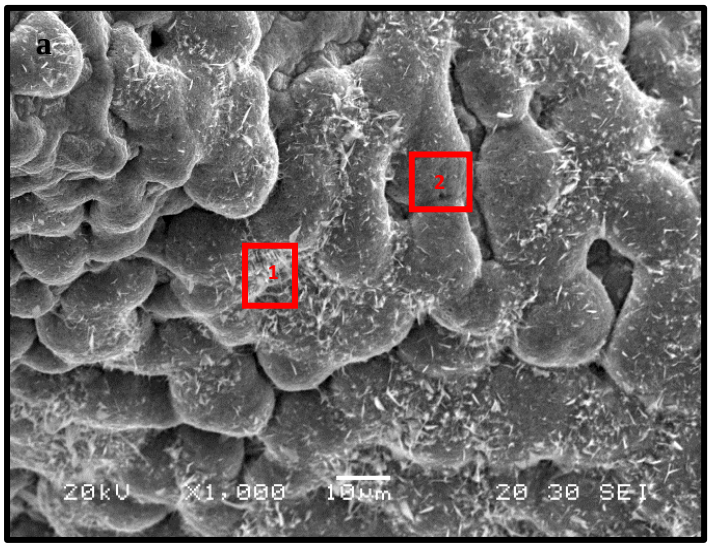

b

Element	Atomic %
Cr K	3
Fe K	96
Ni K	1
Total	100

c

Element	Atomic %
Cr K	2
Fe K	98
Total	100

Figure 4.13. SEM micrograph of (a) SS 314 ox_750_1h_0.1M_ET sample, (b) EDS of point 1 and (c) EDS of point 2 of this sample

Due to the lack of loading and homogeneity on the surface of the impregnated foams, another attempt was made to improve the surface morphology of the foams. In this case, the raw and 750 °C pre-oxidised foam were dip coated in a solution containing ethanol, terpineol and Polyvinyl Butyral (PVB) as a resin. The resin was added to further increase the viscosity of the solution which was expected to adhere a better impregnated layer on the surface of raw or pre-oxidised foams. The metal oxide loading (%) achieved for both substrates dip coated in this solution has been summarised in Table 4.4**.** It can be seen that there was no significant change in the wt. % increase after the addition of resin for the SS 314 raw sample, the loading had almost doubled in the case of the SS 314 ox_750_1h sample.

Table 4.4. Metal oxide loading (%) obtained with raw and oxidised samples impregnated with 0.1M iron nitrate solution in ethanol, terpineol and PVB

Substrate	Metal oxide loading
SS 314 raw	0.8 wt %
SS 314 ox_750_1h	2.0 wt %

Figure 4.14a is a representative micrograph of the SS 314 raw impregnated with 0.1M iron nitrate solution in ethanol, terpineol and PVB sample (SS 314 raw 0.1M_ETP). The surface of the foam resembled closely to that of the raw SS 314 (Figure 4.2) with unevenly agglomerated particles distributed on the surface of the foam.

In this case, three different regions were chosen for EDS point id analysis.in the first instinct by looking at the morphology only, it seemed that the impregnation had not worked very well and was perhaps only found on the agglomerated particle. However, upon looking at point 1 (Figure 4.14b) showing the Fe content to be of 85 %, Cr to be of 9 % and Ni to be of 6 %, it was clear that some iron oxide impregnation had occurred on the surface of the foam The thick grain boundaries (Figure 4.14c) consisted of Fe (78 %), Cr (9 %) and Ni (13 %) as shown in Figure 4.14c.. The high Ni content found on this region was not surprising, as it was also observed during EDS mapping of the SS 314 raw sample (Figure 4.2). The small agglomerated region was high in Fe and O only as shown in Figure 4.14d. The lack of homogeneity and agglomeration was observed in the previous case also with SS 314 raw 0.1M_ET sample (Figure 4.13a), this indicated that the addition of resin in this case did not have a positive impact on surface morphology of the SS 314 raw foam.

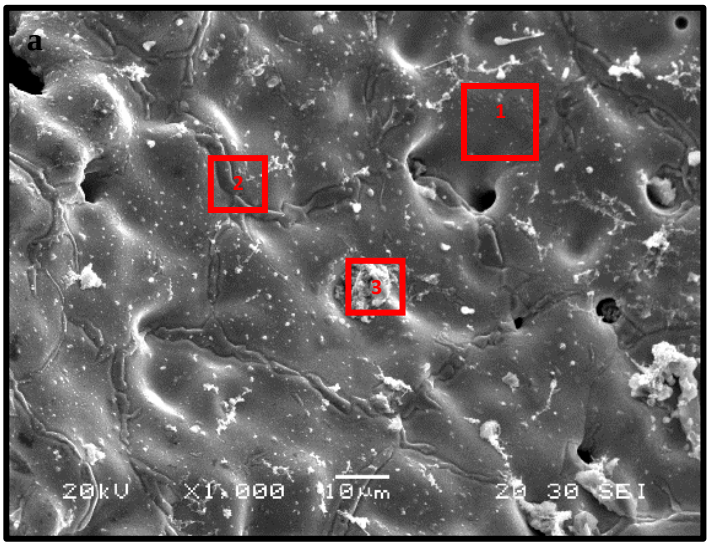

b

Element	Atomic %
Cr K	9
Fe K	85
Ni K	6
Total	100

c

Element	Atomic %
Cr K	9
Fe K	78
Ni K	13
Total	100

d

Element	Atomic %
Fe K	100
Total	100

Figure 4.14. SEM micrograph of (a) SS 314 raw_0.1M_ETP sample, (b) EDS of point 1, (c) EDS of point 2 and (d) EDS of point 3

After raw, SS 314 ox_750_1h was also impregnated under same conditions. Figure 4.15a shows the surface morphology of the SS 314 oxidised at 750 °C for 1h dip coated with 0.1M iron nitrate solution in ethanol, terpineol and PVB sample (SS 314 750_0.1M_ETP). A much better surface coverage compared to any of the previous attempts discussed earlier was obtained. Moreover, the wt. % loading (Table 4.4) was also a little higher than the SS 314 raw sample. Two separate regions were chosen for EDS point analysis. The metallic content of the smooth region was close to that of the peroxidised substrate (Figure 4.4b). The smooth region consisted Fe (86 %) oxide mainly with some Cr (10 %) and Ni (3 %) also

being observed as shown in Figure 4.15b. The impregnation had resulted in formation of agglomerated particles which were high in iron oxide (Figure 3.14c).

a

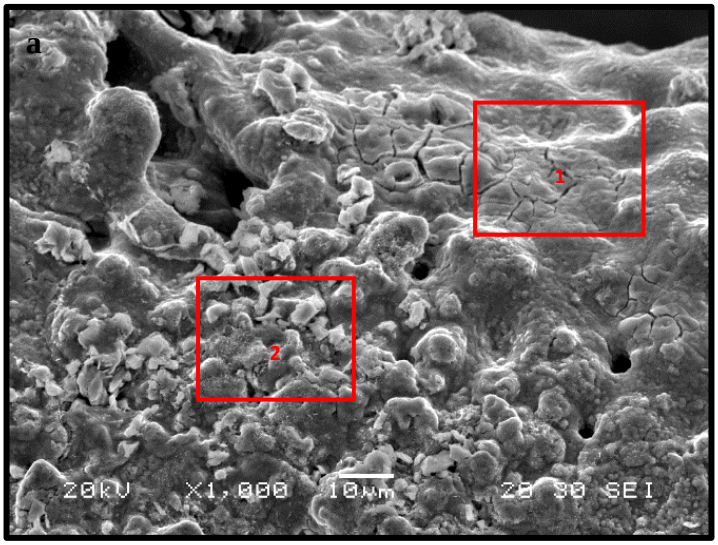

b

Element	Atomic %
Cr K	10
Fe K	86
Ni K	4
Total	100

c

Element	Atomic %
Cr K	6
Fe K	94
Total	100

Figure 4.15. SEM micrograph of (a) SS 314 ox_750_1h_0.1M_ETP, (b) EDS of point 1 and (c) EDS of point 2 of this sample

Despite an improvement in the surface morphology of the pre-oxidised foam, the loading was still not high enough and the morphology of the raw or pre-oxidised foams was not ideal to be used for catalytic testing. Therefore, to improve the metal oxide loading and homogeneity of the coating layer, a re-impregnating strategy was evaluated.

4.3.4.1 Influence of re-impregnating substrates

SS 314 raw 0.1M_ETP and SS 314 ox_750_1h_0.1M_ETP samples discussed previously were re-impregnated. The overall increase in metal oxide loading (%) has been summarised in Table 4.5. Reimpregnation resulted in a further increase of metal oxide loading (%).

Table 4.5. Total increase in metal oxide wt. % observed after being re-impregnated on raw SS 314 0.1M_ETP and SS 314 ox_750_1h_0.1M_ETP samples.

Substrate	Metal oxide loading after re-impregnating
SS 314 raw 0.1M_ETP	1.6 wt %
SS 314 ox_750_1h_0.1M_ETP	2.0 wt %

Figure 4.16a shows a representative of the re-impregnated SS 314 raw 0.1M_ETP sample (SS 314 raw 0.1M_ETP_RC). This morphology was similar to that of the one observed with SS 314 raw 0.1M_ETP sample (Figure 4.14a). The impregnation on top layer was scattered on different regions and the rest of the surface of the foam still looked smooth. Both of these regions were chosen for EDS point analysis. This metallically high in Fe (74 %), Cr (17 %) and Ni (9 %) which was similar to that observed in the case of the single coated sample (Figure 4.14b). The unevenly distributed top coating on the surface of the substrate shown in Figure 4.16c scattered impregnated region consisted of Fe (93 %) oxide mainly.

Re-impregnation was expected to bridge the uneven agglomerated chunks of metal oxides seen deposited on the surface of the single coat sample (Figure 4.14a). However, this was not seen to be the case. One possible explanation could be that the new layer agglomerated on top of the previous chunks instead of spreading homogeneously.

a

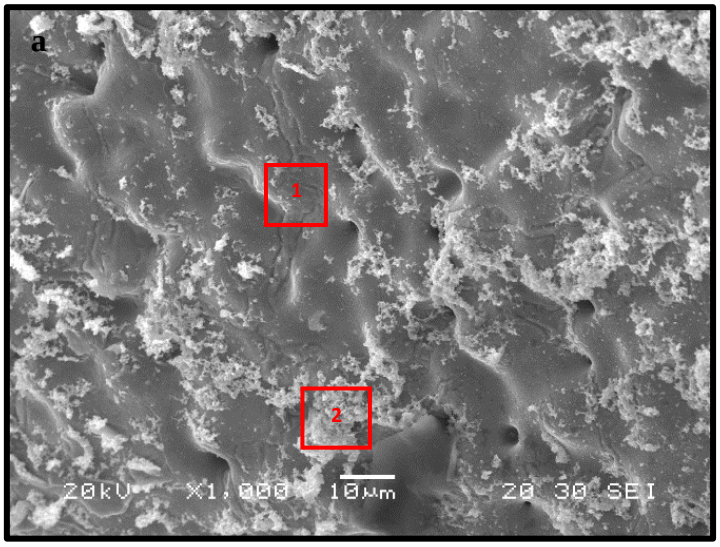

b

Element	Atomic %
Cr K	17
Fe K	74
Ni K	9
Total	100

c

Element	Atomic %
Cr K	7
Fe K	93
Total	100

Figure 4.16. SEM micrograph of S 314 raw 0.1M_ETP_RC sample, (b) EDS of point 1 and (c) EDS of point 2 of this sample

SS 314 750_0.1M_ETP sample was also re-impregnated in order to improve loading and homogeneity in the sample. The increase in this case again (Table 4.5) was not satisfactory. Figure 4.17a is a representative of the SS 314 ox_750_0.1M_ETP re-impregnated with the same ETP solution. The SEM analysis revealed presence of rough regions, chunks of impregnated layer and agglomerated regions randomly scattered on the surface of the foam. All three of these regions were chosen for EDS point analysis. After being re-impregnated, Ni had disappeared from the elemental point analysis in all three regions (Figure 4.17b, c and d). The smooth region had a higher Fe (92 %) content compared to the previous attempt (Figure 4.15b). The chunks also had high Fe (89 %) content and finally, the agglomerated region had the highest content of Fe (97 %). The new impregnated layer in this case had spread better than previous attempts as Cr present in the elemental analysis (Figure 4.17b, c and d) overall (5 % average) was less than seen

previously (Figure 4.15b and c). The nature of SS foam makes it harder for the metal nitrates to be displaced on the surface homogenously therefore, agglomeration was seen in some regions of the foam.

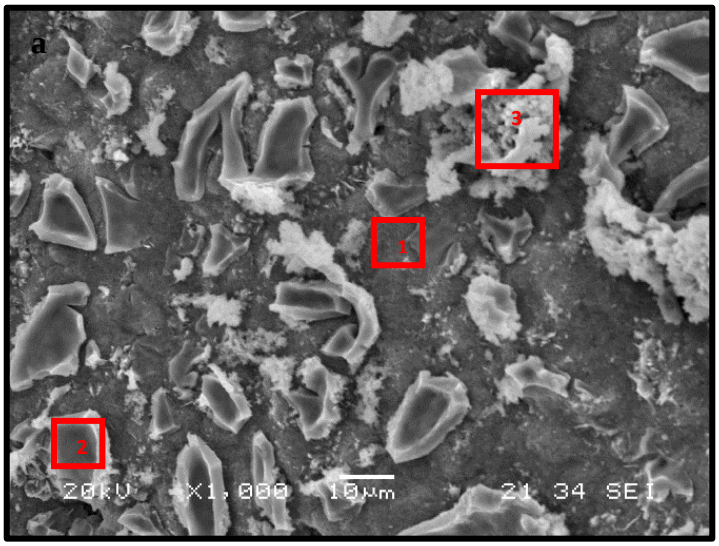

b

Element	Atomic %
Cr K	8
Fe K	92
Total	100

c

Element	Atomic %
Cr K	11
Fe K	89
Total	100

d

Element	Atomic %
Cr K	3
Fe K	97
Total	100

Figure 4.17. SEM micrograph of (a) SS 314 ox_750_0.1M_ETP_RC sample, (b) EDS of point 1, (c) EDS of point 2 and (d) EDS of point 3 of this sample

After considering the outcomes of this set of data, it was decided that the re-impregnating of this material does not have a positive impact on the morphology of the foams. Despite changing various experimental parameters, a higher metal loading was still not achieved. Therefore, another attempt was made to improve the loading and surface morphology of the foam by increasing the molarity of the solution.

4.3.4.2 Influence of iron nitrate concentration

To begin with, 1 M solution of ethanol and terpineol were used. The resin was not used any further as it did not have much impact on the wt. % loading. Increasing the molarity from 0.1 to 1 M had a dramatic affect on the metal oxide wt. % loading on raw (SS 314 raw 1M_ET_FeOx) and pre-oxidised foam (SS 314 750_1h_1M_ET_FeOx) as shown in Table 4.6. Not only was the loading improved, an overall of 5 wt. % iron oxide loading was obtained with the SS 314 750_1h_1M_ET_FeOx sample which was comparable to the 5 wt. % increase observed with the SS 314 750_1h sample. Having the same amount of loading will make it easier for samples to be compared in catalytic testing.

Table 4.6. Metal oxide loading (wt. %) on SS 314 foams impregnated with iron nitrate (1 M)

Substrate	Metal oxide loading
SS 314 raw 1M_ET_FeOx	4.2 wt %
SS 314 ox_750_1h_1M_ET_FeOx	5.4 wt %

In addition to the weight increase, the morphology of the raw foam had also improved by increasing the solution molarity. Figure 4.18a shows a representative micrograph of the SS 314 raw 1M_ET surface. As can be seen from this figure, the coating was still dispersed into chunks on the surface of the foam. The surface was more covered as more of the randomly distributed metal oxides chunks were seen at the surface of this foam. EDS point analysis of the top and bottom layers has been shown in Figures 4.18b and c respectively. The bottom layer consisted of mostly Fe (93 %) oxide and some Cr (7 %) was also detected (Figure 4.18b). The top chunks were high in Fe oxide only (Figure 4.18c). Ni was not present in either regions which indicated a better spread of iron oxide impregnation.

a

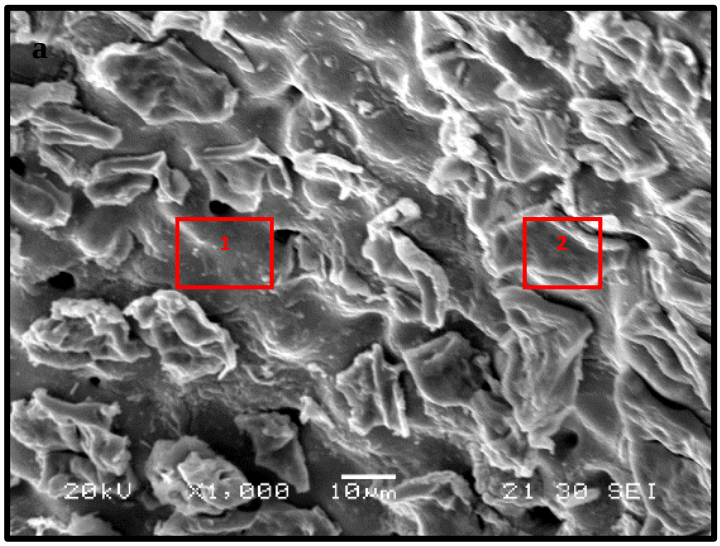

b

Element	Atomic %
Cr K	7
Fe K	93
Total	100

c

Element	Atomic %
Fe K	100
Total	100

Figure 4.18. SEM micrograph of (a) SS 314 raw 1M_ET sample, (b) EDS of point 1 and (b) EDS of point 2 of this sample

In the case of pre-oxidised foam, the surface morphology had changed dramatically. Figure 4.19a shows a representative micrograph of the SS 314 ox_750_1h_1M_ET sample. The difference observed in the morphology of this sample was not comparable to any other previous attempts made regardless of whether the foam was oxidised or not. EDS analysis revealed presence of Fe oxide mainly as shown in Figure 4.19b.

a

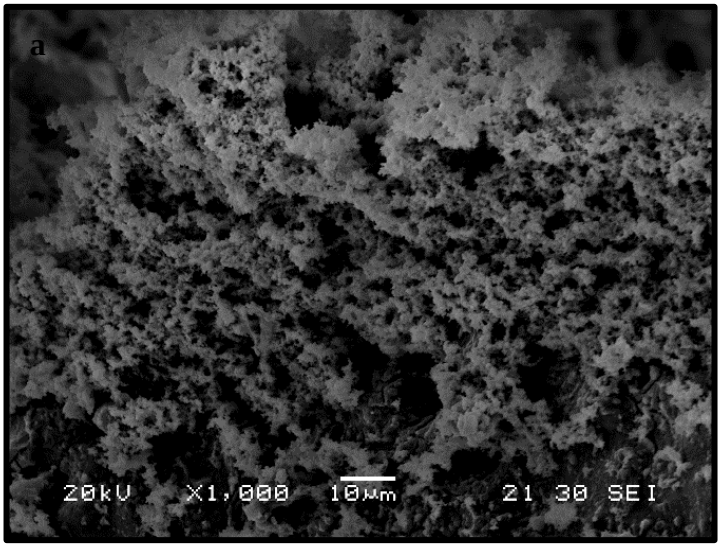

b

Element	Atomic %
Cr K	4
Fe K	96
Total	100

Figure 4.19. SEM micrograph of (a) SS 314 ox_750_1M_ET sample and (b) EDS analysis of SS 314 ox_750_1M_ET sample

For the purpose of catalytic testing, it was decided that the sample pre-oxidised at 750 °C for 1 hour, impregnated in 1M solution would be the best candidate to be tested. The impregnation in this case had resulted in the formation of an Fe oxide rich layer on the surface of the foam with 5 wt. % metal oxide loading which seemed to be a good starting point for the metal oxide impregnated foam. After this, SS 314 750_1h sample was also dip coated with 1M Mn nitrate solution with the ethanol and terpineol to obtain a homogeneous 5 wt. % Mn oxide rich surface on the foam.

Mn oxide was chosen based on the previous performance of Mn based catalysts in oxidation of toluene [150, 56, 151]. The SEM micrograph of SS 314 750_1h_1M_ET_Mn can be seen in Figure 4.20a. The Mn oxide coating in this case resulted in a very good spread of Mn oxide on the surface of the foam. The elemental composition revealed presence of a mixed Mn (64 %), Fe (31 %) oxide (Figure 4.20b).

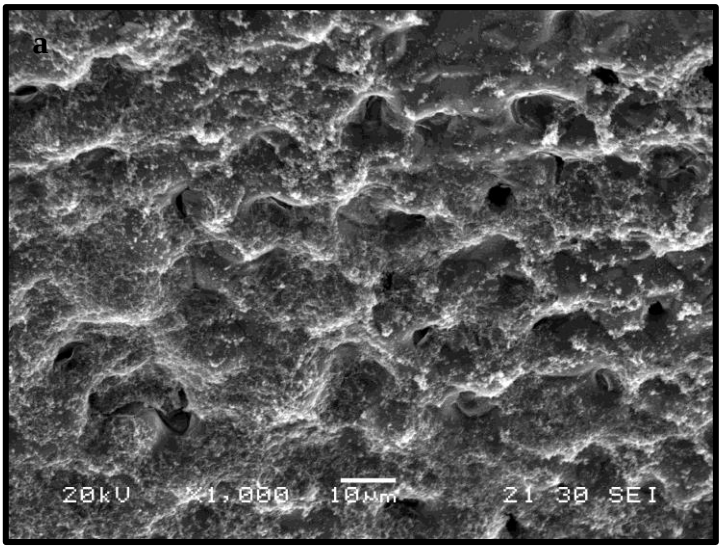

b

Element	Atomic %
Cr K	5
Mn K	64
Fe K	31
Total	100

Figure 4.20. SEM micrograph of (a) SS 314 ox_750_1h_1M_ET_Mn sample and (b) EDS analysis of this sample

The raw, SS 314 750_1h, SS 314 750_1h_1M_ET_FeOx and SS 314 750_1h_1M_MnOx foams were tested in a lab scale rig for their performance in toluene oxidation.

4.4 Catalytic testing of stainless steel 314 foams for oxidation of toluene

The selected foams were used as catalysts for toluene oxidation. A lab-scale rig with a fixed bed reactor was used for these experiments. A detailed description of the rig can be found in the experimental section. The calibration of the mass spectrometer for the expected oxidation product, CO_2, has also been explained in the experimental section. For the purpose of catalytic testing, the background for the experiments was air only which was the first blank experiment conducted at all temperatures. For instance, in the case of CO_2, the signal appears at m/z 44. The signal for m/z 44 for air was subtracted from the signal obtained through the catalytic testing. All the catalytic calculations were therefore calculated as such:

m/z signal of fragment from test- m/z signal of fragment from air

A second blank experiment was conducted with toluene only without any catalyst. This was to see what signals would be obtained in toluene upon heating it between 200 and 500 °C.

4.4.1 Blank experiment – toluene only

The main aim of this study was to completely oxidise toluene into CO_2 therefore, the mass spec was calibrated with CO_2 to allow for quantification of the products. This blank experiment, in absence of catalyst, was important to determine the difference that the catalyst would make in the toluene decomposition/ oxidation. The initial fragmentation for toluene was chosen based on NIST data [152]. Toluene has the main M-1 ion peak at 91 and therefore, the toluene conversion was followed by monitoring the changes of m/z 91. The fragmentations between 14-91 were monitored however, the signals that were changing have been plotted in Figure 4.21. It can be seen that the initial drop of toluene (approximately 40% conversion) was obtained when toluene was heated to 200 °C. The decrease in initial concentration showed an increase in two main fragments of m/z 27 (molecular ion peak for C_2H_4) and 31 (molecular ion peak for CH_3OH) and a slight increase in m/z 39 (molecular ion peak for C_3H_4) and 65 (molecular ion peak for C_5H_6). With an increase in temperature, toluene conversion can be seen to increase as the amount of toluene decreased and the main fragments that remained were of C_2H_4 and CH_3OH. Overall, 90 % of the toluene was converted mainly in to ethene and methanol. These trends were the same regardless of the catalyst used and for blank experiments without any CO_2 and H_2O being produced. The introduction of catalyst lead to oxidation of toluene and an example of trends observed have been discussed in the next section. To summarise, when oxidation does not occur, toluene can break down into C-based species on the left and when it does occur, CO_2 alongside methanol can be formed, the general schematic is as follows:

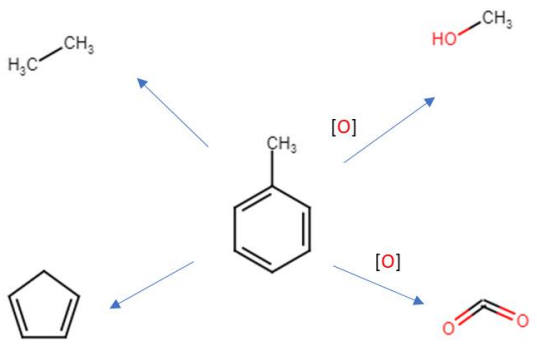

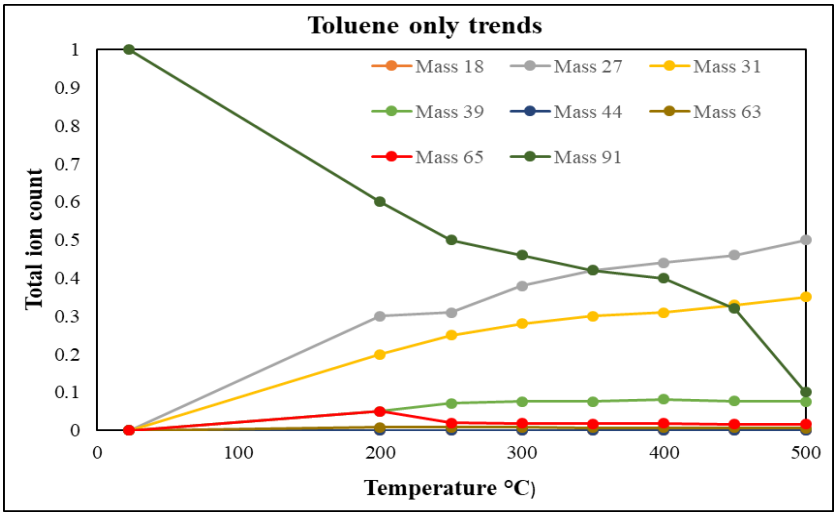

Figure 4.21. Decomposition of toluene over different temperatures

The results show that toluene in air at the operating temperatures does not oxidise into CO_2 itself and instead, it forms fragments of different ions at ~90 % conversion. After carrying out the blank experiment, different SS 314 foams in raw, pre-oxidised or impregnated forms were tested under the same conditions and the oxidation reaction was followed based on the selectivity of toluene decomposition towards CO_2 (g).

4.4.2 Stainless steel 314 raw as a catalyst for toluene oxidation

SS 314 raw was tested as a first catalyst. Figure 4.22 represents the change in toluene selectivity towards CO_2 with SS 314 raw foam as a catalyst. In terms of toluene conversion, at 200 °C, 65 % of toluene had converted and by 350 °C, this had increased to 98 % which was the highest conversion obtained. The main fragments seen were the same as the one seen without the presence of catalyst.

Compared to the blank experiment, raw SS 314 foam became catalytically active towards oxidation of toluene as a rise in the CO_2 selectivity was seen between 350 and 400 °C. Alongside CO_2, traces of methanol were observed qualitatively as by product of oxidation. There is also a possibility of carbon being deposited on the catalyst.

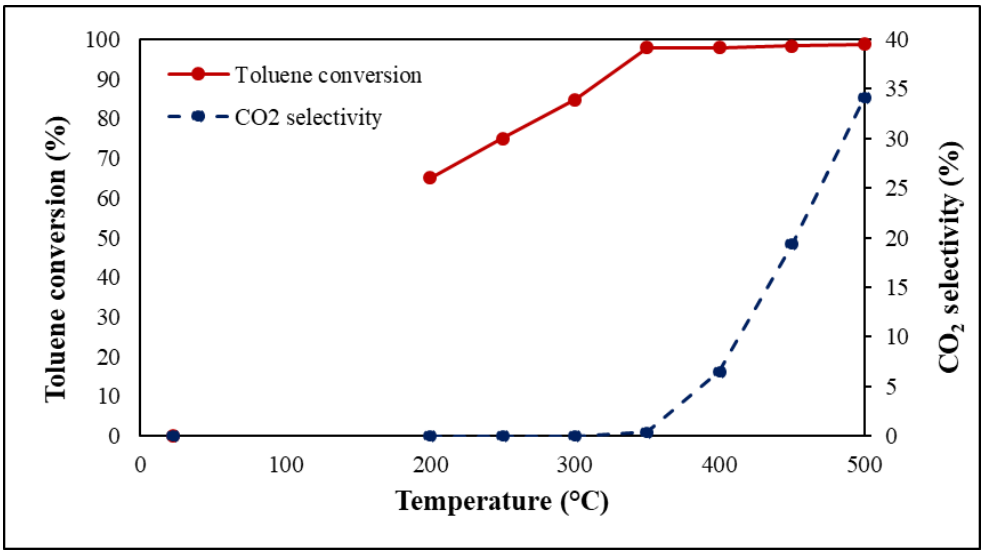

Figure 4.22. Toluene conversion (%) and selectivity towards CO_2 (%) at different temperatures with SS 314 raw foam as a catalyst

The amount of CO_2 produced constantly increased from 350 to 500 °C and the maximum selectivity of 35 % was obtained at the highest operating temperature of the application. Although the overall selectivity was low, the presence of CO_2 denoted that the foam could potentially act as an oxidation catalyst. The general trends observed have been summarised in Figure 4.23. The trends plotted show how the toluene initially breaks down into ethanol and ethene alongside the other fragments observed in the case of blank experiment. The main change occurs when the catalyst becomes active towards oxidation of toluene. It can be seen that the

fragmentations produced further break down to produce CO_2 and H_2O. As the trends observed were the same, for the rest of the results chapters, only the quantitative analysis of toluene and CO_2 has been discussed.

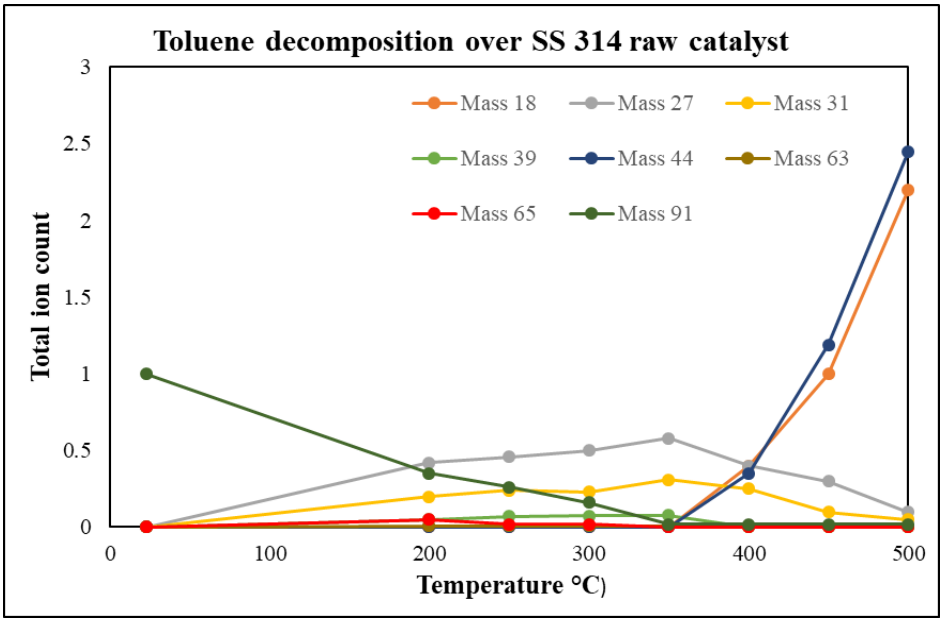

Figure 4.23. Toluene decomposition over different temperatures in the presence of SS 314 raw catalyst

Due to the formation of CO_2 (v) upon the use of catalyst, it was decided to look at the type of mechanism that was involved in the process of oxidising toluene. Oxidation through heterogeneous catalysis can occur via three mechanisms. A short explanation of each one has been given below:

1. Langmuir-Hinshelwood (L-H) model – this model states that the oxidation takes place when there is a reaction between the adsorbed oxygen and the adsorbed VOC [153].

2. Eley-Rideal (E-R) model - this model assumes that oxidation occurs between the adsorbed oxygen and the VOC in the gas phase. The rate determining step is the reaction between the contaminant in the gas phase and the adsorbed oxygen on the surface [154].

3. Mars Van Krevelen (MVK) model – this model considers that the oxidation reaction occurs between the lattice oxygen of the catalyst and the

adsorbed VOC to produce oxidation product. This model predicts oxidation based on oxygen present in the catalyst rather than the oxygen present in the air [155].

According to previous literature review on oxidation of toluene, the aromatic compound oxidises via the MVK model [149], keeping this in mind an experiment was set up. Instead of using compressed air, pure nitrogen was fed into the contaminant and passed over the raw catalyst. This resulted in formation of CO_2 which meant that oxidation had occurred. As there was no oxygen in the gas stream, the oxidation could have only occurred through the lattice oxygen present in the catalyst which meant that the oxidation mechanism in this case followed the MVK model.

Figure 4.24a represents the SS 314 raw after being tested. SEM revealed that the raw sample which was smooth (Figure 4.1a) in surface and had the elemental composition of Fe (54), Cr (26) and Ni (20) according to EDS analysis had oxidised after being in the reactor. The presence of increased Fe oxygen in the sample gave a good indication of oxidation. The morphology of the before (Figure 4.1a) and after sample (Figure 4.24a) showed a drastic change. The oxidation could be attributed to the catalytic activity observed. The SS 314 had oxidised to form mixed metal oxide layer on the surface which was catalytically active. Prior to 300 °C, the temperature was too low for the formation of the oxide layer therefore, no CO_2 production was seen. An increase in temperature increases the amount of CO_2 produced, the foam oxidises more readily at higher temperatures which could be the cause of increase in oxidation of toluene. A ~98 % toluene conversion was observed eventually at 350 °C however, the selectivity towards CO_2 was rather low (35 %). This meant that the toluene upon reacting with raw SS 314 forms different intermediates that then form CO_2 which in this case were not breaking down/oxidising further. The increase however, in CO_2 (Figure 4.23) compared to the blank experiment (Figure 4.21) was a positive outcome nevertheless therefore, SS 314 pre-oxidised at 750 °C for 1 h was tested next.

a

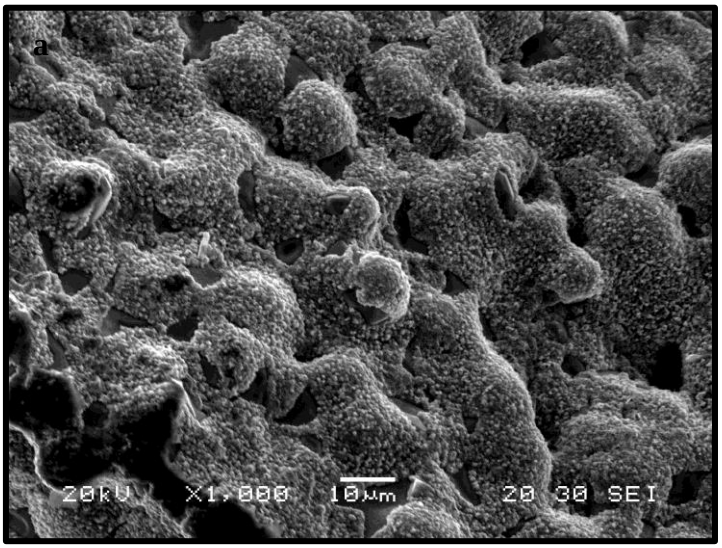

b

Element	Atomic %
Cr K	24
Fe K	71
Ni K	5
Total	100

Figure 4.24. SEM micrograph of (a) SS 314 raw sample after being used as a catalyst and (b) EDS analysis of this sample

4.4.3 SS 314 ox_750_1h as a catalyst for toluene oxidation

SS 314 ox_750_1h was tested next. Figure 4.25 summarises toluene conversion and selectivity of this sample towards main oxidation product over different temperatures. The pre-oxidised sample was more active towards toluene conversion compared to the raw foam (Figure 4.24). A dramatic increase in the toluene conversion of 95 % was observed when the reactor temperature had reached 200 °C. The maximum conversion in this case was significantly higher (100 %) at a much lower temperature (300 °C) compared to that of the raw sample.

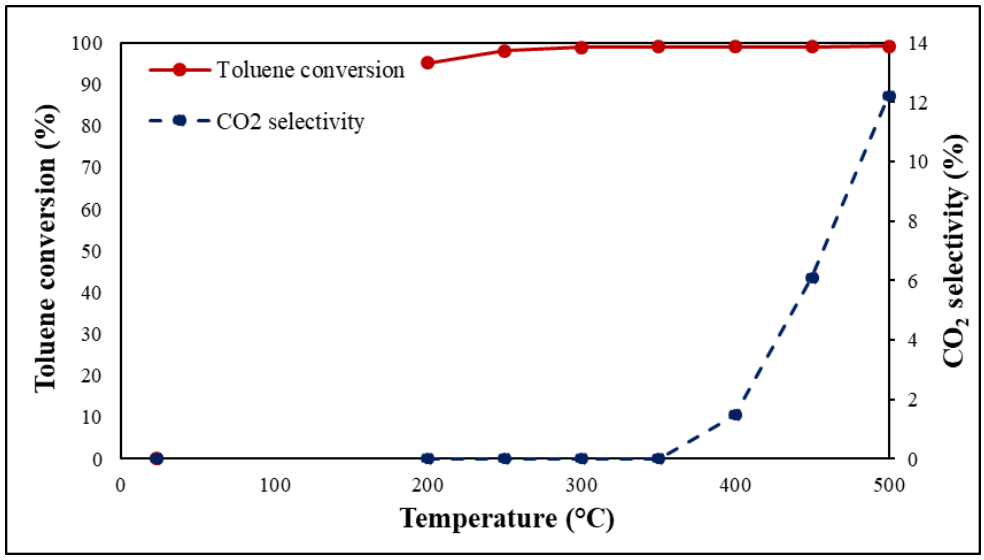

Figure 4.25. Toluene conversion (%) and selectivity towards CO_2 (%) at different temperatures with SS 314 ox_750_1h sample

The SS 314 750_1h sample became catalytically active at 350 °C. The amount of CO_2 produced constantly increased similarly to that of the raw sample from 350 to 500 °C however, the maximum selectivity in this case was 12 % which was obtained at the highest operating temperature of the application. The main reason behind testing the oxidised foam was that this foam gave a 5 wt. % increase (Table 4.1) upon oxidation at 750 °C for 1 h, which meant that this foam would be comparable to other foams that would be impregnated with the same amount of metal oxide loading. Figure 4.26a represents SS 314 ox_750_1h sample after being tested. The SEM analysis of before (Figure 4.6a) and after revealed that the foam had oxidised

even further upon being tested, there were no drastic changed to the morphology of the foam. According to the EDS analysis (Figure 4.26b), the Fe content had increased from 82 to 89 % and Cr content had decreased from 15 to 11 %, also Ni was not found after the sample had been tested. Although overall low selectivity was obtained, these results still indicated that the foam was still catalytically active in oxidation of toluene. After this, the impregnated foams were tested next.

a

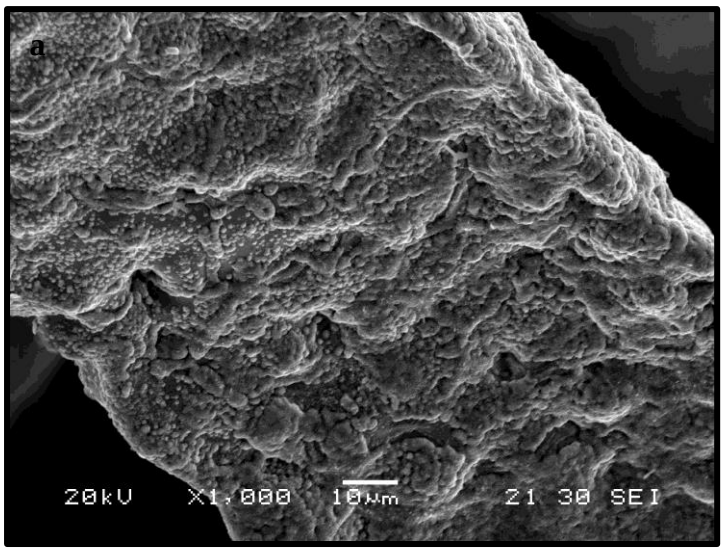

b

Element	Atomic %
Cr K	11
Fe K	89
Total	100

Figure 4.26. SEM micrograph of (a) SS 314 ox_750_1h sample after being used as a catalyst and (b) EDS analysis of this sample

4.4.4 SS 314 ox_750_1h_1M_ET_FeOx as a catalyst for toluene oxidation

In the case of the iron oxide impregnated sample, the toluene conversion followed same trend as that of the oxidised sample. Figure 4.27 summarises the trends observed when SS 314 ox_750_1h_1M_ET_FeOx was used. Using the Fe oxide impregnated foam had resulted in 97 % toluene decomposition at 200 °C. Full conversion of toluene was obtained at 400 °C.

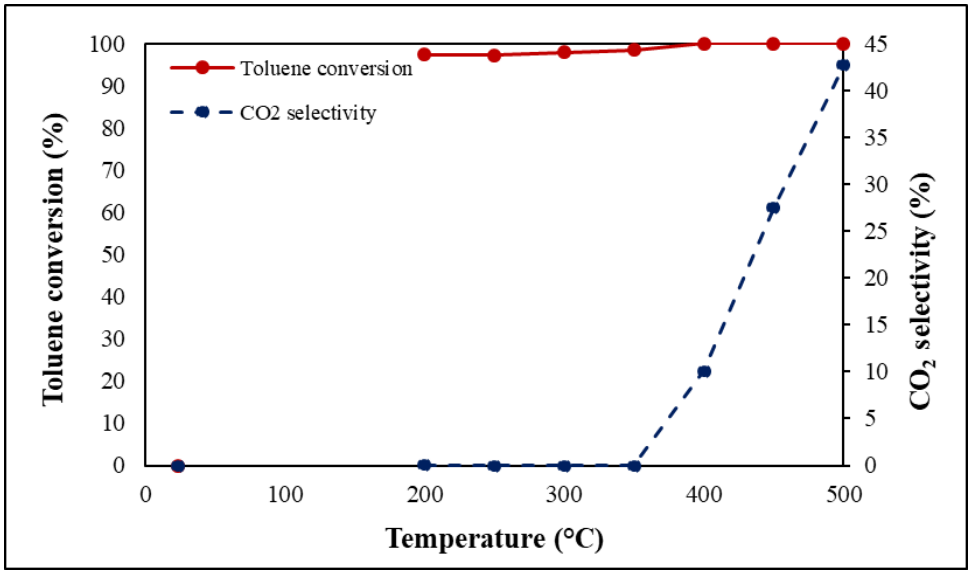

Figure 4.27. Toluene conversion (%) and selectivity towards CO_2 (%) at different temperatures with SS 314 ox_750_1h_1M_ET_FeOx sample.

In terms of selectivity towards CO_2, the Fe oxide impregnated foam became catalytically active at 350 °C. The foam followed the same trends as previously seen with the raw and pre-oxidised samples (Figures 4.23 and 4.24 respectively) as the CO_2 selectivity can be seen to increase constantly from 350 to 500 °C. The main difference between this sample and the previous samples is the amount of toluene oxidised to CO_2. The maximum selectivity in this case was 43 %. Methanol was qualitatively observed as a by-product alongside CO_2. The foam prior to being tested was rough and the main composition was of Fe oxide (Figure 4.19a and b). Once tested, the morphology had changed as can be seen in Figure 4.28a. The top layer had agglomerated in different regions of the foam, overall the agglomerated regions looked smoother than before being tested. EDS analysis revealed that the elemental composition of both, the top layer (Figure 4.28b) and the smooth surface

(Figure 4.28c) of the foam were the same. The increase in selectivity towards CO_2 meant that the impregnated foam was more selective towards toluene oxidation than the unoxidized (raw) or oxidised foam.

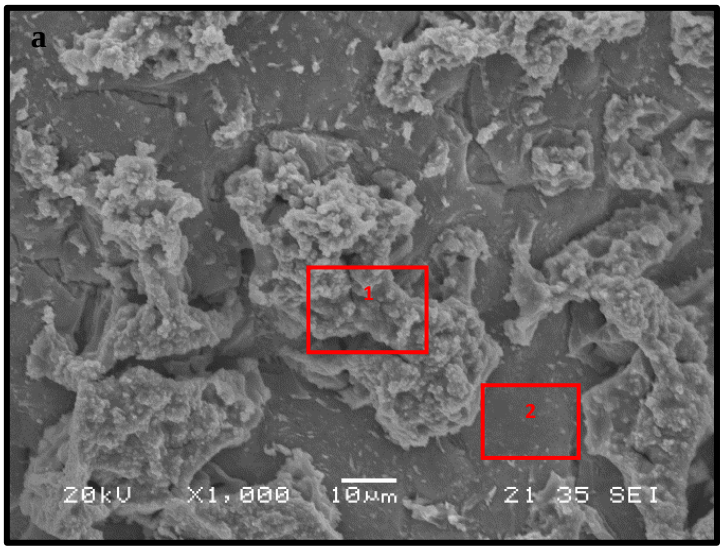

b

Element	Atomic %
Cr K	9
Fe K	91
Total	100

c

Element	Atomic %
Cr K	12
Fe K	88
Total	100

Figure 4.28. SEM micrograph of (a) SS 314 ox_750_1h_1M_ET_FeOx sample after being used as a catalyst and (b) EDS analysis of point 1 and (c) EDS analysis of point 2 of this sample

4.4.5 SS 314 ox_750_1h_1M_ET_MnOx as a catalyst for toluene oxidation

The last 314 foam tested for oxidation of toluene was the MnO impregnated foam. This foam was chosen based on it's previous use in oxidation of VOCs. In previous cases, Mn oxide was catalytically active towards toluene oxidation [156, 81]. Figure 4.29 summarises the trends of toluene conversion and selectivity towards CO_2 observed in the presence of SS 314 ox_750_1h_1M_ET_MnOx at different temperatures. This foam had a slower conversion compared to the oxidised or Fe oxide impregnated foam at 200 °C. The overall conversion of this sample at 200 °C was 75 % (Figure 4.29) compared to 95 and 97 % of the oxidised and impregnated foams (Figures 4.25 and 4.28 respectively). This slowly increased to 100 °C at 350 °C.

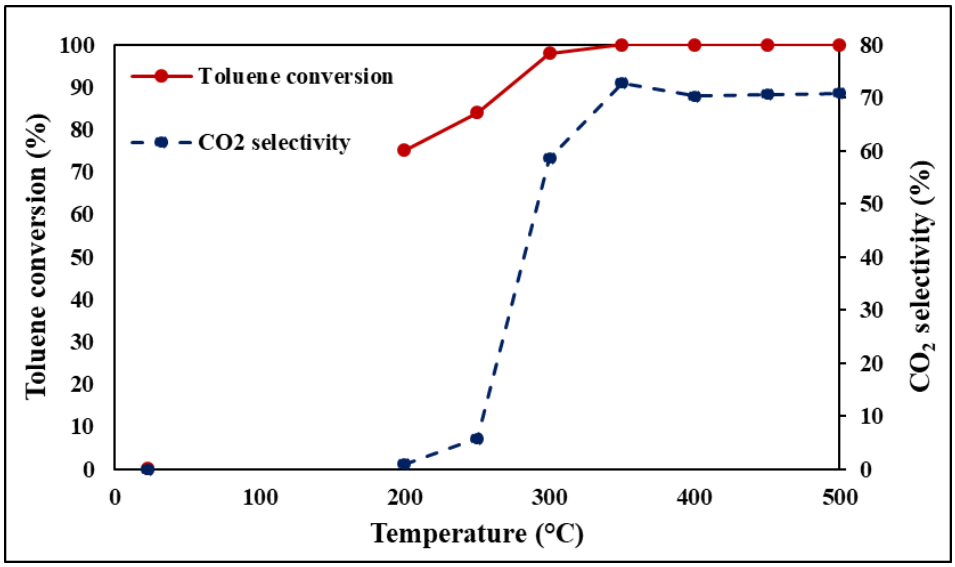

Figure 4.29. Toluene conversion (%) and selectivity towards CO_2 (%) over different temperatures with SS 314 ox_750_1h_1M_ET_MnO sample

The main difference arises when the selectivity of this foam towards CO_2 production is compared to the previous samples. The MnOx impregnated foam became catalytically active at 200 °C. The selectivity increased until 350 °C and a very slight drop was observed at 400 °C but overall, it could be concluded that the selectivity was constant after 300 °C. Maximum selectivity of 71 % of toluene into CO_2 was obtained at 350 °C. Qualitatively, methanol was seen as a by-product of this reaction at a constant rate. There is also a possibility of some carbon deposition

on the surface of the catalyst as methanol was not quantified which can explain lower than 100 % selectivity towards CO_2. Figure 4.20a and Figure 4.30a are representatives of before and after catalysis samples. The morphology of the foam before and after as well as the EDS composition for both, the sample prior to being tested and after being tested were very similar (Figures 4.20a, b and 4.30a, b respectively). This indicated that the Mn ox impregnated foam was not only catalytically active but retained its morphology until the end of the reaction which was a positive outcome. The 71 % selectivity towards CO_2 was the highest observed for any SS 314 foam previously tested under same conditions.

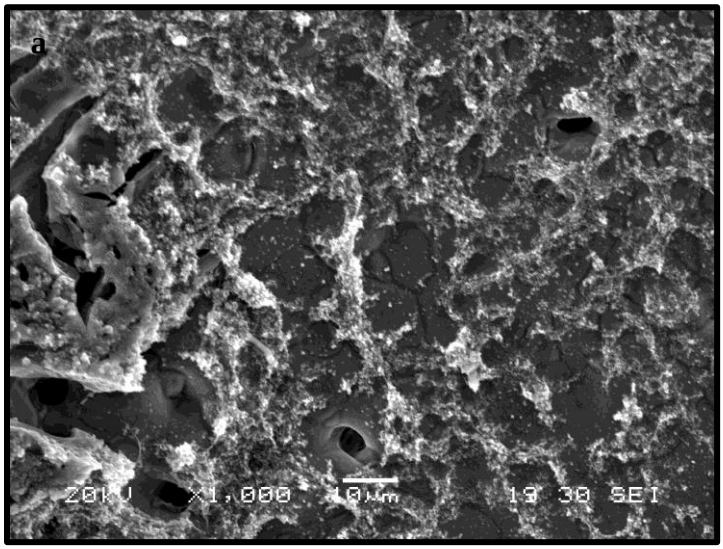

b

Element	Atomic %
Cr K	6
Mn K	63
Fe K	31
Total	100

Figure 4.30. SEM micrograph of (a) SS 314 ox_750_1h_1M_ET_MnOx sample after being used as a catalyst and (b) EDS analysis of this sample

4.5 Chapter Summary

In this chapter, SS 314 foams have been modified using oxidation and/or impregnation to form a metal oxide rich layer on the surface of the foams. In terms of the oxidation study, the SS 314 foam oxidised at 750 °C for 1h gave a 5 wt. % metal oxide loading and an increased surface roughness. For impregnation, a few experimental parameters such as influence of substrate, solution composition and solution molarity were studied. Both the SS 314 raw and SS 314 foam oxidised at 750 °C for 1h were investigated for dip coating. The pre-oxidised foam gave a better surface coverage morphology. In the end, raw, SS 314 ox_750_1h and pre-oxidised foams dip coated with Fe and Mn oxides were tested for catalytic oxidation of toluene. Summary of the elemental composition before and after testing is shown in Table 4.7.

Table 4.7. Elemental enrichment summary for SS 314 foams

Element	Raw SS 314		750_1h SS 314		FeOx SS 314		MnO SS 314	
	Before	After	Before	After	Before	After	Before	After
Cr K	24	26	15	11	4	11	5	6
Fe K	71	54	82	89	96	89	31	31
Ni K	5	20	3	-	-	-	-	-
Mn K	-	-	-	-	-	-	64	64

Mn oxide coated foam gave the highest toluene conversion (100 %) and selectivity towards CO_2 (71 %) at 350 °C. Methanol was observed as a by-product alongside CO_2. As it was not quantified, there is also a possibility of elemental C which can account for lower than 100 % selectivity towards CO_2. This was the lowest temperature for maximum toluene conversion and selectivity compared to all the other foams tested.

Characterisation and catalytic testing of SS 316 foams

5.1 Chapter overview

Due to the unavailability of the SS 314 foams, SS 316 foams were used instead for studying oxidation of toluene further. SS 316 foams were more readily available and cheaper compared to the SS 314 composition. Previous chapter discussed how the pre-oxidised foam gave better surface coverage compared to raw foam. Keeping this in mind, oxidation of SS 316 foams was carried out at various temperatures to increase surface roughness. In this chapter, oxidation, impregnation and catalytic testing of SS 316 foams for toluene oxidation will be discussed. The change in morphology of the foams was investigated with SEM 5600, FEG JSM650 and EDS was used for elemental analysis. The catalytic oxidation was studied at 25, 200 – 500 °C in a lab scale rig and the oxidation products were monitored using MS.

5.2 Oxidation study for SS 316 foams

Figure 5.1a represents low magnification SEM micrograph of SS 316 raw sample. The porosity was similar to that of the SS 314 raw seen in Figure 4.1a. The metallic components of the SS 316 raw also consisted of Fe, Cr and Ni however, the content of each was different to that of the SS 314 raw. In the case of SS 316 raw, the Fe (71 %) content was higher than Fe (54 %) in SS 314 raw (Figure 4.1b). The Cr content (18 % compared to 26 %) and Ni (11 % compared to 20 %) were however lower than the SS 314 composition. This meant that the SS 316 had a much higher Fe content compared to SS 314 raw sample.

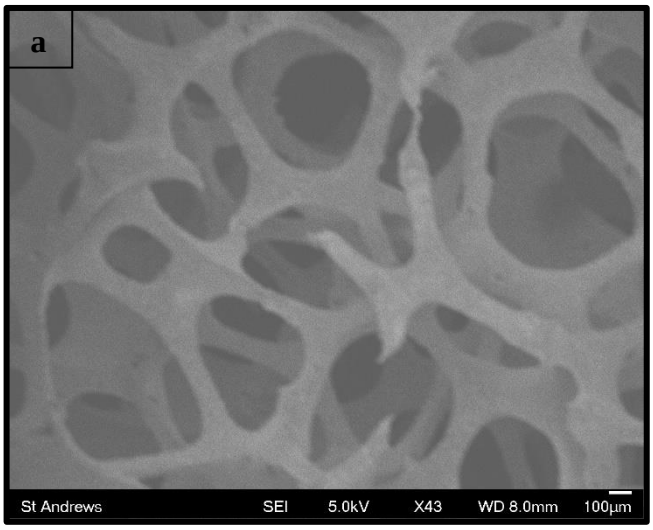

b

Element	Atomic%
Cr K	18
Fe K	71
Ni K	11
Total	100

Figure 5.1. SEM micrograph of (a) SS 316 raw foam and (b) EDS composition of the foam

In terms of the morphology, a closer look at the SS 316 raw foam revealed some interesting features. Figure 5.2 depicts SS 316 raw at higher magnification so that the features of the foam can be seen. The foam compared to SS 314 raw (Figure 4.2a) already had a rough surface area. Instead of smooth islands, roughness was present throughout the surface. The O content was also higher than that of the SS 314 raw.

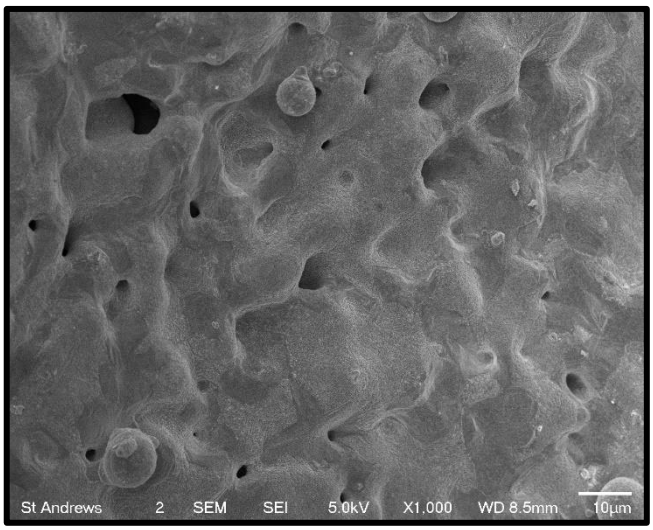

Figure 5.2. SEM micrograph of SS 316 raw at higher magnification

Oxidation study was carried out on SS 316 foam in the same experimental conditions as the ones used for SS 314 foams. In this case, the starting temperature was chosen to be 750 °C as previously this had resulted in formation of a rough surface on the foam which in turn gave positive coating outcome. After 750 °C, lower temperatures such as 600, 450 and 300 °C, all at 1h dwell were investigated. Table 5.1 presents a summary of wt. % increase at respective temperatures. The wt. % after oxidation generally was higher than that observed in the case of SS 314 foams (Table 4.1). At 750, the wt. % increase was similar to that of SS 314 sample (5 %), however, at 600 °C, with the SS 316, the ~2 wt. % increase was a lot higher than 0.1 % observed in the previous case. Even temperature as low as 300 °C had ~1 wt. % increase which was a positive outcome as it meant that the SS 316 foams could potentially be oxidised at lower temperatures provided the surface morphology had increased surface roughness which will be discussed next.

Table 5.1. The increase in wt. (%) obtained at different temperatures at constant dwell time of 1h

Substrate	Metal oxide loading
SS 315 ox_300_1h	0.8 wt %
SS316 ox_450_1h	1.4 wt %
SS316 ox_600_1h	1.9 wt %
SS 316 ox_750_1h	5.8 wt %

The morphology and elemental analysis of the foams was evaluated using FEG SEM and EDS. The first temperature for oxidation was of 750 °C. Figure 5.3a shows representative SEM micrograph of SS 316 ox_750_1h sample, this sample had regions which showed agglomeration and increased surface roughness compared to the SS 316 raw (Figure 5.1a). As shown in Figure 5.3b, the oxidised sample had an increased Fe content 87 % compared to 71 % in the raw sample. The Cr and Ni after oxidation had decreased from 18 to 8 and 11 to 5 % respectively compared to the raw SS 316 foam (Figure 5.1b). This meant that under the chosen oxidation conditions, Fe was still dominating the mixed oxide layer found on the surface of the foam.

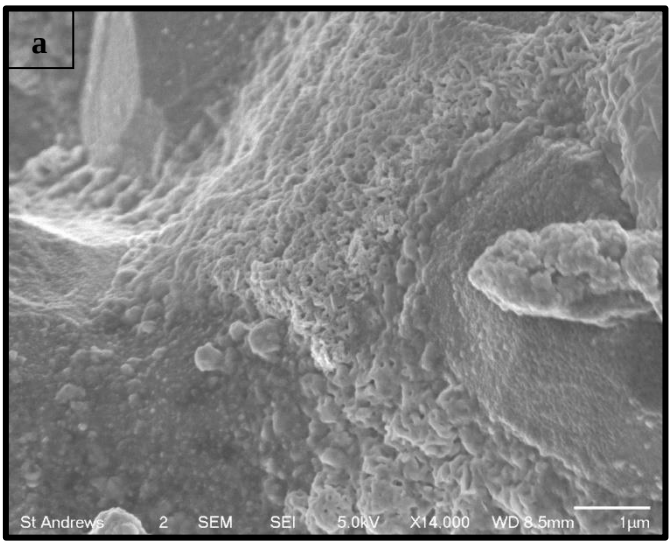

b

Element	Atomic%
Cr K	8
Fe K	87
Ni K	5
Total	100

Figure 5.3. SEM micrograph of (a) SS 316 ox_750_1h sample and (b) EDS analysis of this sample

After seeing that the oxidation at 750 °C had been successful in increasing surface roughness, lower temperature of 600 °C was tested next. Figure 5.4a represents the SS 316 foam oxidised at 600 for 1h dwell time (SS 316 ox_600_1h). This sample also had an increased roughness and showed homogeneity at the surface. The elemental composition as shown in Figure 5.4b comprises of mixed metal oxide layer. The metallic content of Fe (68 %) was similar to that of the SS 316 raw (Figures 5.1b) but lower than that of the SS 316 ox_750_1h sample (Figure 5.3b). The Cr (22 %) had increased compared to the 8 % of the SS 316 ox_750_1h sample and the Ni (10 %) was similar to 11 % that of the SS 316 raw foam but higher than the 5 % of the SS 316 ox_750_1h sample. According to the elemental composition, SS 316 ox_600_1h had a more similar composition to that of the SS 316 raw which was also expected as the wt % increase (Table 5.1) was reasonably lower.

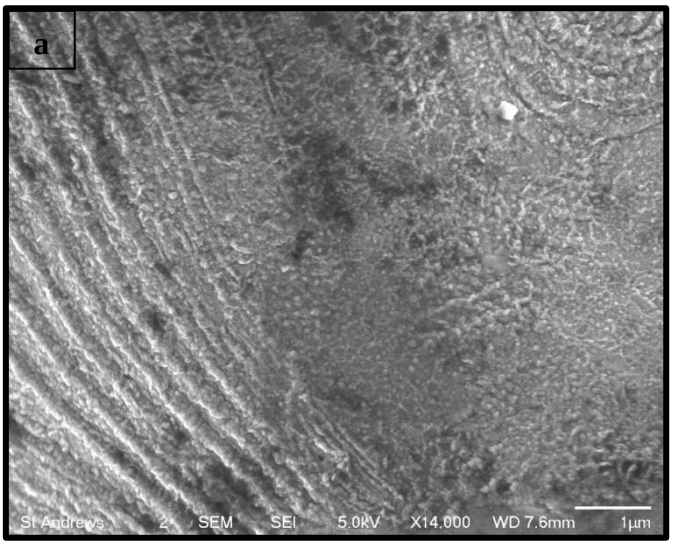

b

Element	Atomic%
Cr K	23
Fe K	68
Ni K	9
Total	100

Figure 5.4. SEM micrograph of (a) SS 316 ox_600_1h sample and (b) EDS analysis of this sample

As the lower temperatures were giving beneficial results, temperature of 450 °C was tested next. The sample oxidised at 450 °C for 1 hour (SS 314 ox_450_1h) also demonstrated increased roughness as shown in Figure 5.5a. The elemental composition consisted of a mixed oxide layer with Fe, Cr and Ni all being present on the surface as seen in Figure 5.5b. The Fe content of 70 % was close to that of the SS 316 raw (Figure 5.1b), the Cr content of 25 % was close to that of the SS 316 raw and ox_600_1h samples (Figure 5.1b and 5.4b) but higher than that of the SS 316 ox_750_1h sample (Figure 5.3b). The Ni (5 %) was close to the SS 316 ox_750_1h sample.

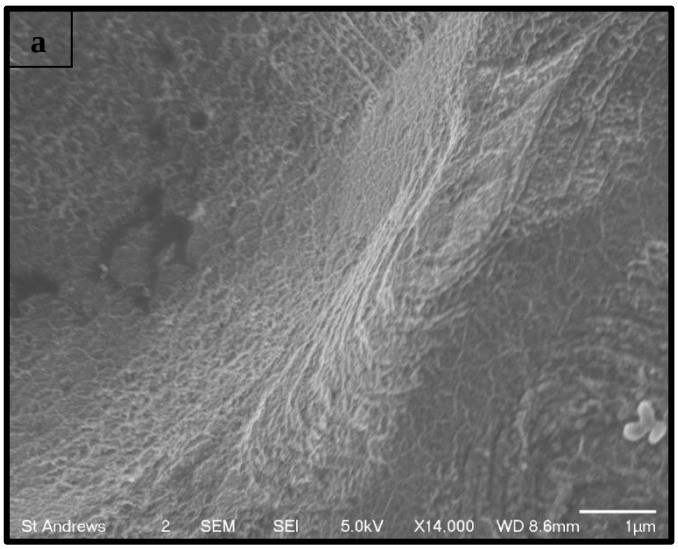

b

Element	Atomic%
Cr K	25
Fe K	70
Ni K	5
Total	100

Figure 5.5. SEM micrograph of (a) SS 316 ox_450_1h sample and (b) EDS analysis of this sample

As oxidation at 450 °C still resulted in an increase roughness on the surface, final attempt was made of oxidation at 300 °C to see whether this would result in an increased roughness on the surface. Figure 5.6a illustrates that the SS 316 ox_300_1h sample also had rough surface morphology. The EDS analysis revealed in Figure 5.6b showed presence of O, Fe, Cr and Ni. In this case, the Fe (72 %) was similar to that of the SS 316 raw and 316 ox_450_1h samples (Figures 5.1b and 5.2b respectively). The Ni (6 %) and Cr (22 %) were also quite similar to the metallic composition of SS 316 ox_450_1h sample (5 and 25 % respectively, Figure 5.5b). The increase in Cr content at lower oxidation temperatures indicated that at lower temperatures, the SS 316 oxidises Cr more readily to form Cr oxide which was a sensible outcome as stainless steels are known to form a Cr oxide rich layer on the surface to avoid corrosion.

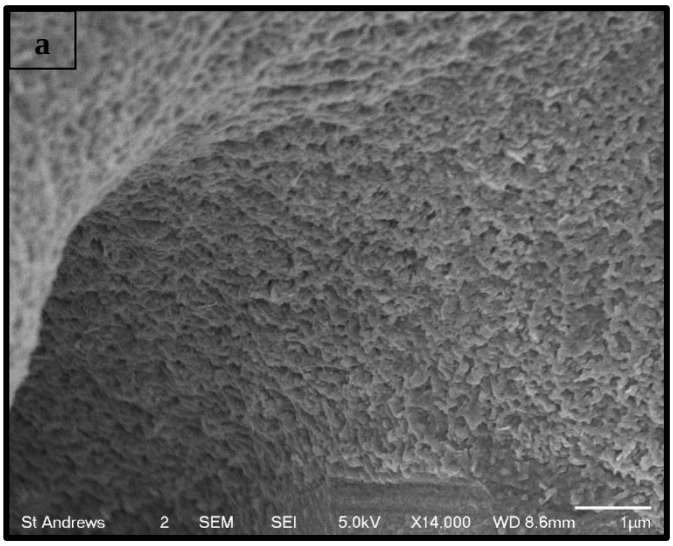

b

Element	Atomic%
Cr K	22
Fe K	72
Ni K	6
Total	100

Figure 5.6. SEM micrograph of (a) SS 316 ox_300_1h sample and (b) EDS analysis of this sample

Switching from SS 314 to SS 316 had beneficial outcome as oxidation at lower temperatures was successful in obtaining a homogeneous rough surface on the SS foams. As temperature as low as 300 °C showed increased roughness, it was decided that the impregnation of different metal nitrates would be tried at the SS 316 raw and SS 316 ox_300_1h foams. Different metal nitrates such as Fe, Ni, Cu, Mn and Ce were used to impregnate SS 316 foams *via* dip coating. The metal nitrates were chosen based on their previous performances as oxidation catalysts which have been discussed in the Introduction and also mentioned in the previous SS 314 results chapter. Instead of starting with Fe nitrate solution, the first impregnations were carried out with Cu nitrate solutions as Cu oxide has previously shown promising results as an oxidation catalyst [157].

The aim of impregnation was to achieve 5 wt. % Cu oxide on the surface of the foam. 5 wt. % was chosen as a constant so that all impregnated samples could be compared when used in catalytic testing.

5.3 Impregnation study with Cu nitrate solution

The foams raw or oxidised were impregnated with 1 M Cu nitrate solution with ethanol, terpineol and binder (PVB) as a starting point. Though ethanol and terpineol worked well in the case of SS 314 foam impregnation, the SS 316 study was a separate study therefore few modifications were made in the solution composition gain to a homogeneous coverage of metal oxide on the surface.

Figure 5.7 shows a representative SEM micrograph of the SS 316 raw foam coated with 1M Cu oxide in ethanol, terpineol and surfactant-based solution (SS 316 raw 1M_ETS_CuOx). A homogeneous surface coverage was obtained in this case. The wt. % increase however, was 17 wt. % which was higher than the required target. Nevertheless, the same solution was tested with the pre-oxidised 300 °C sample to see if that would influence surface coverage and wt. % loading.

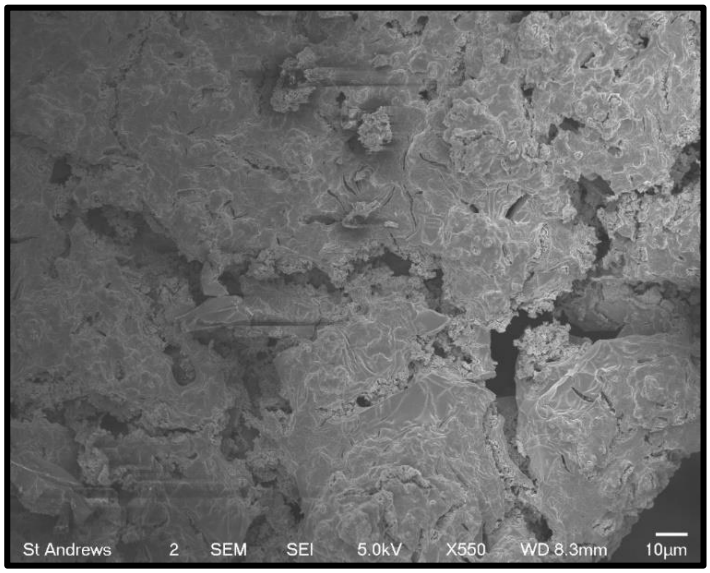

Figure 5.7. SEM micrograph of SS 316 raw 1M_ETS_CuOx sample

Figure 5.8 is a representative micrograph of SS 316 ox_300_1h foam impregnated with 1M Cu oxide in ethanol, terpineol and surfactant-based solution (SS 316 ox_300_1h_1M_ETS_CuOx). This sample had a smooth coverage with cracks that could be seen. The 14 wt. % was again higher than what was required. The high increase in wt. % was attributed to the high molarity of the solution therefore, 0.1M solutions were tested next.

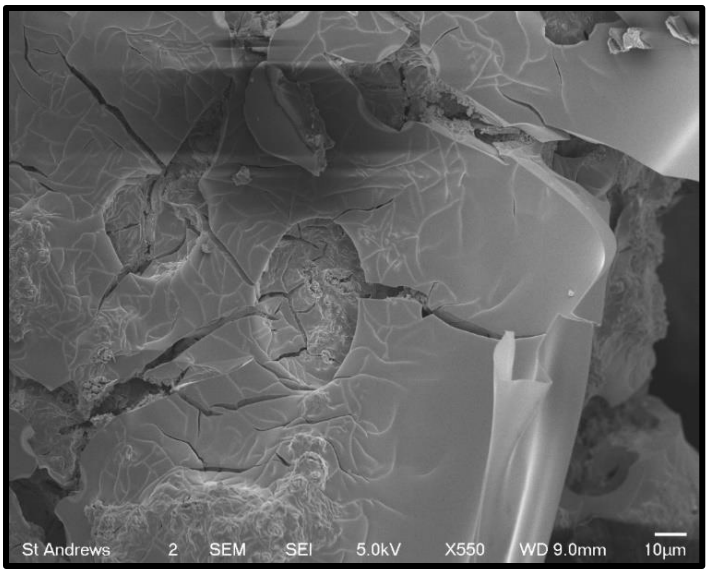

Figure 5.8. SEM micrograph of SS 316 ox_300_1h_1M_ETS_CuOx sample

Figure 5.9 is a representative of SS 316 raw impregnated with 0.5M Cu oxide in ethanol, terpineol and surfactant-based solution (SS 316 raw 0.5M_ETS_CuOx). With this impregnation, some regions of foams were clearly seen to be uncovered. The impregnation had been successful in some areas of the foam however, raw SS 316 could be seen. This sample had an overall wt. % loading of 3.4 % which was close to the target however, it lacked homogeneity therefore the pre-oxidised sample was tested with the same solution composition.

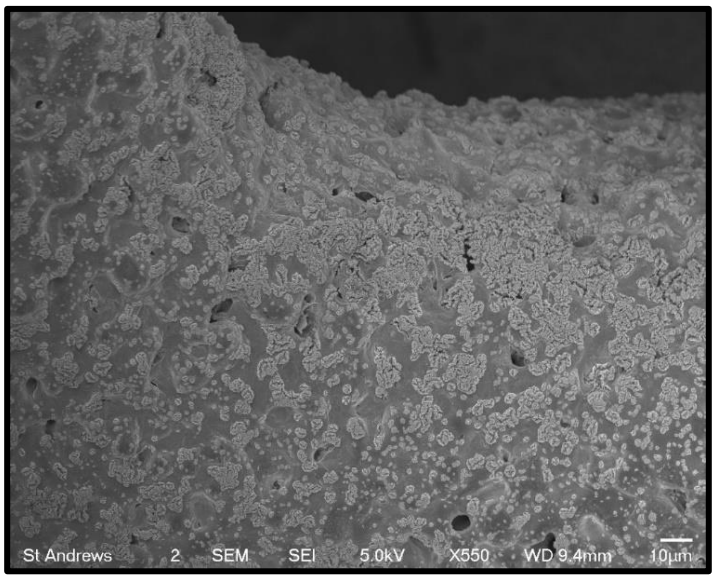

Figure 5.9. SEM micrograph of SS 316 raw 0.5M_ETS_CuOx sample

Figure 5.10 shows that the pre-oxidised sample impregnated with 0.5M Cu oxide in ethanol, terpineol and surfactant-based solution (SS 316 ox_300_1h_0.5M_ETS_CuOx) had a better surface coverage compared to the raw substrate. The Cu oxide impregnation had resulted in 4.0 wt. % increase, this was closer to that of the required loading. Although the morphology of the oxidised foam was better than the raw sample, there was still a need to obtain the 5 wt. % metal oxide loading. It was important to keep the wt. % increase to 5 so that as catalysts, the impregnated samples could be compared against each other and the amount of active catalyst was kept consistent.

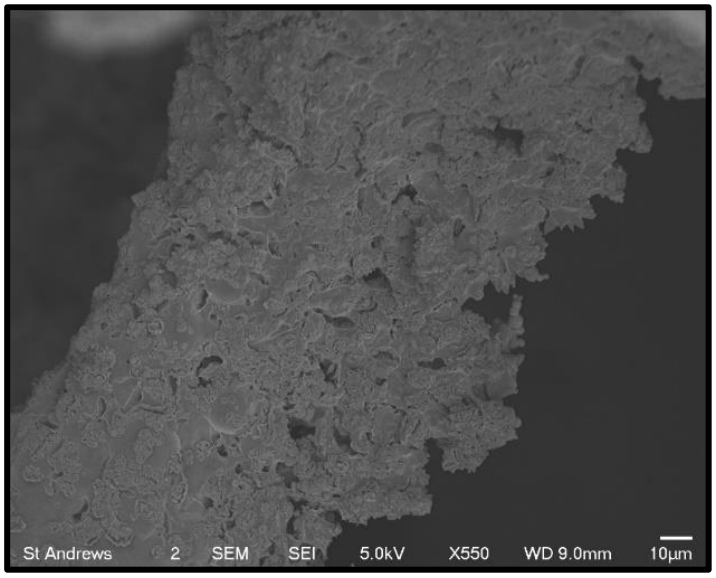

Figure 5.10. SEM micrograph of SS 316 ox_300_1h_0.5M_ETS_CuOx sample

A different set of solution was tested next with the same molarity, mixture of IPA and PVB were used to see the affect of these on the morphology of the foam. The solvent change from ethanol and terpineol to IPA was decided based on PVB having better compatibility with IPA [158]. This compatibility was expected to spread the metal nitrates more evenly on the surface resulting in a better coverage of the surface.

Figure 5.11 shows SEM micrograph representative of the SS 316 raw impregnated with 0.5M Cu oxide in IPA and surfactant-based solution (SS 316 raw 0.5M_IS_CuOx). The morphology was similar to the ones obtained with the SS 316 raw 0.5M_ETS_Cu sample (Figure 5.9). The foam was generally more covered and the metal oxide loading of 4.2 % was getting closer to the required loading as well. Therefore, keeping this in mind, the same solution composition was tested for the pre-oxidised substrate.

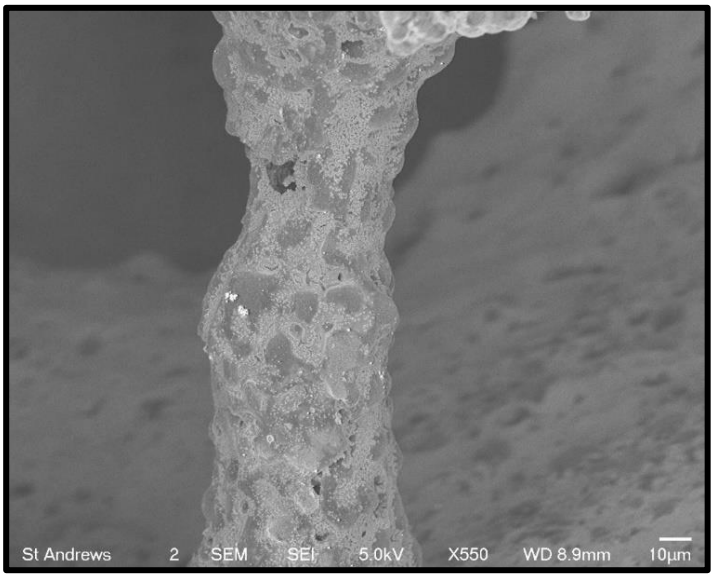

Figure 5.11. SEM micrograph of SS 316 raw 0.5M_IS_CuOx sample

Figure 5.12 illustrates the surface morphology of the SS 316 ox_300_1h impregnated with 0.5M Cu oxide in IPA and surfactant-based solution (SS 316 ox_300_1h_0.5M_IS_CuOx). The morphology of this sample was similar to that of the raw substrate (Figure 5.11) but the impregnation was more dominant. The loading of metal oxide loading obtained in this case was 4.4 %.

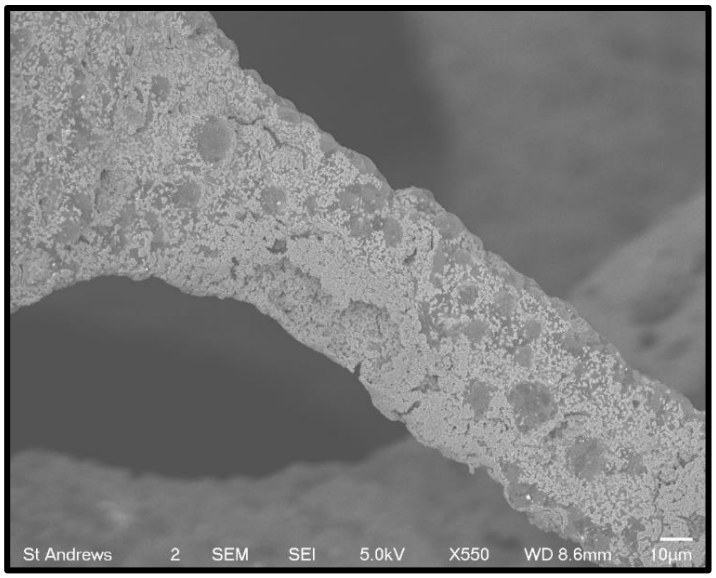

Figure 5.12. SEM micrograph of SS 316 ox_300_1h_0.5M_IS_CuOx sample

Though the wt. % increase and the morphology were very close to that of the target. Few final attempts were made to evaluate their affect on the morphology and wt. % loading. Terpineol previously resulted in a better coating therefore, it was added into the solution with IPA and surfactant. In this case, only the pre-oxidised sample was tested.

Addition of terpineol had a positive impact on the surface morphology of the foam. Figure 5.13 shows that the SS 316 ox_300_1h impregnated with 0.5M Cu oxide in IPA, terpineol and surfactant-based solution (SS 316 ox_300_1h_0.5M_ITS_CuOx) had a homogeneous impregnated layer on the surface. This resembled quite closely to that of the SS 316 ox_300_1h_0.5M_ETS_CuOx sample (Figure 5.10). The metal oxide loading obtained was 4.6 % which was very close to the require 5 wt. % loading.

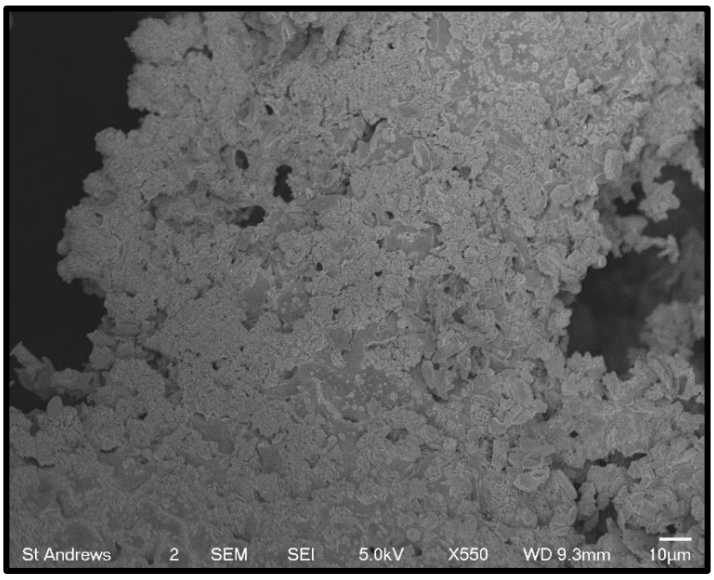

Figure 5.13. SEM micrograph of SS 316 ox_300_1h_0.5M_ITS_CuOx sample

After obtaining homogeneous surface coverage of metal oxides, final few attempts were made to see whether the surfactant was a necessity. Same molarity of 0.5 M was used but with ethanol and terpineol only as solvents.

Figure 5.14 is a representative micrograph of the SS 316 raw impregnated with 0.5M Cu oxide in ethanol and terpineol-based solution (SS 316 raw 0.5M_ET_CuOx). The morphology of the raw sample in this case resembled

closely to the SS 316 raw 0.5M_ETS_CuOx sample (Figure 5.9) as this sample also consisted of some scattered impregnated regions with smooth raw foam being shown. The metal oxide loading of 4.6 % of was higher than that of the SS 316 raw 0.5M_ETS_CuOx sample. Seeing that the morphology had not changed drastically and there was no detrimental effect on the metal oxide loading either without the presence of surfactant, it was decided that surfactant will not be used in any further impregnations.

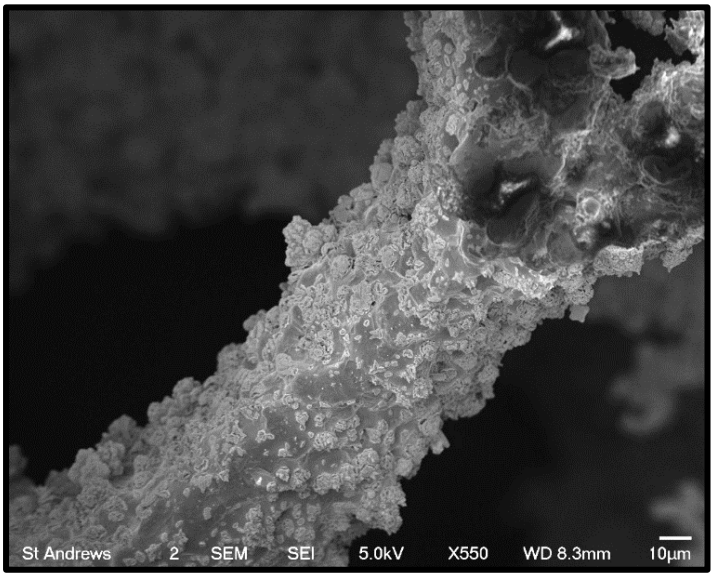

Figure 5.14. SEM micrograph of SS 316 raw 0.5M_ET_CuOx sample

The peroxidised sample was also tested with the same solution composition. Figure 5.15 illustrates that the SS 316 ox_300_1h impregnated with 0.5M Cu oxide in ethanol and terpineol-based solution (SS 316 ox_300_1h_0.5M_ET_CuOx) had an excellent surface coverage. The sample seemed to have a homogeneous layer on the surface. The overall wt. % loading of this sample was 5.2 % which was also ideal as for the purpose of this project.

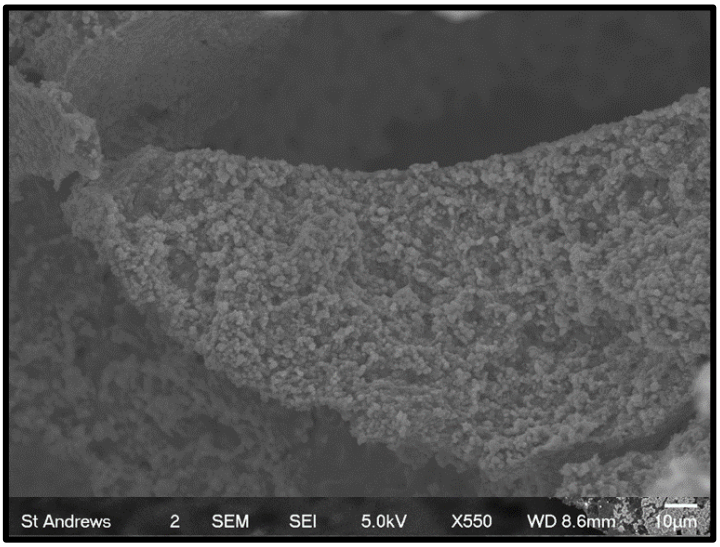

Figure 5.15. SEM micrograph of SS 316 ox_300_1h_0.5M_ET_CuOx sample

It was clear from the results obtained with different solution compositions and concentrations that the ethanol and terpineol had a positive impact on the surface morphology. Although the loading and homogenous morphology was obtained with the final test, one further last test was carried out on the raw sample to see if terpineol makes a difference in morphology or wt. % loading therefore, raw foam impregnated with 0.5 M of Cu nitrates in ethanol only was tested.

Figure 5.16 depicts surface morphology of the SS 316 raw impregnated with 0.5M Cu oxide in ethanol only based solution (SS 316 raw 0.5M_E_CuOx). This sample had a very close resemblance to the SS 316 raw sample (Figure 5.1a), the only difference observed was the scattered impregnation which in wt. % was only of 0.8 %. This meant that the addition of terpineol was vital in obtaining a higher and, in some cases more homogeneous surface coverage.

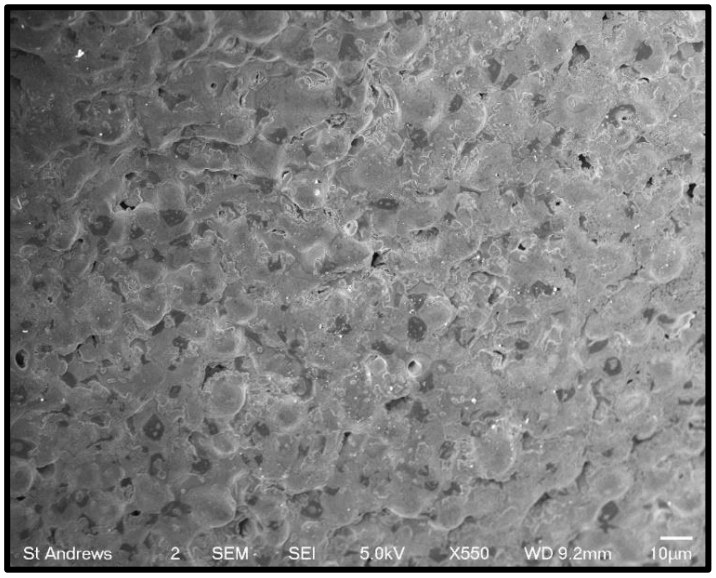

Figure 5.16. SEM micrograph of SS 316 raw 0.5M_E_CuOx sample

As the surface morphology and the metal oxide (%) loading were both not satisfactory, no further modifications were made in solution compositions for impregnation of metal nitrates. It was decided that SS 316 pre-oxidised foams would be impregnated in solution containing ethanol and terpineol as solvents for impregnation of other metal nitrates (Fe, Ni, Mn and Ce). Overall ~5 wt. % metal oxide loadings were obtained by coating the peroxidised foam with respective metal nitrates and calcining them. The morphologies of these have been discussed in the following section. The raw/oxidised/impregnated foams were tested for catalytic oxidation of toluene.

5.4 Catalytic testing

The catalytic testing was carried out in the same reaction conditions as described earlier in the Experimental section. Raw, oxidised or pre-oxidised impregnated samples of the SS 316 foams were investigated for oxidation of toluene at 200-500 °C.

5.4.1Oxidation of toluene

5.4.1.1 Oxidation of toluene with SS 316 raw foam

The first sample tested was the SS 316 raw foam. This foam showed promising results towards toluene conversion even at 200 °C. Figure.5.17 shows toluene conversion of 90 % was achieved at 200 °C, compared to the SS 314 (Figure 4.24) this conversion was a lot higher. The products obtained were still the same as the ones seen in the case of SS 314. Selectivity towards the main product of CO_2 was also better with the SS 316 foam. This foam became catalytically active towards oxidation of toluene at 350 °C. The oxidation selectivity started at 2 % and increased to 90 % at 500 °C. The by-product similarly as SS 314 foam was methanol.

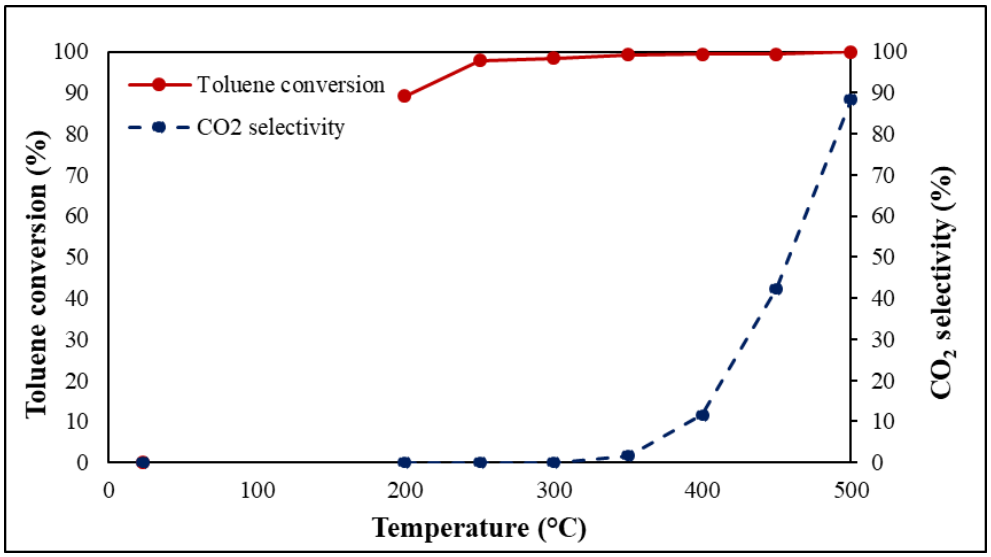

Figure 5.17. Toluene conversion and selectivity towards CO_2 over SS 316 raw catalyst at different temperatures

The foams were analysed using SEM and EDS analysis. Interestingly, in the case of raw SS 316, the morphology of before (Figure 5.1a) and after (Figure 5.18a) catalytic testing was very similar which was in contrast to what was observed previously in the case of SS 314. A drastic change in morphology was obtained with the SS 314 (Figure 4.1a and 4.23a respectively) however, the SS 316 raw foam retained its morphology. The EDS analysis revealed higher oxygen presence compared to the SS 316 raw sample prior to being tested. As expected, the foam had oxidised in the reaction conditions, the elemental composition revealed that the Cr content stayed the same at 18 %, Ni content had slightly increased from 11 to 14 % and the Fe content in this case had decreased from 74 to 68 %. The elemental composition gave an indication that the foam during catalytic testing had developed a mixed oxide on the surface. The catalytic selectivity observed could be due to more Ni on the surface of the foam. These results were different to the ones observed in the case of SS 314 raw (Figure 4.23b**)** as in that case, Ni content had decreased, and Fe had increased. In the case of raw SS 316 sample, better toluene conversion and catalytic oxidation selectivity could be attributed to the balance of elemental composition. The presence of Ni and Cr after the reaction indicated that having these elements was helpful in giving better oxidation of toluene. The improved conversion and oxidation of toluene with the SS 316 raw foam meant that the SS 316 foams could be used as a substitute for the SS 314 foam. For this reason and to keep the comparison of the foams consistent, the next foam tested was the foam oxidised at 750 °C for 1 hour.

a

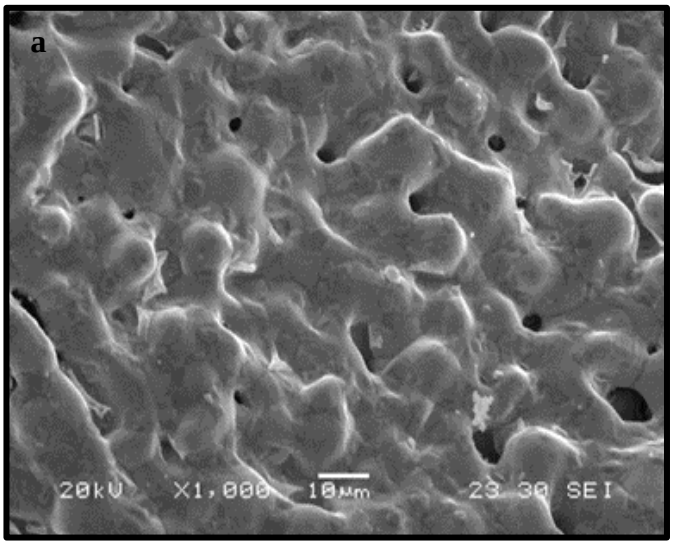

b

Element	Atomic%
Cr K	18
Fe K	68
Ni K	14
Totals	100

Figure 5.18. SEM micrograph of (a) SS 316 raw sample after being tested and (b) EDS analysis of this sample

5.4.1.2 Oxidation of toluene with SS 316 ox_750_1h foam

Figure 5.19 shows that the peroxidised sample (SS 316 ox_750_1h) gave a 100 % toluene conversion at 250 °C and this foam became active towards oxidation of toluene at 400 °C. Prior to this, the same products were observed as with the case of previous foams. The highest selectivity of 88 % towards CO_2 was obtained at the highest temperature of 500 °C. Alongside CO_2, traces of methanol were also observed. The performance of this foam again was better compared to the SS 314 oxidised foam as seen previously in Figure 4.24.

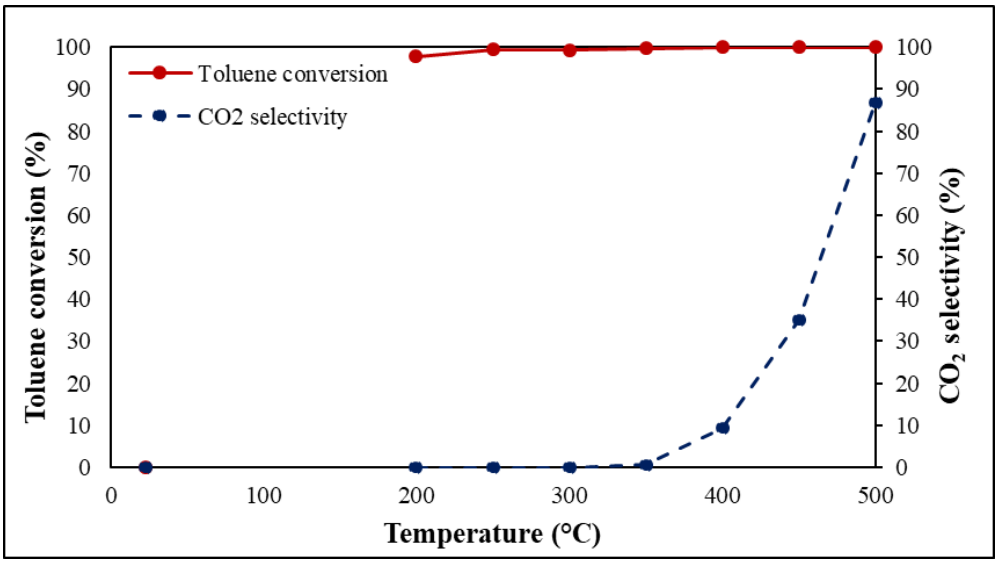

Figure 5.19. Toluene conversion and selectivity towards CO_2 over SS 316 ox_750_1h catalyst at different temperatures

Figure 5.20a shows that a smooth layer had formed on the surface of the foam compared to the rough surface seen in the post catalyst sample (Figure 5.3a). Figure 5.20b shows that this layer was rich in Fe (73 %) oxide mainly with Cr (17 %) and Ni (10 %) mixed oxides being also present. The Cr (8 %) and Ni (5 %) observed in the pre catalysis sample (Figure 5.3b) had almost doubled in the post catalysis sample. The Fe content of 87 % in the pre sample had decreased to 73 % after being used in catalysis. This meant that under the reaction conditions, the sample had been oxidised further and, in this case, Cr and Ni were oxidised more. The SS 316 raw foam became active towards toluene oxidation at 350 °C (Figure 5.17) however,

the oxidised foam became active at 400 °C. There was no great difference between the total oxidation results of the raw and oxidised samples as their elemental composition had become similar in the reactor hence the oxidation followed the same trends in both cases. The next sample tested was the Fe oxide impregnated foam, the oxidised foam contained high amount of elemental Fe so it was interesting to see whether externally impregnating oxides would change the way the foam oxidises toluene or not.

a

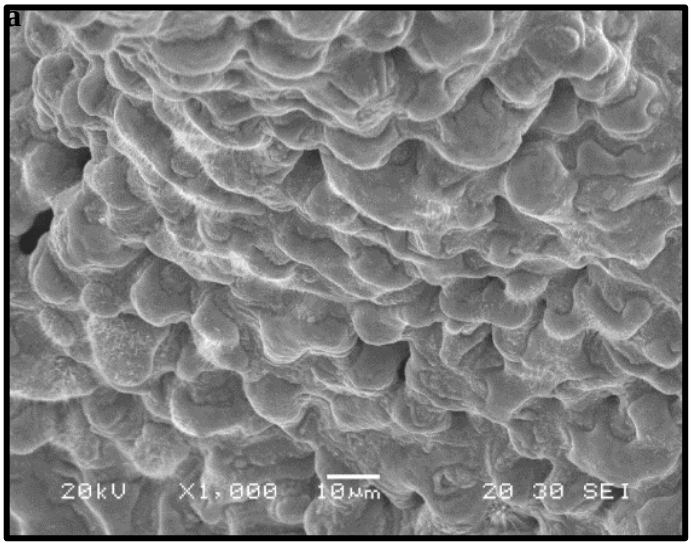

b

Element	Atomic%
Cr K	17
Fe K	73
Ni K	10
Total	100

Figure 5.20. SEM micrograph of (a) SS 316 ox_750_1h sample after being tested and (b) EDS analysis of this sample

5.4.1.3 Oxidation of toluene with SS 316 ox_300_1h FeOx foam

The toluene conversion over the Fe oxide impregnated foam (SS 316 300_1h_0.5M_ET_FeOx) was rather interesting. Figure 5.21 illustrates that the conversion was slow at the start and eventually 100 % conversion was obtained at 400 °C. In comparison with the raw and oxidised samples, which almost had 90 % above conversions even at 200 °C, the 45 % conversion obtained was unexpected. The foam became active towards oxidation at 350 °C and eventually 90 % selectivity was obtained at 500 °C. Methanol was observed as a by-product which can account for the selectivity being lower than 100 %.

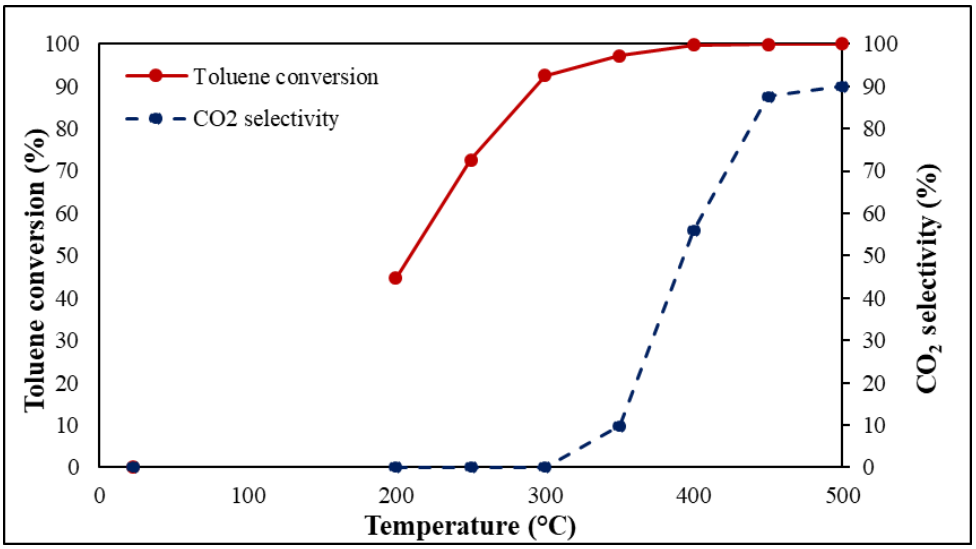

Figure 5.21. Toluene conversion and selectivity towards CO_2 over SS 316 ox_300_1h_0.5M_ET_FeOx catalyst at different temperatures

Figures 5.22a and Figure 5.22b are representatives of the pre catalysis and post catalysis sample. Figure 5.22a shows that the morphology of the impregnated foam had an oxide layer on the surface. The foam after being tested had formed a smoother homogeneous layer on the surface compared to the island like impregnation instead of having a rough layer on the surface as seen in SS 314 sample. The impregnation on pre oxidised SS316 resulted in a smoother surface. Figures 5.22c and d reveal that according to the EDS analysis, both, the pre and post catalysis samples were rich in Fe (82 and 84 %) and Cr (18 and 16 %) oxide only unlike the raw and oxidised foams (Figures 5.17b and 5.19b) which were rich

in Fe, Cr and Ni. Figure 5.21b shows that this foam only consisted of Fe (81 %) and Cr (19 %) oxide. Previously, it was thought in the case of the raw foam that the Cr and Ni presence both improved catalytic oxidation ability of the foam. The slow conversion of toluene (Figure 5.21) at lower temperatures could be attributed to the lack of Ni present in the sample. The performance of this SS 316 ox_300_1h_0.5M_ET_FeOx impregnated foam was similar to the raw or oxidised SS 316 samples however, the results in comparison with the SS 314 1M_ET_FeOx impregnated foam (Figure 4.26) were still marginally better.

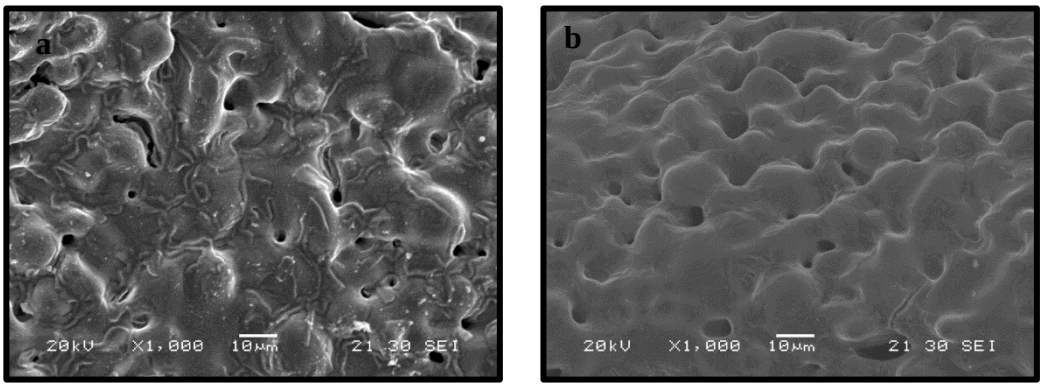

c

Element	Atomic%
Cr K	18
Fe K	82
Total	100

d

Element	Atomic%
Cr K	16
Fe K	84
Total	100

Figure 5.22. SEM micrograph of (a) SS 316 ox_300_1h_0.5M_ET_FeOx before catalysis, (b) after catalysis, (c) EDS analysis of pre catalysis and (d) EDS analysis of post catalysis of this sample

5.4.1.4 Oxidation of toluene with SS 316 ox_300_1h NiOx foam

Figure 5.23 illustrates toluene conversion and selectivity towards CO_2 with SS 316 ox_300_1h_0.5M_ET_NiOx foam. Toluene conversion of 40 % was obtained at 200 °C which eventually increased to 100 % at 350 °C. This trend was similar to the one observed with the SS 316 ox_300_1h_0.5M_ET_FeOx sample. The selectivity, however, was improved compared to raw, oxidised and impregnated samples. The Ni oxide impregnated foam became active towards oxidation of toluene at 300 °C. Initially 14 % selectivity towards CO_2 was observed which eventually increased to 82 % at 350 °C. After this point, there was a small drop in the overall selectivity however, this was still within the experimental error. Though this foam was active towards toluene oxidation at lower temperature, the overall selectivity of 82 % was still lower than that observed with SS 316 ox_300_1h_0.5M_ET_FeOx foam of 88 %.

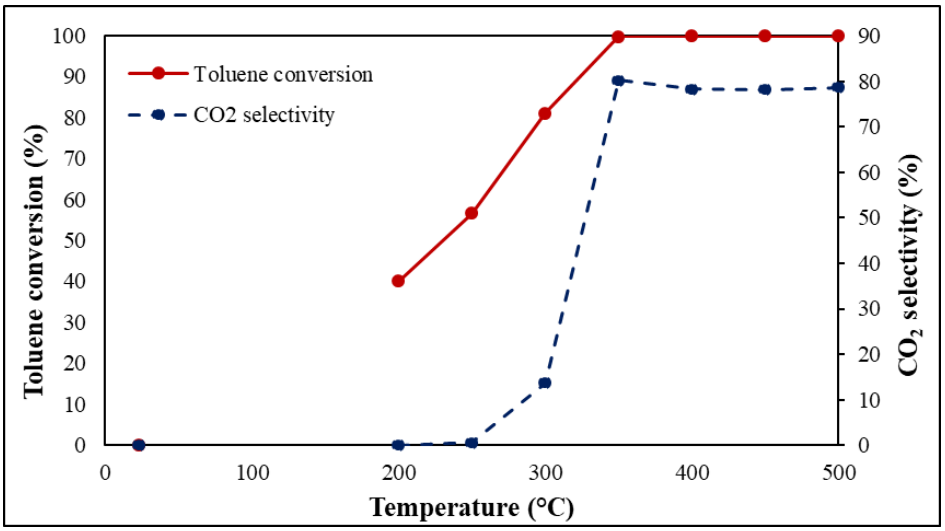

Figure 5.23. Toluene conversion and selectivity towards CO_2 over SS 316 ox_300_1h_0.5M_ET_NiOx catalyst at different temperatures

Figures 5.24a shows the morphology of the foam prior to being tested. Before testing, two regions could be seen under the SEM. Figure 5.24b shows that the top layer-the impregnated layer had a high content of Ni (91 %) as expected. The smoother area underneath (Figure 5.24c) had Fe (43 %), Cr (17 %) and Ni (40 %), compared to the SS 316 ox_300 sample (Figure 5.6) which was the substrate for coating, the Ni content was marginally high due to the impregnation. Figure 5.25a

shows that the morphology of this sample had very slightly changed, it had become a little smoother however, the elemental composition of Fe (8 %) and Ni (92 %) on the top layer was still the same as can be seen from Figure 5.25b. This meant that the change in morphology observed was due to the air causing compression of the impregnated layer causing it to come together to form a smoother overall surface of the foam.

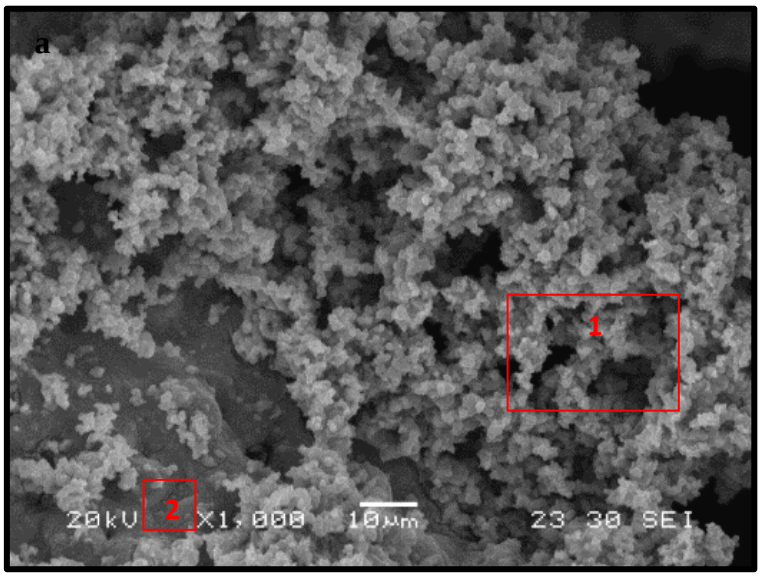

b

Element	Atomic%
Fe K	9
Ni K	91
Total	100

c

Element	Atomic%
Cr K	17
Fe K	43
Ni K	40
Total	100

Figure 5.24. SEM micrograph of (a) SS 316 ox_300_1h_0.5M_ET_NiOx before catalysis, (b) EDS analysis of point 1 and (c) EDS analysis of point 2 of this sample

a

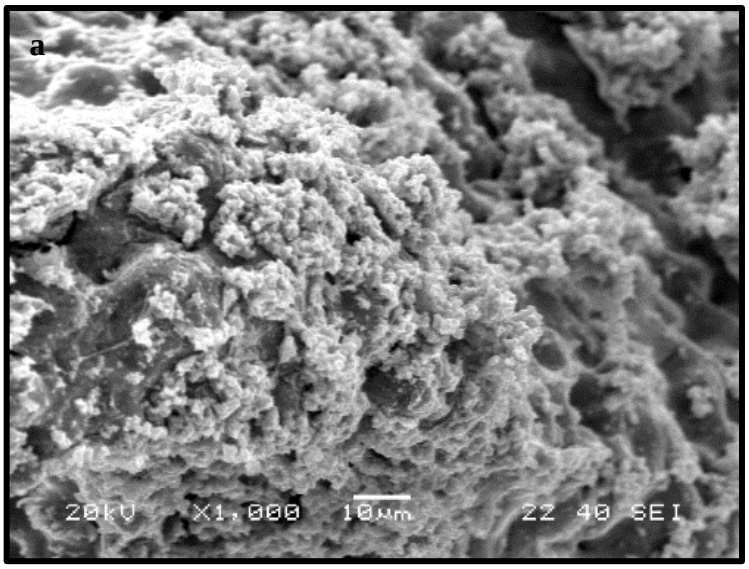

b

Element	Atomic%
Fe K	8
Ni K	92
Total	100

Figure 5.25. SEM micrograph of (a) SS 316 ox_300_1h_0.5M_ET_NiOx after catalysis and (b) EDS analysis of this sample

5.4.1.5 Oxidation of toluene with SS 316 ox_300_1h CuOx foam

Copper oxide is a good oxidation catalyst and has been used previously for toluene oxidation[156]. Figure 5.26 shows that the SS 316 ox_300_1h_0.5M_ET_CuOx sample was successful in converting 72 % of toluene at 200 °C which eventually increased to 100 % at 350 °C. The foam became active towards oxidation at 300 °C and the overall selectivity of 86 % towards CO_2 was obtained at 400 °C. The amount of CO_2 was constant at temperatures after 400 °C.

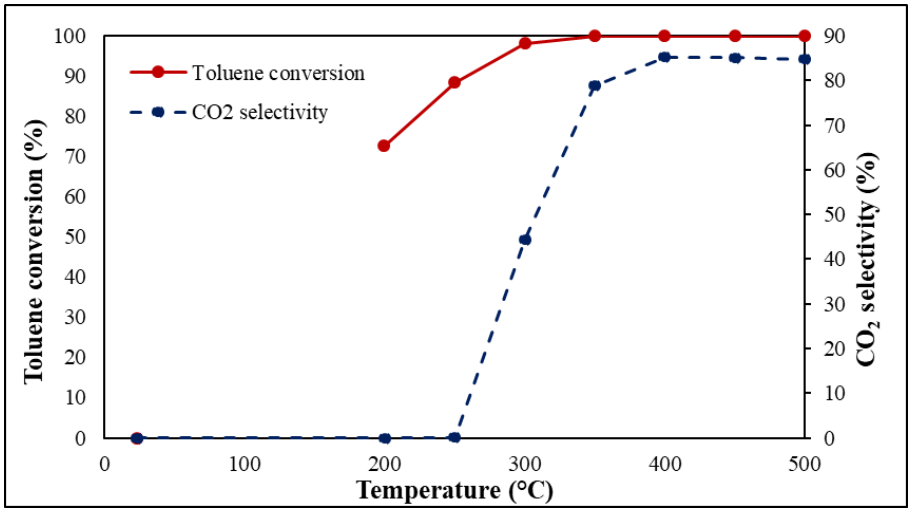

Figure 5.26. Toluene conversion and selectivity towards CO_2 over SS 316 ox_300_1h_0.5M_ET_CuOx catalyst at different temperatures

Figure 5.14 shows that the SS 316 ox_300_1h_0.5M_ET_CuOx foam had a rough oxide layer on the surface of the foam. This was rich in Cu (92 %) oxide mainly and the Fe (8 %) was also observed before the sample was tested. Figure 5.27a shows that this foam retained its original morphology after being tested. The elemental composition revealed in Figure 5.27b shows that the elemental composition had remained unchanged as the Cu (93 %) and Fe (7 %) were observed. Using SS 316 as a support for Cu oxide had a positive affect on the performance of the foam. The oxidation was specifically improved compared to the previous attempts as better selectivity towards CO_2 (88 %) was observed at lower temperature (400 °C) The results obtained were comparable to the ones reported in the literature [149].

a

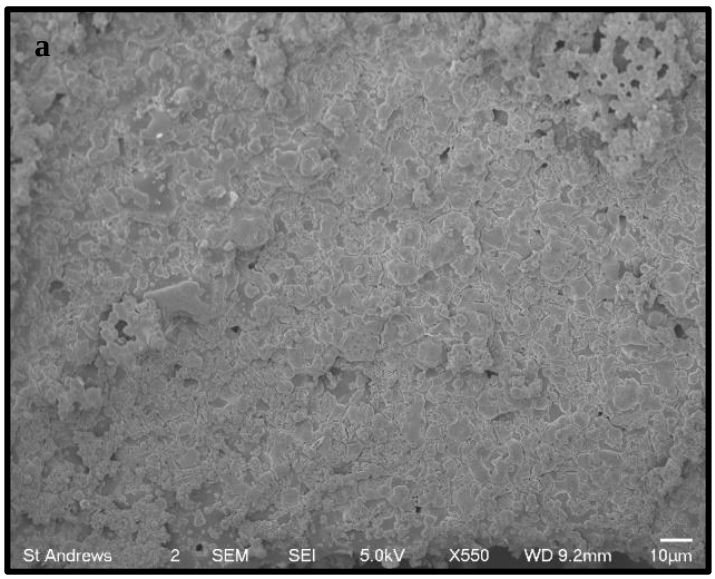

b

Element	Atomic%
Fe K	7
Cu K	93
Total	100

Figure 5.27. SEM micrograph of (a) SS 316 ox_300_1h_0.5M_ET_CuOx after catalysis, (b) EDS analysis of this sample

5.4.1.6 Oxidation of toluene with SS 316 ox_300_1h MnOx foam

Manganese oxide has extensively been used for oxidation of VOCs in the past. Keeping this in mind, Mn oxide impregnated SS 316 foam (SS 316 ox_300_1h_0.5M_ET_MnOx) was tested for the total oxidation of toluene. Figure 5.28 shows toluene conversion of 98 % was observed at 200 and at 300 °C, toluene had fully converted when SS 316 ox_300_1h_0.5M_ET_MnOx was used. The Mn oxide impregnated foam became active towards oxidation at 250 °C, this was the lowest temperature for activation of a catalyst compared to any previous attempts. The overall CO_2 production was 90 % and was first obtained at 300 °C, this stayed constant at all temperatures after this.

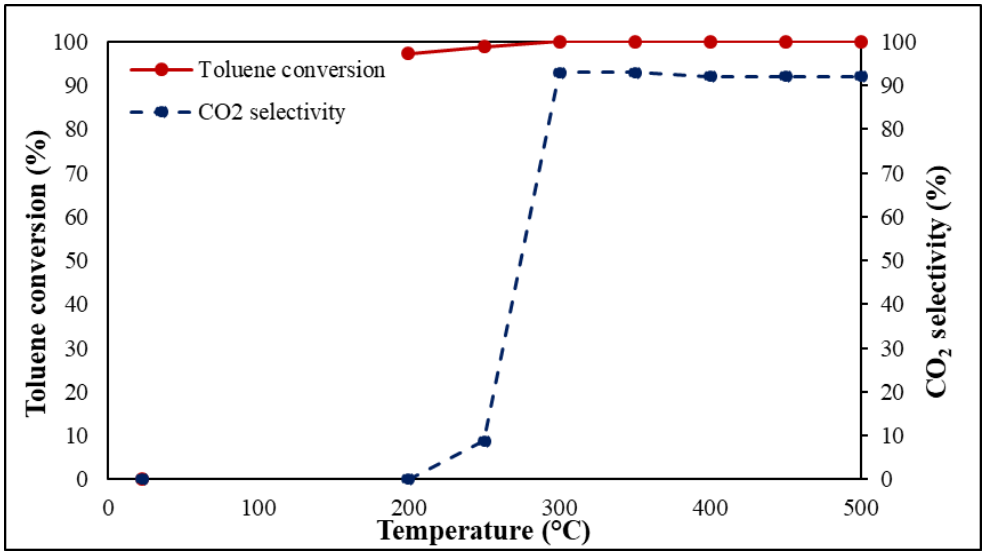

Figure 5.28. Toluene conversion and selectivity towards CO_2 over SS 316 ox_300_1h_0.5M_ET_MnOx catalyst at different temperatures

Figure 5.29a is a representative SEM micrograph of the SS 316 ox_300_1h_0.5M_ET_MnOx prior to being tested. The impregnation had worked well and could be visibly seen. This was also proven further by the elemental composition which consisted mainly of Mn (86 %) and small amount of Fe (14 %) oxide was quantified. Presence of Mn not only improved the conversion of toluene, it also increased the selectivity towards CO_2 at rather low temperatures. Figure 5.30a illustrates the sample after being used as a catalyst, the sample had a smoother overall surface which could be due to the compression from high flow of toluene

and air entering the reactor. Though it visibly looked different, the EDS analysis as shown in Figure 5.30b had almost no change in the metallic components. After being tested, Mn (83 %) and Fe (17 %) oxide were observed which was almost identical to that of the sample prior to being tested (Figure 5.29a**).** The conversion and oxidation were both better with Mn oxide impregnated foam compared to the foams that were previously tested.

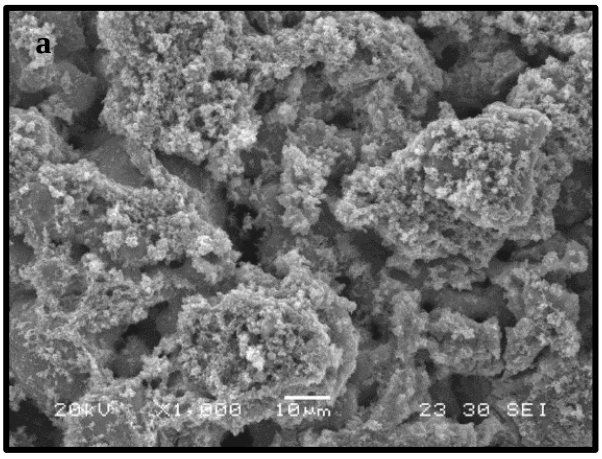

b

Element	Atomic%
Mn K	86
Fe K	14
Total	100

Figure 5.29. SEM micrograph of (a) SS 316 ox_300_1h_0.5M_ET_MnOx before catalysis and (b) EDS analysis of this sample

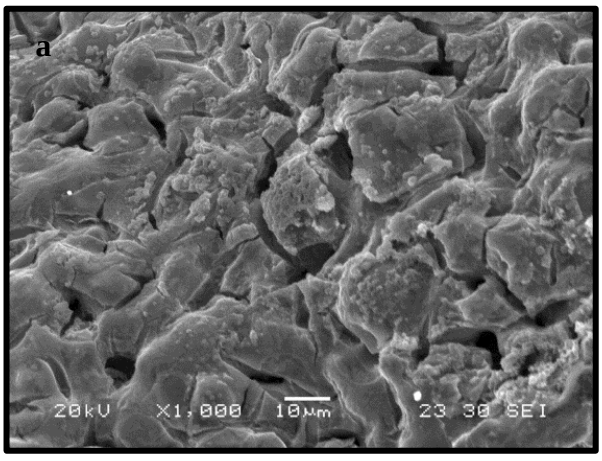

b

Element	Atomic%
Mn K	83
Fe K	17
Total	100

Figure 5.30. SEM micrograph of (a) SS 316 ox_300_1h_0.5M_ET_MnOx after catalysis and (b) EDS analysis of this sample

5.4.1.7 Oxidation of toluene with SS 316 ox_300_1h CeOx foam

Ceria is also known to be a good oxidation catalyst and has been used vastly in the past for oxidation of VOCs. Figure 5.31 shows toluene conversion and total oxidation of toluene observed when Ce ox impregnated sample (SS 316 ox_300_1h_0.5M_ET_CeOx) was tested. At 200 °C, 80 % conversion was observed which increased to 100 % at 300 °C. Interestingly, this sample was active towards total toluene oxidation even at 200 °C as a slight increase in CO_2 was observed at that temperature. The selectivity increased with an increase in temperature and overall, the highest selectivity of 88 % was observed at 400 °C.

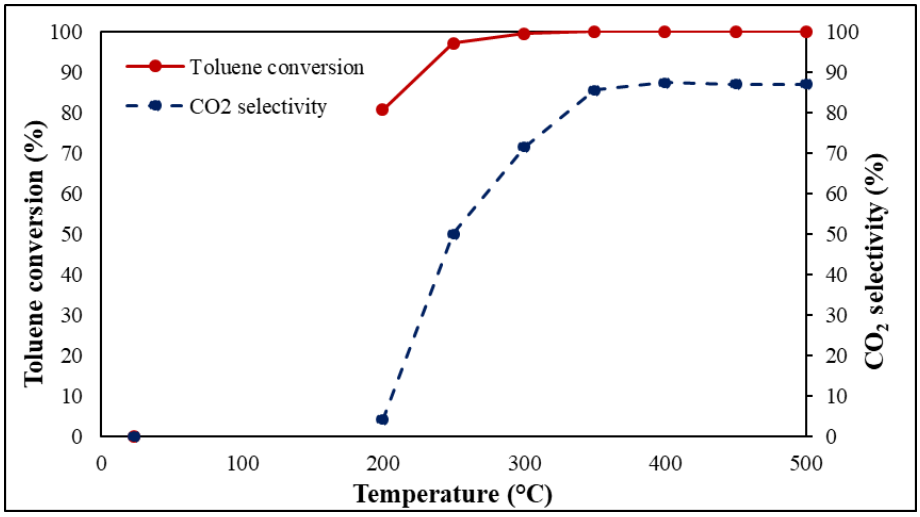

Figure 5.31. Toluene conversion and selectivity towards CO_2 over SS 316 ox_300_1h_0.5M_ET_Ce catalyst at different temperatures

Ce ox impregnated foam had a very interesting morphology. Figure 5.32a shows the foam before testing. The Ce ox impregnated had formed a thin layer on the surface of the foam which had cracks. Due to a thin layer presence, the elemental analysis picked up Fe (14 %) signal from the bulk of the material Ce (86 %) was still present in excess comparatively (Figure 5.32b). Figure 5.33a shows that the morphology had changed after the foam was tested; the top impregnated layer had agglomerated together in chunks revealing more of the oxidised foam from underneath. This can be seen from the metallic composition of the sample after being used as a catalyst in Figure 5.33b. Large presence of Fe (58 %), Cr (12 %),

Ni (8 %) alongside small amount of Ce (22 %) overall indicated that the layer top layer had perhaps detached during catalysis. The change in morphology could explain why this sample did not perform as well as other oxidation catalysts such as Mn oxide.

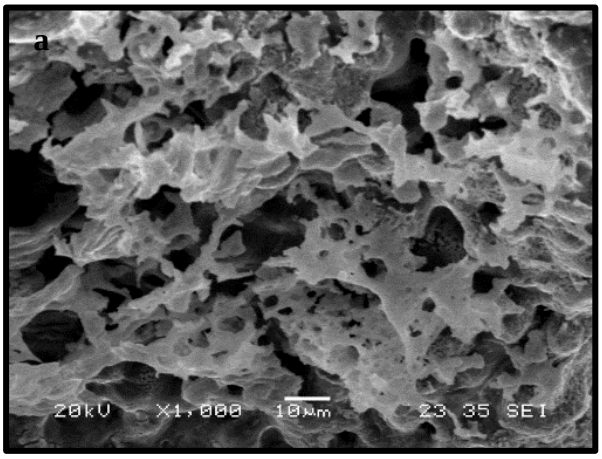

b

Element	Atomic%
Fe K	14
Ce K	86
Total	100

Figure 5.32. SEM micrograph of (a) SS 316 ox_300_1h_0.5M_ET_CeOx before catalysis and (b) EDS analysis of this sample

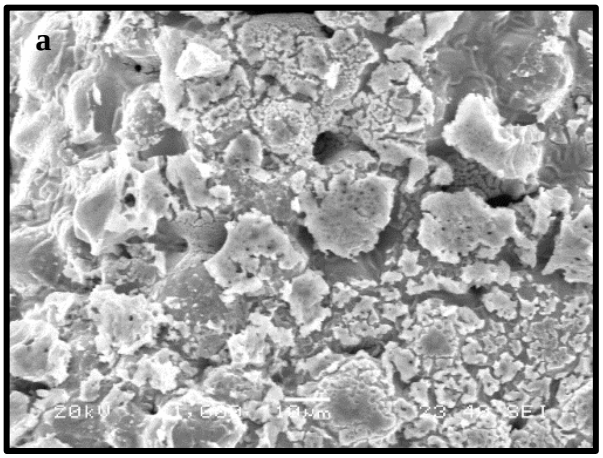

b

Element	Atomic%
Cr K	11
Fe K	59
Ni K	8
Ce K	22
Total	100

Figure 5.33. SEM micrograph of (a) SS 316 ox_300_1h_0.5M_ET_CeOx after catalysis and (b) EDS analysis of this sample

After scanning the chosen materials, it was clear that the Mn oxide impregnated foam had the best toluene conversion and selectivity towards CO_2. It was decided

that a higher wt. % loading of the Mn oxide sample would be tested so that the influence of wt % loading could also be examined. It was thought that the higher loading would cause more active sites which would therefore enhance the reactivity of the sample. As a starting point, the wt % loading was doubled.

5.4.2 Catalytic oxidation test with SS 316 ox_300_1h MnO_10wt. foam

Figure 5.34 shows toluene conversion and total oxidation over 10 wt. % Mn oxide impregnated foam (SS 316 ox_300_1h_1M_MnOx_10wt.). Previously, in the 5 wt. % SS 316 ox_300_1h_0.5M_ET_MnOx sample the overall toluene conversion of 100 % was observed at 300 °C (Figure 5.28), using more loading, the full conversion was obtained at 250 °C. The selectivity towards CO_2 was initially higher with the 10 wt. % loaded sample in both at 250 °C as 82 % of toluene had successfully oxidised compared to the previous 10 % at 250 °C. The overall selectivity towards CO_2, however, was the same in both, the 5 wt % sample and the 10 wt % samples was similar at 300 °C.

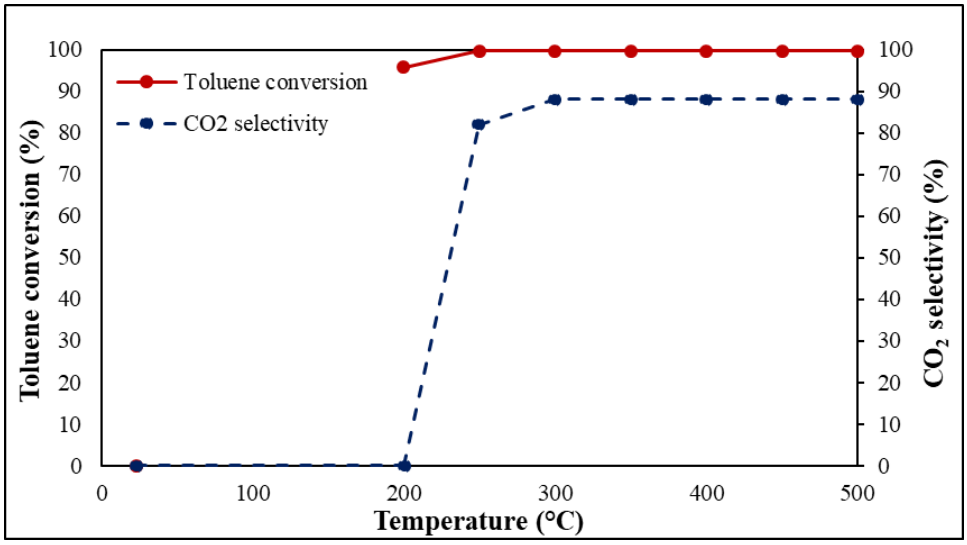

Figure 5.34. Toluene conversion and selectivity towards CO_2 over SS 316 ox_300_1h_1M_ET_MnOx_10wt. catalyst at different temperatures

Figure 5.35a depicts morphology of the foam before being tested. The morphology prior to being tested had a rough impregnated layer on the surface of the foam. This impregnation seemed to have blocked the smaller pores found with in the structure of SS 316 foam. The rough layer on top consisted of Mn oxide only which meant that this layer was thicker than the one previously obtained with lower loading as this EDS did not pick any signals from the bulk of material (Figure 5.35b). Figure 5.36a depicts that after being tested, this sample looked more like the lower loading sample (Figure 5.29a). It had regained some pores which was perhaps due to constant flow of air through the foam at constant speed. The elemental composition after being tested as depicted in Figure 5.36b of Mn (89 %) and Fe (11 %)

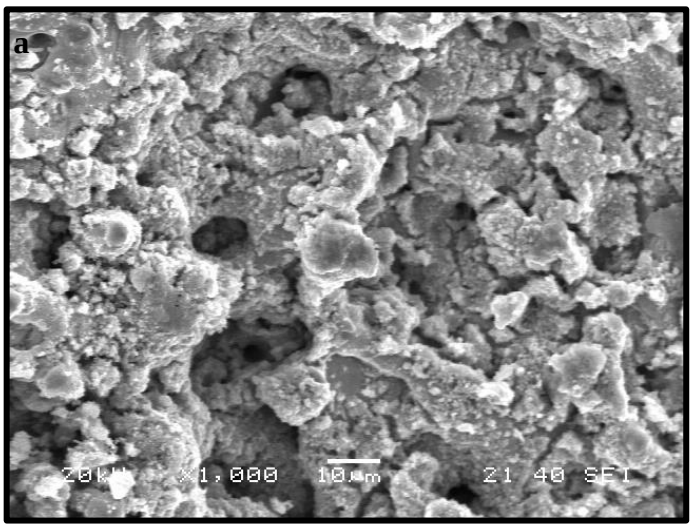

b

Element	Atomic%
Mn K	100
Total	100

Figure 5.35. SEM micrograph of (a) SS 316 ox_300_1h_1M_ET_MnOx_10wt before catalysis and (b) EDS analysis of this sample

a

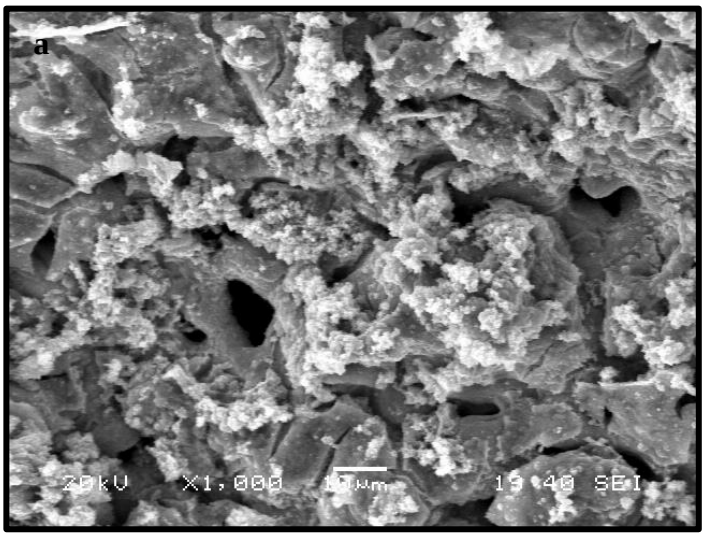

b

Element	Atomic%
Mn K	100
Total	100

Figure 5.36. SEM micrograph of (a) SS 316 ox_300_1h_1M_ET_MnOx_10wt. after catalysis and (b) EDS analysis of this sample

It was found that increasing the loading of the metal oxide did not affect the performance of the catalyst as much in the reaction conditions that were being used therefore no further modification were made on the morphology of the foam. The final test carried out with the SS 316 foams for toluene oxidation was the stability test of the best sample, in this case, 5 wt. % Mn ox impregnated sample was tested for 8 hours duration.

5.4.3 Long term testing with SS 316 ox_300_1h MnOx foam

For the long-term test, the reactor temperature was increased to 300 °C as this was the temperature that the SS 316 ox_300_1h_0.5M_ET_MnOx sample was most active towards conversion and oxidation of toluene. An 8-hour flight representative time at 300 °C was used for this experiment. Figure 5.37 depicts that the SS 316 impregnated with Mn ox was stably selective towards CO_2 production for the 8 hours interval. The CO_2 production remained constant throughout the experiment.

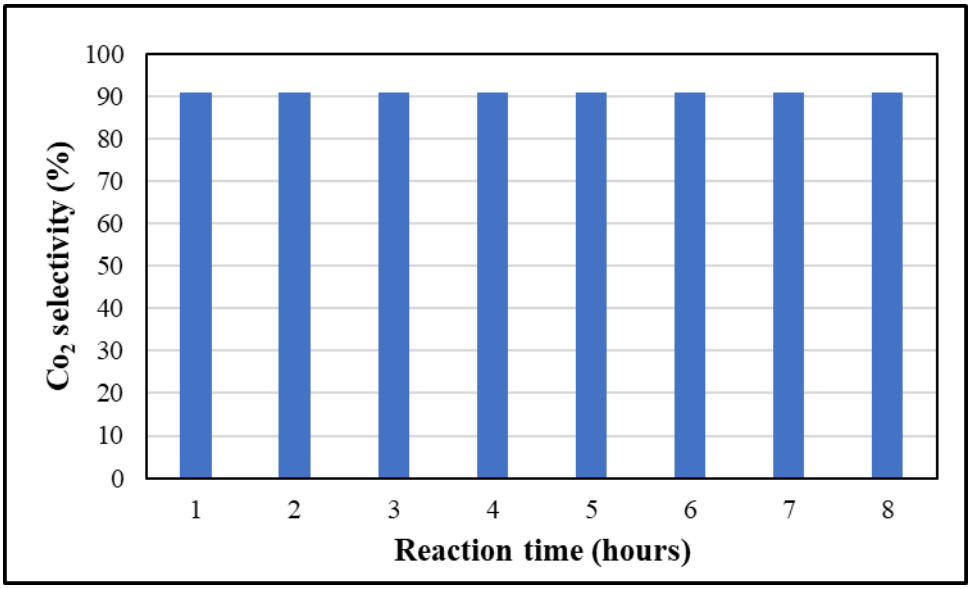

Figure 5.37. Toluene conversion and selectivity towards CO_2 over SS 316 ox_300_1h_1M_ET_MnOx for 8 hours at 300 °C

Figure 5.38a and 5.38b shows the morphology of the foam before and after being tested for 8 hours. It can be clearly seen that there was no change in the morphology. Previously, after being tested, the SS 316 ox_300_1h_0.5M_ET_MnOx sample had a smooth layer on the surface (Figure 5.29a) however, this was not the case observed. This change could be attributed to the reactor temperature being lower, the change previously observed was after the sample had been in the reactor at 500 °C. The good conversion, selectivity and stability observed with the MnO impregnated sample illustrated that this could be potentially used as a catalyst for oxidation of toluene.

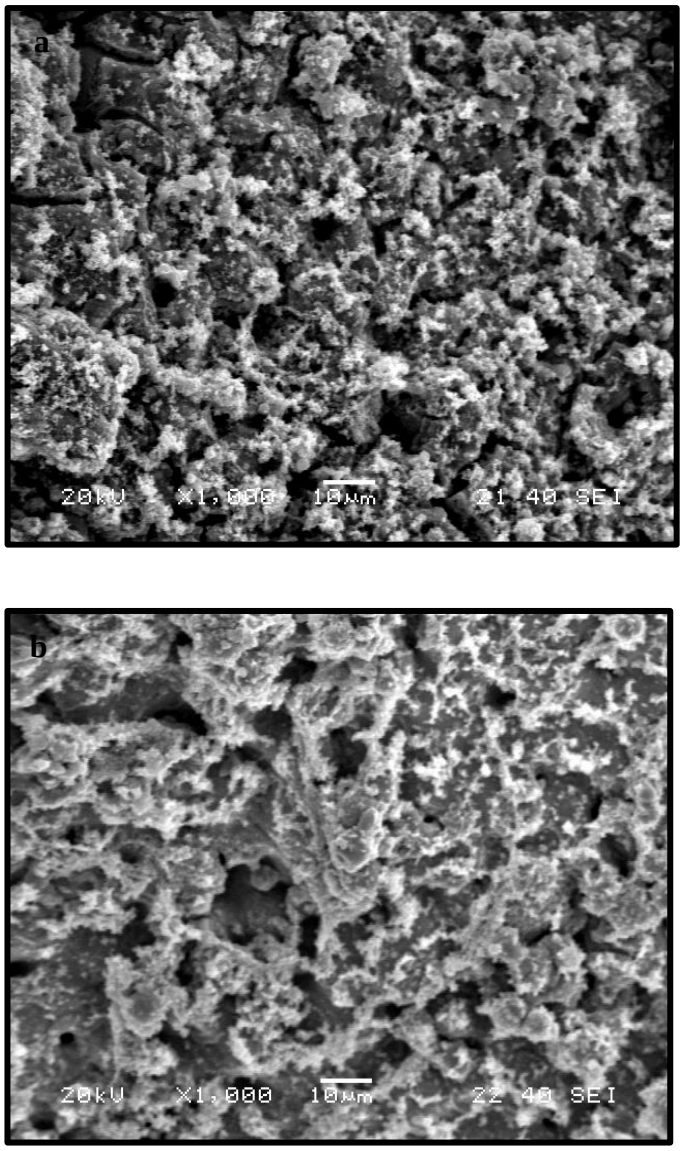

Figure 5.38. SEM micrograph of (a) SS 316 ox_300_1h_0.5M_ET_MnOx foam before long term catalysis and (b) after catalysis

5.5 Chapter summary

Overall in this chapter, different SS 316 raw/oxidised/impregnated foams were tested for total oxidation of toluene. The first optimisation was carried out in the oxidation step where a rough layer was required to get better metal nitrates impregnation on the surface of the foams. Oxidation at 300 °C for 1 h resulted in a positive outcome and was used as a substrate for impregnation of different metal nitrates to obtain oxides on the surface. The metal oxides (Fe, Ni, Cu, Mn and Ce) were chosen based on their previous good performance as oxidation catalysts. For impregnation, substrate and solution composition were modified to get the best outcome. It was found that ethanol and terpineol were ideal to be used as solvents as these gave good coverage of metal oxides on the surface. The before and after catalysis elemental enrichment of SS 316 foams has been summarised in Table 5.2.

Table 5.2. Elemental enrichment for SS 316 foams

Element	Raw SS 316		750_1h SS 316		Feox SS 316		Ni ox SS 316	
	Before	After	Before	After	Before	After	Before	After
Cr K	18	18	8	17	18	16		
Fe K	71	68	87	73			9	8
Ni K	11	14	5	10	82	84	91	92

	CuOx SS 316		MnOx SS 316		CeOxox SS 316	
Element	Before	After	Before	After	Before	After
Ce K	-	-	-	-	86	22
Cu K	7	93	-	-	-	-
Fe K	7	93	14	17	14	59
Mn K	-	-	86	83	-	-
Ni K	-	-	-	-		11

From the impregnated samples, SS 316 ox_300_1h impregnated with Mn oxide (5 wt. %) had the best conversion of toluene (100 %) and selectivity towards CO_2 (90 %) at 300 °C. This combination occurred at the lowest temperature compared to other metal oxides. Attempts of increasing loading were made however, this did not result in any improved results. The Mn ox (5 wt. %) was tested for an 8-hour flight representation at 300 °C and the results showed that this catalyst was stable throughout therefore, it could potentially be used for oxidation of toluene.

Characterisation and catalytic testing of SS 316 foams for ethyl acetate

6.1 Chapter overview

From previous results, it was clear that the SS 316 foam had good potential to be used as an oxidation catalyst. The attempts with toluene had shown a positive outcome. Toluene was a conjugated hydrocarbon system and to increase the scope of the work, it was decided that an ester would also be tested. Ethyl acetate was chosen as an ester to see how well the same catalysts would work with a non conjugated system containing oxygens. Ethyl acetate in the past has been found in the cabin air of the aircraft therefore, the decomposition of it was studied with SS 316 foams. The SS raw and impregnated foams were chosen based on toluene oxidation. The foam oxidised at 750 °C was not tested for ethyl acetate as it did not have a positive oxidation outcome. Raw foam was tested however, to keep comparison between impregnated and un-impregnated foams.

6.2 Catalytic testing for oxidation of ethyl acetate

To begin with, a blank experiment was carried out. The rig in this case was modified to dilute the air containing ethyl acetate with fresh air. In this case, lower temperatures of 50-100 °C were also examined. This was done because ethyl acetate has a lower boiling point than toluene and autoignition temperature of 410 °C therefore, the maximum testing temperature was 400 °C.

6.2.1 Blank experiment

Figure 6.1 depicts the change in conversion of ethyl acetate. As the temperature increased, so did the conversion. Starting at 40 % at 50 °C, this gradually increased to 95 % at the maximum operating temperature. There was no CO_2 produced at any stage, instead qualitatively signals for m/z 15 (molecular ion peak for CH_4), 27 (molecular ion peak for C_2H_4), 31 (molecular ion peak for CH_3OH, OCH_4) and 42 (molecular ion peak for C_3H_6) were produced. As the main quantitative product was

of CO_2 and none was produced at any temperature, it was clear that oxidation of ethyl acetate if any, would occur between the temperature tested would be due to the presence of a catalyst.

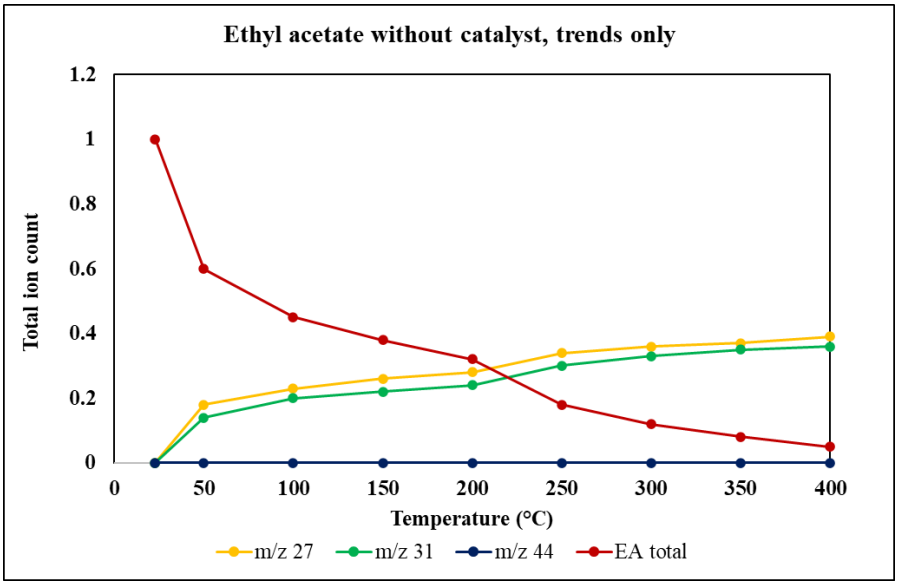

Figure 6.1. Ethyl acetate conversion and selectivity towards CO_2 over different temperatures without a catalyst

After blank experiment, the next experiment was conducted under same conditions in the presence of SS 316 raw foam.

6.2.2 Oxidation of ethyl acetate with SS 316 raw foam

Figure 6.2 shows the trends observed when SS 316 raw foam was introduced in the reactor. The conversion of ethyl acetate even in the presence of a raw catalyst, followed the same trend as before, starting at 38 % at room temperature and gradually increased to 100 % at maximum operating temperature. Ethyl acetate can convert into acetic acid which cokes the catalyst, this can explain the initial slow increase in conversion of ethyl acetate. Eventually, at slightly increased temperatures, the acetic acid starts to break down resulting in an increase in conversion [159].

Qualitatively, products of m/z 27 (molecular ion peak for C_2H_4) and 31 (molecular ion peak for CH_3OH, OCH_4) were observed however, the catalyst became active towards oxidation at 300 °C and an increase in CO_2 (2 %) was observed. This

gradually increased to 6 % at 350 °C and a huge increase in CO_2 (66 %) was observed at 400 °C. Alongside CO_2, methanol was observed as a by-product. As methanol was not quantified, it is possible that there was carbon deposition which can explain lower than 100 % CO_2 selectivity in all oxidation cases. Though the catalyst did not affect the conversion of ethyl acetate, it improved the overall selectivity towards CO_2. Such positive outcome meant that the SS 316 foams could potentially be used as oxidation catalysts for esters also.

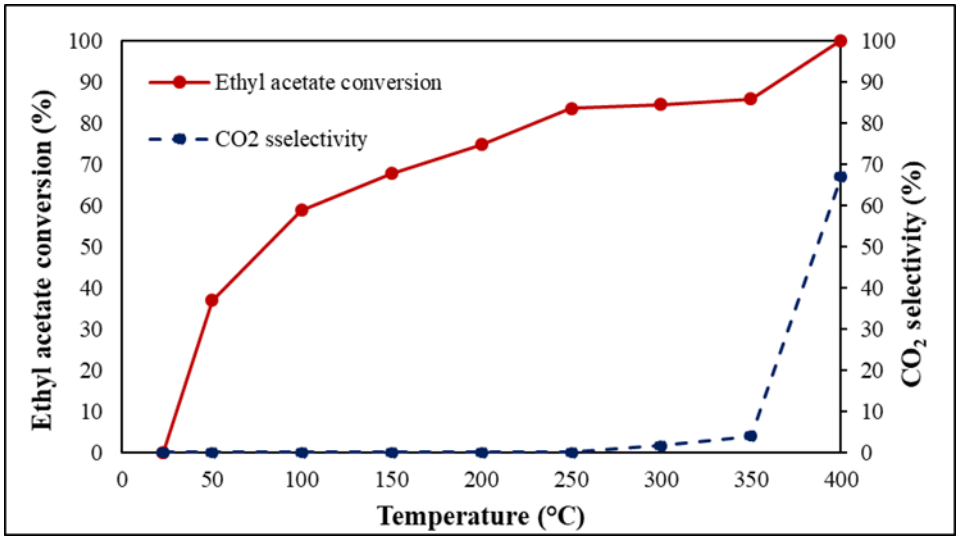

Figure 6.2. Ethyl acetate conversion and selectivity towards CO_2 over different temperatures with SS 316 raw catalyst

Figures 6.3a and 6.3b show the morphology and elemental composition of the foam before being used in the reactor. SS 316 raw had a smoother surface compared to the SS 316 raw (Figure 5.2) used previously, this could just be due to the previous foam being more oxidised at room temperature. The rest of the metallic composition was the same as seen before. Fe (71 %), Cr (16 %) and Ni (13 %) were all 2-3 +/- error of the instrument. Figures 6.4a and 6.4b represent the morphology and elemental composition of the foam after it was tested. It seemed that the foam had oxidised in the reaction conditions as some islands were formed on the surface compared to the smooth surface observed before (Figure 6.3a). The other indicator of oxidation was the increased O content revealed by the EDS analysis of before (16 %) and after samples (28 %) was indictive of formation of rich oxide layer. The

contents Fe (76 %) and Cr (19 %) had increased whereas Ni (5 %) had decreased indicating that Fe and Cr were contributing to the catalytic activity observed. The SS 316 raw sample was successful in oxidising 66 % of the ethyl acetate to CO_2 at 400 °C. The main by product of m/z 27 ($C_2H_3^+$) was observed alongside CO_2.

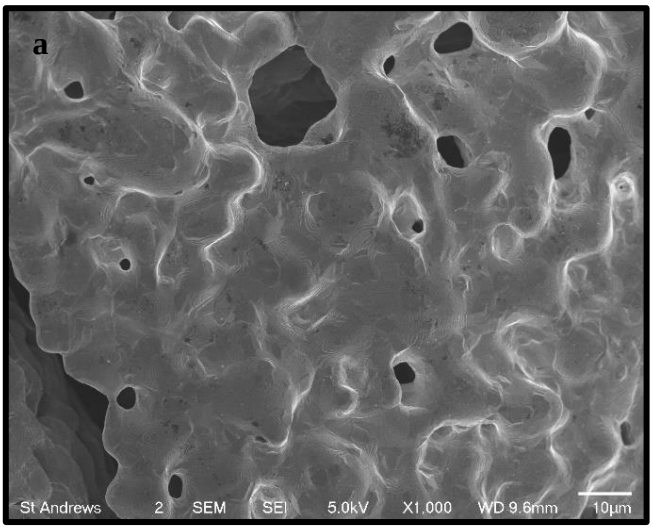

b

Element	Atomic%
Cr K	15
Fe K	71
Ni K	14
Total	100

Figure 6.3. SS 316 raw (a) prior to being tested and (b) the EDS composition of the foam

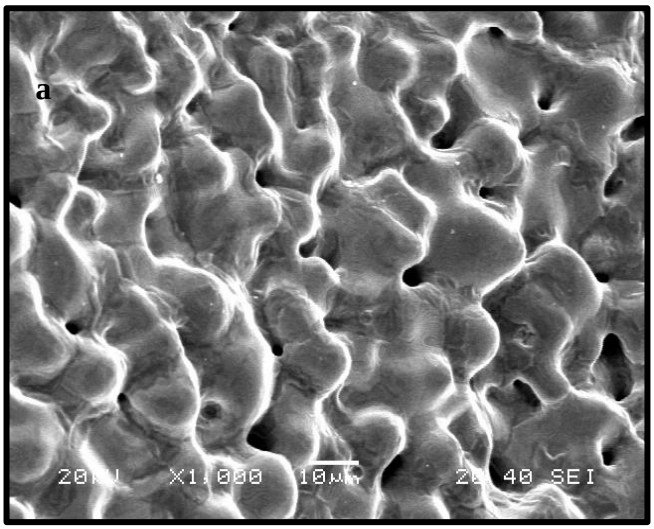

b

Element	Atomic%
Cr K	19
Fe K	76
Ni K	5
Total	100

Figure 6.4. SS 316 raw (a) after being tested and (b) the EDS composition of the foam

6.2.3 Oxidation of ethyl acetate with SS 316 Fe ox impregnated foam

Figure 6.5 depicts the change in conversion and selectivity towards oxidation product in the presence of SS 316 imp_Fe ox sample. The conversion followed the same trends as the ones observed previously (Figure 6.1 and 6.2 respectively). At the start 40 % conversion was observed at 50 °C which eventually increased to 100 % at 350 °C. Similar qualitative products of m/z 27 and 31 were observed. This sample became active towards oxidation at 250 °C which eventually increased to 80 % at 350 °C. Alongside CO_2, qualitatively, methanol was also observed. Carbon deposition can also be a possible explanation of lower selectivity towards CO_2.

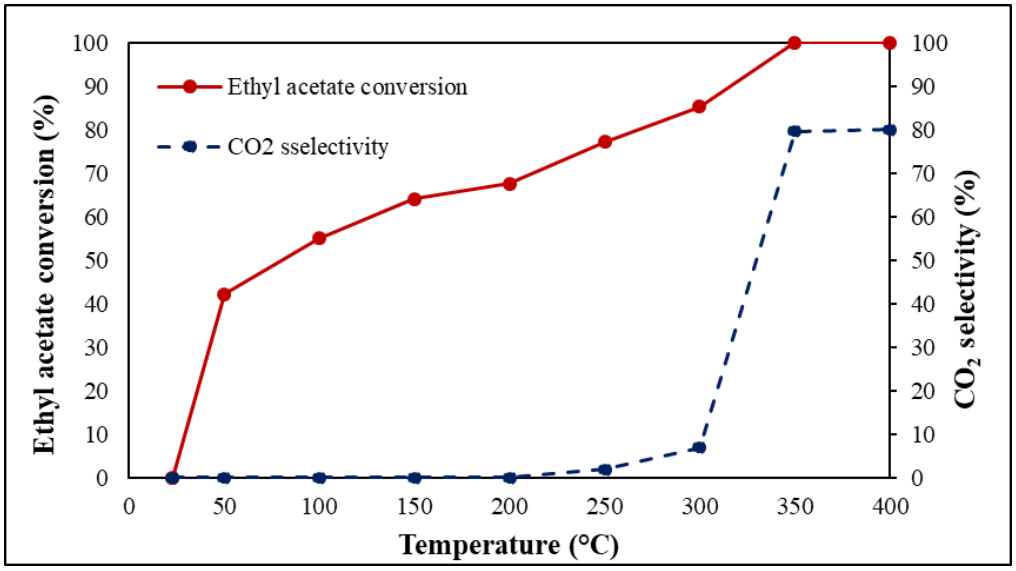

Figure 6.5. Ethyl acetate conversion and selectivity towards CO_2 over different temperatures with SS 316 imp_Fe ox foam

Figures 6.6a and 6.6b depict the morphology and EDS elemental composition of the foam before catalysis. The catalyst prior to being tested had a rough oxide layer on the surface which was metallically rich in Fe (78%) and Cr (22 %). This was similar to that of the SS 316 ox_300_1h_0.5M_ET_FeOx (Figure 5.21c). Figure 6.7a shows that the top impregnated layer had become smoother after being tested. This could be due to the compression from the air fed into the reactor or the oxidation of the substrate. Figure 6.7b illustrates that after being tested, the elemental composition had remained very similar to the pre catalysis sample. Fe

(82 %) and Cr (18 %) were present metallically indicating similarity in the elemental composition and stability of the foam.

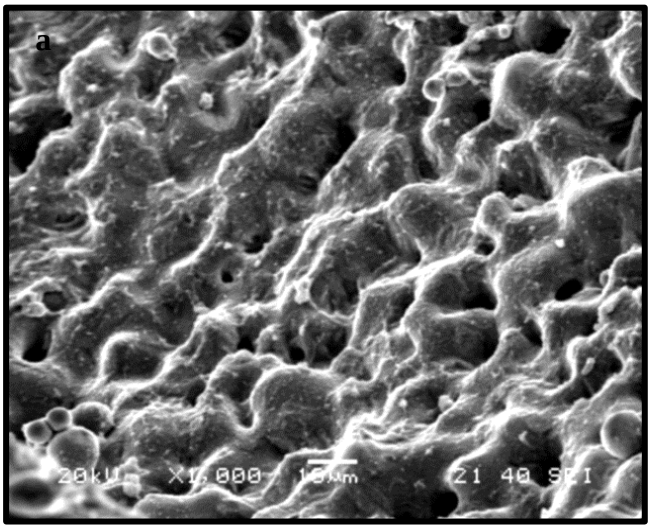

b

Element	Atomic%
Cr K	22
Fe K	78
Total	100

Figure 6.6. SS 316 imp_Fe ox (a) prior to being tested and (b) the EDS composition of the foam

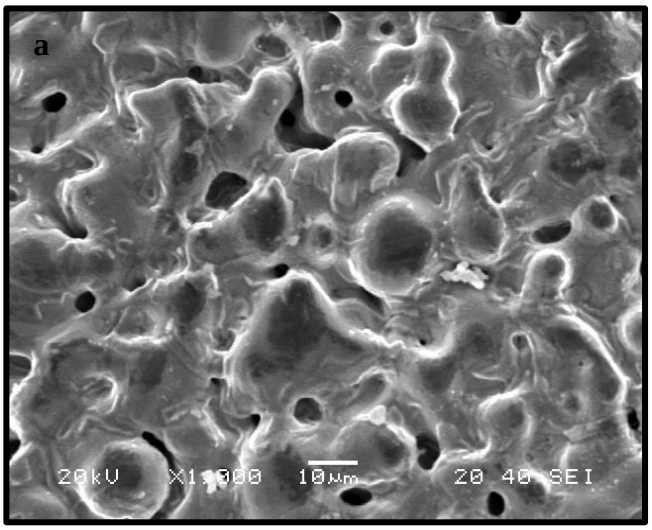

b

Element	Atomic%
Cr K	18
Fe K	82
Total	100

Figure 6.7a. SS 316 imp_Fe ox (a) after being tested and (b) the EDS composition of the foam

6.2.4 Oxidation of ethyl acetate with SS 316 Ni ox impregnated foam

Figure 6.8 demonstrates the conversion and oxidation trends observed at different temperatures in the presence of SS 316 imp_Ni ox foam. The conversion in this case at 50 °C was lower (28 %) compared to previously observed (approx. 40 %) with or without the catalyst (Figures 6.1, 6.2, 6.5). The overall conversion of 100 % however was observed at 300 °C, this temperature was lower than previous samples SS 316 raw or SS 316 imp_Fe ox samples (Figures 6.2 and 6.5 respectively). This foam became active towards oxidation at 250 °C, 73 % selectivity was observed at 300 °C which increased to 75 % at the highest operating temperature of the reactor. Prior to oxidation, same products were formed as observed in the case of raw and Fe ox samples.

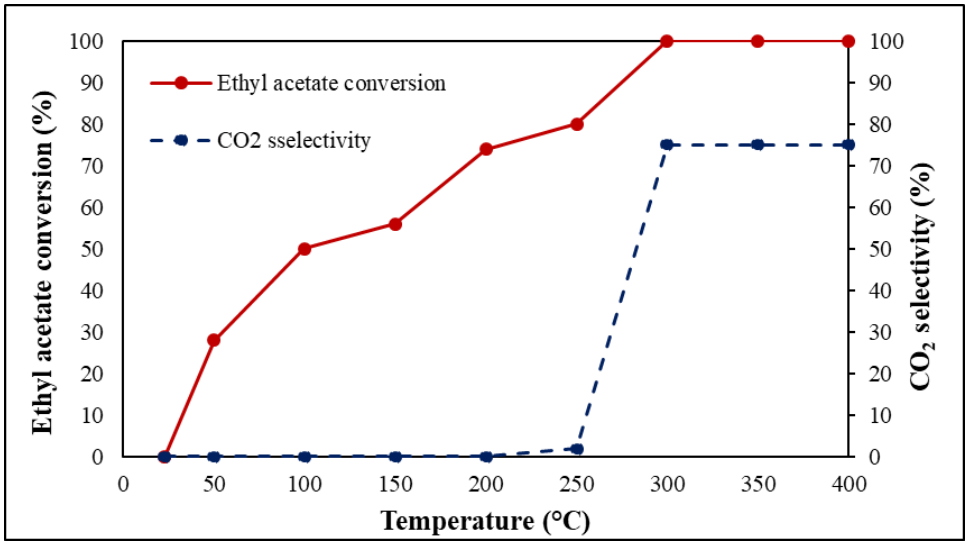

Figure 6.8. Ethyl acetate conversion and selectivity towards CO_2 over different temperatures with SS 316 imp_Ni ox foam

Figures 6.9a and 6.9b demonstrate the morphology, alongside the elemental composition of the catalyst prior to being tested. Ni oxide previously (Figure 5.23a) formed a conjugated thick layer on the surface of the substrate and this was the case again when the impregnation was repeated (Figure 6.9a). A full EDS spectral analysis was carried out which revealed presence of mixed oxides. Metallically, a high presence of Ni (78 %) alongside some Fe (18 %) and Cr (4 %) from the bulk were observed. Figures 6.10a and 6.10b represent morphology and EDS analysis of the sample after catalysis. Both, the surface and the metallic composition of Ni (74

%), Fe (17 %) and Cr (9 %) had remained similar to that of the sample before testing.

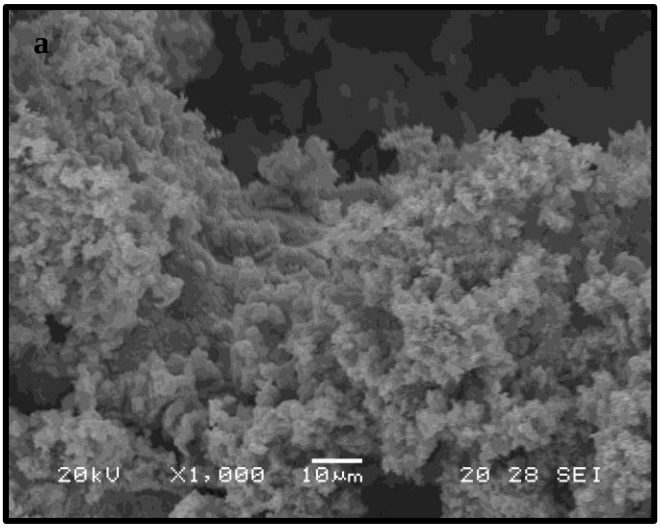

b

Element	Atomic%
Cr K	4
Fe K	18
Ni K	78
Total	100

Figure 6.9. SS 316 imp_Ni ox (a) prior to being tested and (b) the EDS composition of the foam

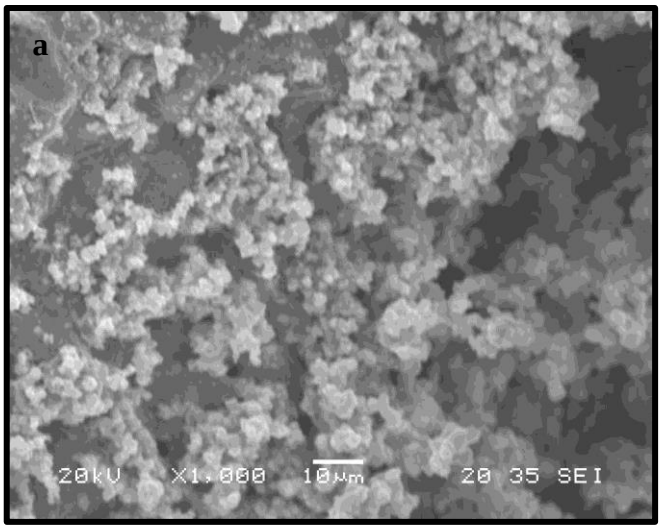

b

Element	Atomic%
Cr K	9
Fe K	17
Ni K	74
Total	100

Figure 6.10. SS 316 imp_Ni ox (a) after being tested and (b) the EDS composition of the foam

6.2.5 Oxidation of ethyl acetate with SS 316 Cu ox impregnated foam

Figure 6.11 illustrates the change in ethyl acetate conversion and oxidation in presence of SS 316 imp_Cu ox foam. The conversion of 40 % was observed at 50 °C which gradually increased to 70 % at 250 °C and finally to 100 % at 300 °C. This foam became active towards selectively producing CO_2 at 300 °C, at this temperature 88 % selectivity towards CO_2 was observed. Unlike the previous samples, in this case there was a sharp overall increase in production of CO_2 rather than a gradual increase. After 300 °C, the conversion and selectivity stayed constant until the highest operating temperature.

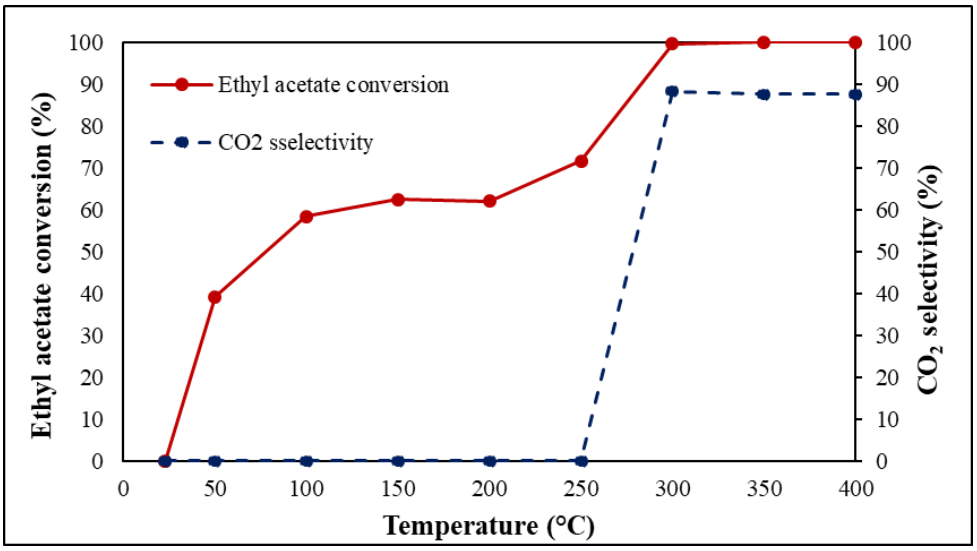

Figure 6.11. Ethyl acetate conversion and selectivity towards CO_2 over different temperatures with SS 316 imp_Cu ox foam

Figure 6.12a and b depict the morphology and elemental composition of the SS 316 imp_Cu ox sample prior to being used as a catalyst. This sample had impregnated regions and some of the support substrate was also visible. For elemental analysis, point ID was not used as it was already understood that the smoother regions were from the pre oxidised material. The metallic composition consisted of Cu (90 %) from the impregnation and Fe (7 %), Cr (3 %) from the bulk of the material. Figure 6.13a demonstrates that after being used as a catalyst, there were no drastic changes in the morphology of the foam. The foam had oxidised under the reaction conditions as indicated by the increase in O, the metallic composition, however, was rather similar. Figure 6.13b shows the elemental composition of the foam after being

tested, metallically, Cu (84 %), Fe (14 %) and Cr (2 %) were still present in the same amounts. This indicated that the foam was able to stay intact under the reaction conditions.

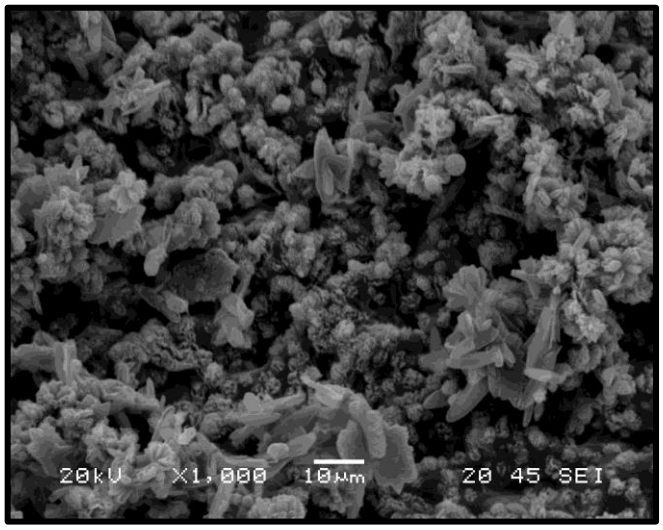

b

Element	Atomic%
Cr K	3
Fe K	7
Cu K	90
Total	100

Figure 6.12. SS 316 imp_Cu ox (a) before being tested and (b) the EDS composition of the foam

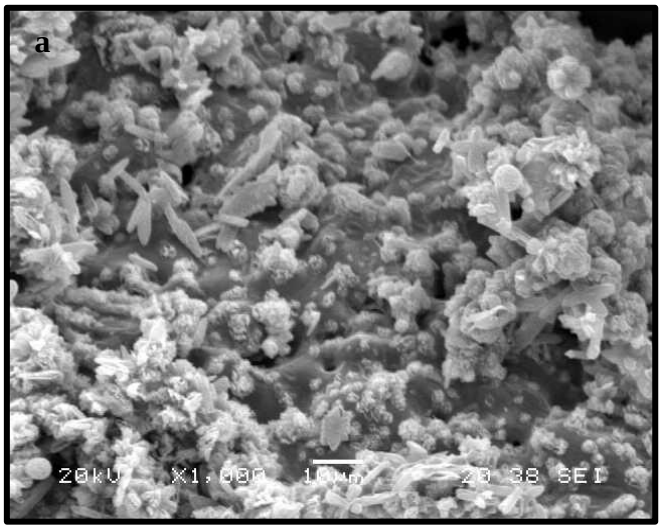

b

Element	Atomic%
Cr K	2
Fe K	14
Cu K	84
Total	100

Figure 6.13. SS 316 imp_Cu ox (a) after being tested and (b) the EDS composition of the foam

6.2.6 Oxidation of ethyl acetate with SS 316 Mn ox impregnated foam

Previous tests with toluene revealed that the Mn ox was most suited for the oxidation and conversion of toluene. Figure 6.14 shows trends observed when SS 316 imp_Mn ox sample was placed in the reactor. The conversion followed the same trend as of the Ni ox sample (Figure 5.8) as 20 % conversion was observed at 50 °C. This eventually increased to 100 % at 300 °C. This foam became active towards oxidation of ethyl acetate at 250 °C which increased to 72 % overall at 300 °C. This was constant at all higher operating temperatures.

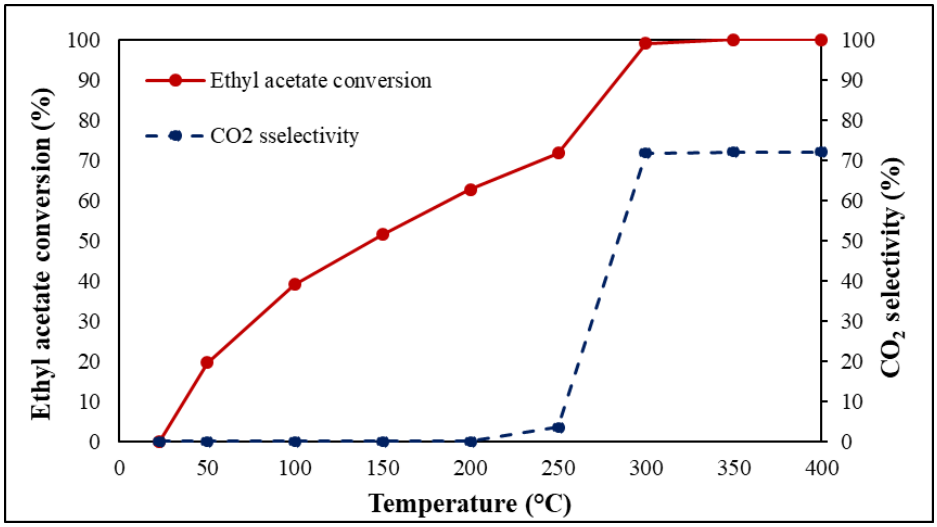

Figure 6.14. Toluene conversion and selectivity towards CO_2 over different temperatures with SS 316 imp_Mn ox foam

Figure 6.15a and 6.15b represent the morphology and elemental composition of the foam before being tested. The morphology of the foam before testing was seen to be rough on top which was the impregnated Mn oxide and the smoother regions underneath belonged to the oxidised foam which was used as a substrate for dip coating. The overall elemental composition as shown in Figure 6.15b consisted of Mn, Fe, Cr, Ni and O. Metallically, Mn (80 %) was found in excess, signals of Fe (14 %), Cr (4 %) and Ni (2 %) were picked from the substrate. Figure 6.16a and 6.16b shows the morphology and the elemental analysis the sample after being used in the reactor. Post catalysis, it can be seen that the top layer had become smooth. Though the morphology had changed, this was not surprising as this was previously seen in the case of toluene oxidation (Figure 5.30a). The elemental composition as shown in Figure 6.16b consisted of the same elements Mn, Fe, Cr, Ni and O.

Quantitively in terms of the metallic content, Mn (88 %) and Fe (12 %). The foam had successfully stayed intact during the process of oxidation of ethyl acetate. The overall selectivity of 72 % was lower than the 88 % of SS 316 imp_Cu (Figure 6.11). It was expected that the Mn oxide impregnated SS 316 would work better as that was the trend followed by toluene however, this change shows that the Cu oxide impregnated sample worked better at oxidising a linear ester than a conjugated hydrocarbon.

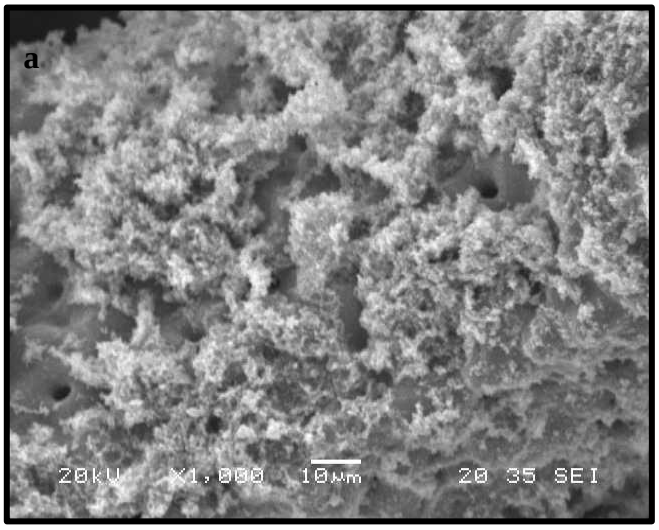

b

Element	Atomic%
Cr K	4
Mn K	80
Fe K	14
Ni K	2
Total	100

Figure 6.15. SS 316 imp_Mn ox (a) before being tested and (b) the EDS composition of the foam

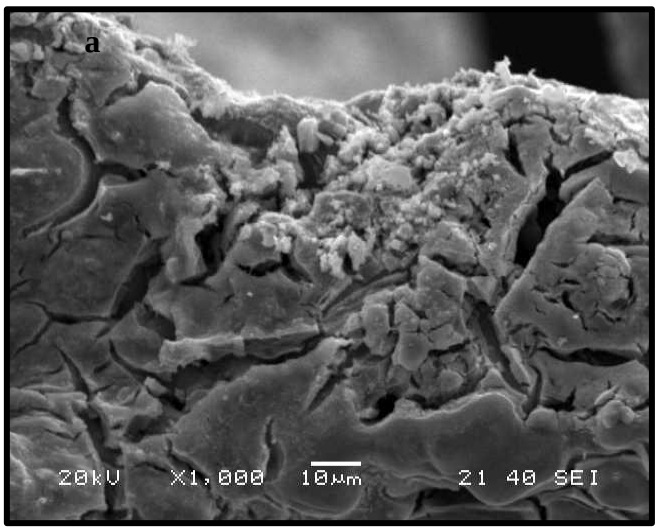

b

Element	Atomic%
Mn K	88
Fe K	12
Total	100

Figure 6.16. SS 316 imp_Mn ox before (a) after tested and (b) the EDS composition of the foam

6.2.7 Oxidation of ethyl acetate with SS 316 Ce ox impregnated foam

The final foam tested for oxidation of ethyl acetate was SS 316 imp_Ce ox foam. Figure 6.17 illustrates changes observed in conversion and selectivity towards oxidation as Ce ox impregnated foam was introduced into the reactor. The conversion at the start was low (20 %) at 50 °C which then gradually increased with increasing reactor temperature and 100 % conversion was observed at 250 °C. This was the lowest temperature for conversion compared to all the previous catalysts that were scanned. This catalyst became active towards oxidation of ethyl acetate at 250 °C. An overall 74 % selectivity towards CO_2 was observed at 250 °C. There was a very small decrease after this point however, it was very small so did not impact the selectivity.

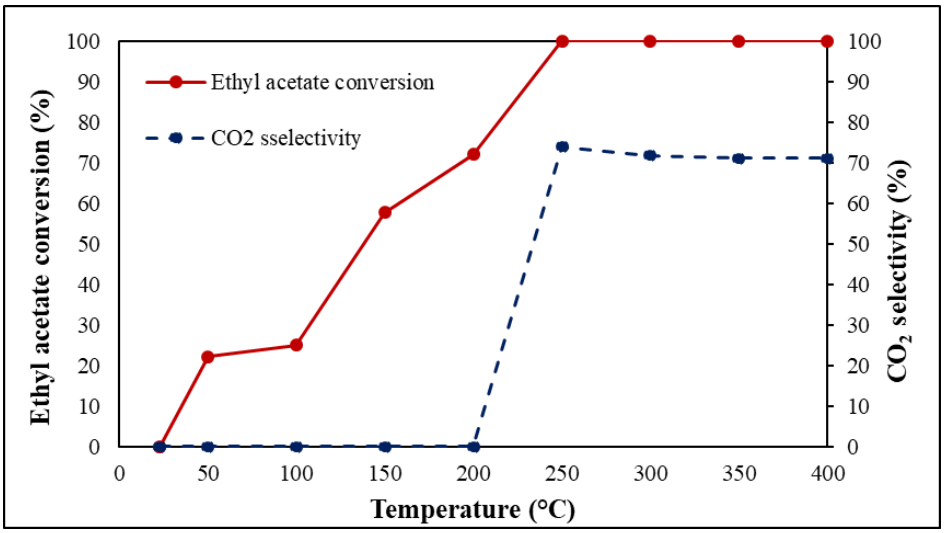

Figure 6.17. Ethyl acetate conversion and selectivity towards CO_2 over different temperatures with SS 316 imp_Ce ox foam

Figure 6.18a and 6.18b depict morphology and the elemental composition of the SS 316 foam imp_Ce ox foam prior to being tested. Ce ox impregnation resulted in a flaky layer being observed at the top of the foam. The overall elemental composition consisted of Ce, Fe, Cr, Ni and O as shown in Figure 6.18b. In terms of the metallic content, Ce (65 %) was detected due to impregnation whereas the Fe (21 %), Cr (11 %) and Ni (3 %) were picked up from the substrate used for impregnation. Figure 6.19a and 6.19b represent the morphology and elemental composition of the SS 316 imp_Ce ox after being tested. It can be seen that the surface of the foam had not

changed after being in the reactor as scattered impregnated regions can be observed in Figure 6.19a. The elemental composition as shown in Figure 6.19b also consisted of the same elements Ce, Fe, Cr, Ni and O. In terms of the metallic components, Ce (52 %), Fe (35 %), Cr (9 %) and Ni (4 %) all stayed similar as before the oxidation.

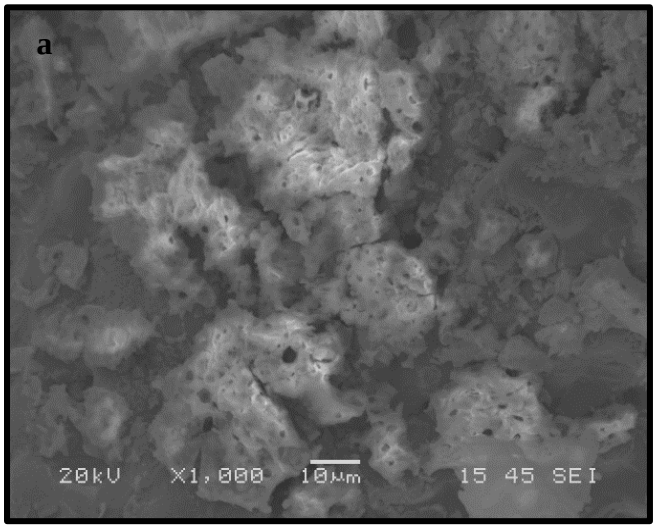

b

Element	Atomic%
Cr K	11
Fe K	21
Ni K	3
Ce L	65
Total	100

Figure 6.18. SS 316 imp_Ce ox (a) before being tested and (b) the EDS composition of the foam

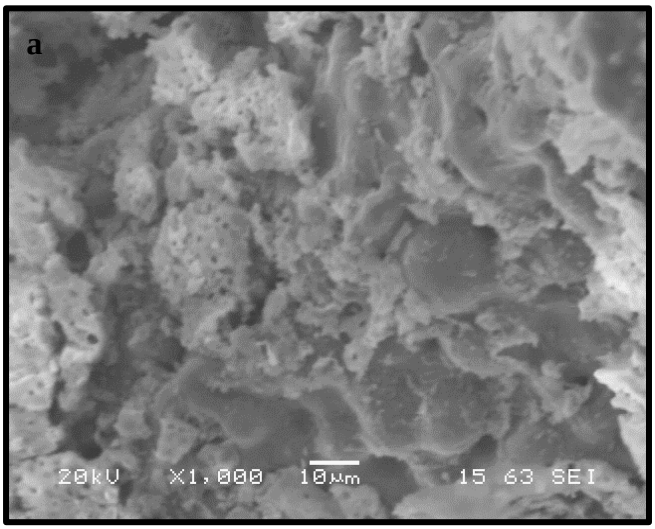

b

Element	Atomic%
Cr K	11
Fe K	35
Ni K	4
Ce L	50
Total	100

Figure 6.19. SS 316 imp_Ce ox (a) after being tested and b) the EDS composition of the foam

6.3 Chapter summary

To conclude, SS 316 foams have been tested for conversion and oxidation of ethyl acetate. The main product observed alongside CO_2 which was qualitatively observed was of m/z 27 ($C_2H_3^+$). The before and after catalysis elemental enrichment of different SS 316 foams has been summarised in Table 7.1.

Table 7.1. Elemental enrichment summary of SS 316 foams with ethyl acetate

	Raw SS 316		FeOx SS 316		NiOx SS 316	
Element	**Before**	**After**	**Before**	**After**	**Before**	**After**
Cr K	15	19	22	18	4	9
Fe K	71	76	78	82	18	17
Ni K	14	5			78	74

	CuOx SS 316		MnOx SS 316		CeOx SS 316	
Element	**Before**	**After**	**Before**	**After**	**Before**	**After**
Ce K	-	-	-	-	65	
Cr K	3	2	4		11	11
Cu K	90	84	-	-	-	-
Fe K	7	14	14	12	21	35
Mn K	-	-	80	88	-	-
Ni K	-	-	2	-	3	4

Different catalysts were active towards conversion and oxidation of ethyl acetate at different temperatures. From the scanned catalysts, SS 316 impregnated with Ce oxide was successful in converting 100 % ethyl acetate at the lowest temperature of 250 ℃ whereas the highest selectivity of 88 % towards oxidation was obtained with SS 316 impregnated with Cu oxide at 300 ℃. SS 316 impregnated Mn oxide was previously the best oxidation catalyst as well as for conversion however, in this case this, the selectivity of 72 % was obtained which meant it had not performed as well, this catalyst was more ideal for a conjugated system rather than a linear system. Overall, in terms of conversion and oxidation the impregnated SS 316 Cu oxide foam gave satisfying results with 100 % conversion and 88 % selectivity towards CO_2 at 300 ℃. which meant that this could also be potentially used in the application.

Synthesis and catalytic testing of $MnFeCrO_4$ and $MnNiCrO_4$ spinels

7.1 Chapter overview

Various studies have been published on the synthesis, electrical properties and applications of spinel oxides. This chapter investigates the synthesis of spinels *via* solution combustion synthesis. The prepared materials were reduced in different conditions, such as, temperature, dwell times and the type of reducing environment. There were two main compositions of spinels which were synthesised, $MnFeCrO_4$ and $MnNiCrO_4$. The $MnFeCrO_4$ were reduced for 2, 20 and 50 hours in tube furnace under 5 % H_2/Ar at 950 °C. Reduction for 2 hours was also conducted in a vacuum furnace for comparison. The reduced samples were taken out of the furnace and were then placed into the reactor so were exposed to air prior to being tested. Reduction was carried out to achieve metallic Fe on the surface of the spinels. The concept was then to etch the metal from the surface with acid which would leave a porous support spinel oxide structure, similar to that seen in the case of SS foams. The porous scaffold could be impregnated with various active materials depending upon the required application. The same reduction idea was repeated with the $MnNiCrO_4$. The phase identification of the synthesised materials was carried out with XRD. The morphological changes were observed with SEM. Finally, the synthesised materials were tested in the lab scale rig for oxidation of toluene.

7.2 $MnFeCrO_4$ spinel oxide

7.2.1 Synthesis of $MnFeCrO_4$

The $MnFeCrO_4$ spinels were synthesised using solution combustion mentioned in the experimental chapter of this thesis. Citric acid was used as a fuel and the prepared materials were calcined and sintered to form the desired spinel structure. Reduction was carried out at 2, 20 and 50 h in tube furnace with 5 % H_2/Ar and for comparison, the 2 h reduction was also carried out in a vacuum furnace. After reduction, etching was also carried out on the reduced sample. For etching, 0.1, 1,

2.5 and 5 M of HNO_3 were used. The powders were left in the acid for 12 h, filtered and washed with de-ionised water until pH was obtained. Finally, the reduced samples were tested for oxidation of toluene in the lab scale rig mentioned in the experimental chapter of this thesis.

7.2.2 Characterisation of synthesised $MnFeCrO_4$ materials

The sintered ceramic powder resulted in formation of a single-phase spinel structure, upon reduction segregation of secondary phases were observed which can be seen in Figure 7.1. The PXRD pattern shows presence of a mixed oxide composition in the sintered sample. Metallic Fe has distinct signals at 45 and 66 marked as *****). These signals were observed in the case of reduced samples, the 50 hours reduction sample had a very intense peak at 45 indicating a large amount of reduction had occurred. The 2- and 20-hours samples showed small presence of these peaks. MnO was another phase that was identified once the samples were reduced. The 2- hours reduced sample can be seen with additional peaks at 41 and 59 2θ values which correspond to MnO segregated phase (marked as●). These were also present in the 20- and 50 – hours sample. The peak intensities of the MnO secondary phase did not differ between the samples. This indicated that although the reduction results in formation of secondary phases, the metallic Fe was more predominant phase under the chosen reducing conditions. Increasing reduction temperature caused a slight shift towards lower 2θ values at 40 and 60, indicating reduction had caused cell parameter to shrink for the MnO phase.

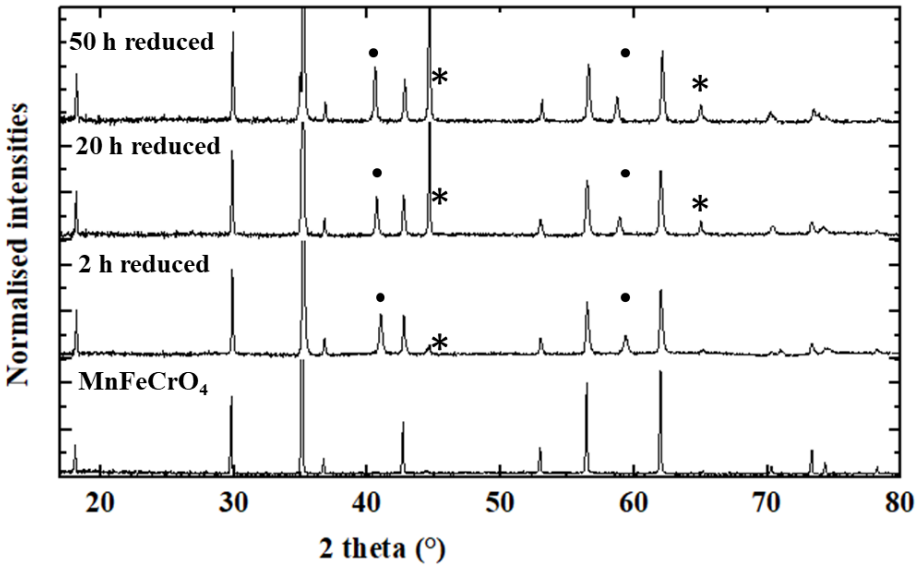

Figure 7.1. PXRD of sintered and reduced $MnFeCrO_4$ spinels

The morphology of the sintered and reduced ceramics can be seen in Figure 7.2. A lower (i) and higher (ii) scale micrograph have been shown parallel to one another to show an overview and detailed view of the samples respectively. The sintered powder had large grain sizes with defined grain boundaries (Figure 7.2a (i) and (ii). Upon reduction, at 2 hours, the sample can be seen to have smaller grain sizes with a few pores (Figure 7.2bi and ii). These pores are the decomposed Fe particles coming together in island like structures, this has been explained by previous work carried out in the JTSI group by Stefan et al [146]. The sample reduced at 20- hours had more of the decomposed Fe as can be seen by the number of increased pores on the surface (Figure 7.3c (i) and (ii)). The sample at 50-hours reduction had a more agglomerated surface which could be due to the dwell time being so long that the decomposed Fe fused together to form a layer on the surface rather than metallic Fe channels connecting in form of pores (Figure 7.3d (i) and (ii)).

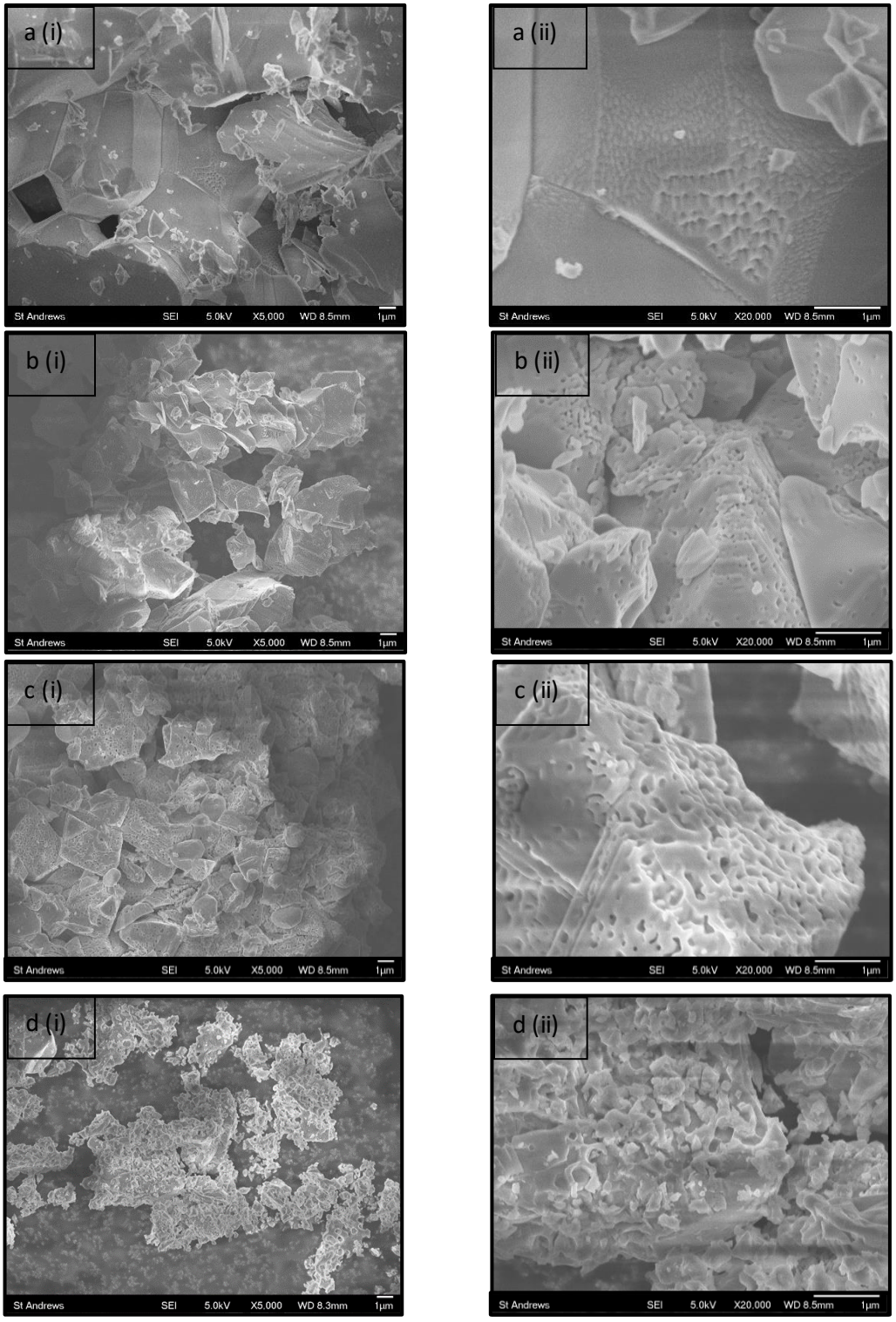

Figure 7.2.SEM micrographs of a) Sintered $MnFeCrO_4$ at low (i) and high (ii) magnification, b)$MnFeCrO_4$ reduced for 2 h at low (i) and high (ii) magnification, c)$MnFeCrO_4$ reduced for 20 h at low (i) and high (ii) magnification and d) $MnFeCrO_4$ reduced for 50 h at low (i) and high (ii) magnification

To compare the effect of reduction environment, the reduction at 2 hours was also carried out in a vacuum furnace at 900 °C. Figure 7.3 shows that there was no phase change difference observed between the sample reduced in a tube furnace or under vacuum. In fact, the 2θ peaks at 45 and 66 indicating presence of metallic Fe (marked as *****)were only observed in the 2 hours tube furnace reduced sample. The peaks were also more intense upon reduction in the tube furnace under 5 % H_2/Ar which indicated better reduction occurred in the tube furnace.

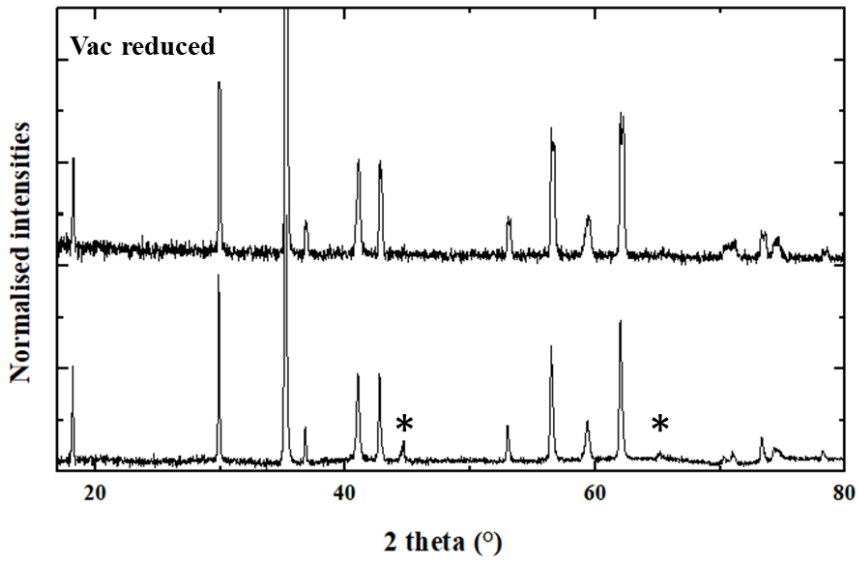

Figure 7.3. PXRD pattern for MnFeCrO4 reduced in tube and vacuum furnace for 2 h at 900 °C

The morphology of the sample reduced in vacuum furnace shown in Figure 7.4 (i) at low and higher magnifications (ii) was similar to that of the sintered sample (Figure 7.2 a (i) and (ii)). This meant that the tube furnace provided better reducing conditions thus leading to formation of more intense peaks and difference in morphology compared to sintered material.

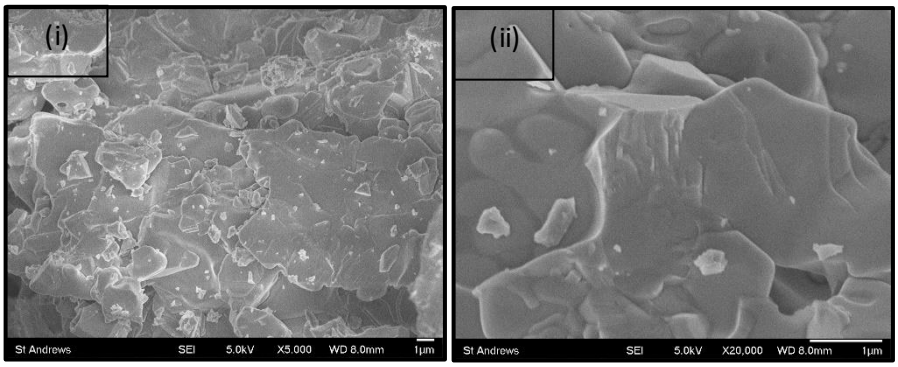

Figure 7.4. SEM micrographs of $MnFeCrO_4$ spinel oxide reduced at 2 h in vacuum furnace at (i) low and (ii) high magnification

As the tube furnace reduction conditions gave better results, all further reduction tests were carried out in tube furnace under 5 % H_2/Ar environment.

7.2.2.1 Metallic Fe etching

In an attempt to see if the reduced samples could be etched to gain a porous structure, different molarities of acid were tested. 0.1, 0.5, 1 and 5 M of nitric acid were used to etch the reduced Fe from the surface of 50 h reduced sample. Figure 7.5 shows that once etched regardless of the concentration of the acid used, the samples had a smooth surface with well defined grain boundaries. The samples after etching looked close to that of the sintered sample (Figure 7.2a). The idea to obtain a porous spinel oxide support with etching treatment was not successful in this case. The main reason was the composition of the spinel oxide. Reduction of these ceramics resulted in formation of decomposed metallic Fe rather than exsolved particles. When there are exsolved particles on the surface, acidic etching can result in cleansing those particles which results in formation of pores. Not having exsolved nanoparticles meant that etching only was successful in cleaning the surface. Though the etching had not given a positive outcome, the reduced 2- and 50- h spinels were tested for oxidation of toluene. Toluene is more toxic and is more problematic than ethyl acetate therefore reduced spinels were tested for toluene oxidation only.

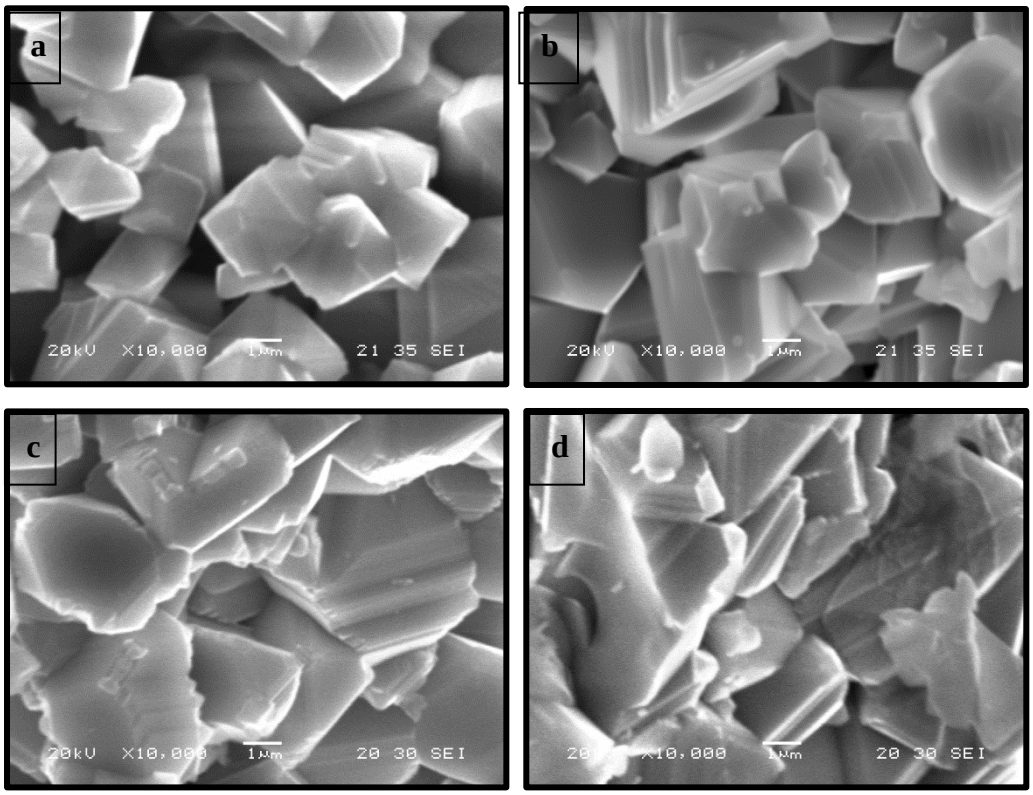

Figure 7.5. SEM micrographs of 50 h reduced $MnFeCrO_4$ sample etched at (a) 0.1 M, (b) 1 M, (c) 2.5 M and (d) 5 M of HNO_3

7.3 Catalytic oxidation of toluene

7.3.1 $MnFeCrO_4$ 2 h reduced sample

Figure 7.6 shows that over the 2 h reduced sample, the toluene conversion was slow at first. Conversion of 50 % was obtained at 200 °C which slowly increased to 100 % at 500 °C. For temperatures up to 300 °C, toluene was converted in to $C_2H_3^+$ (m/z 27), CH_2OH/OCH_3^+ (m/z 31) and $C_3H_3^+$ (m/z 39), unlike with the SS foams, $C_5H_3^+$ (m/z 63) and $C_5H_5^+$ (m/z 65) were not observed. This sample became active towards oxidation at 350 °C, selectivity of 50 % was obtained which very gradually increased to an overall of 43 % at 500 °C. This meant that the 2 h reduced sample was less active towards toluene conversion generally and selectively oxidising it to CO_2 than SS 316 foams.

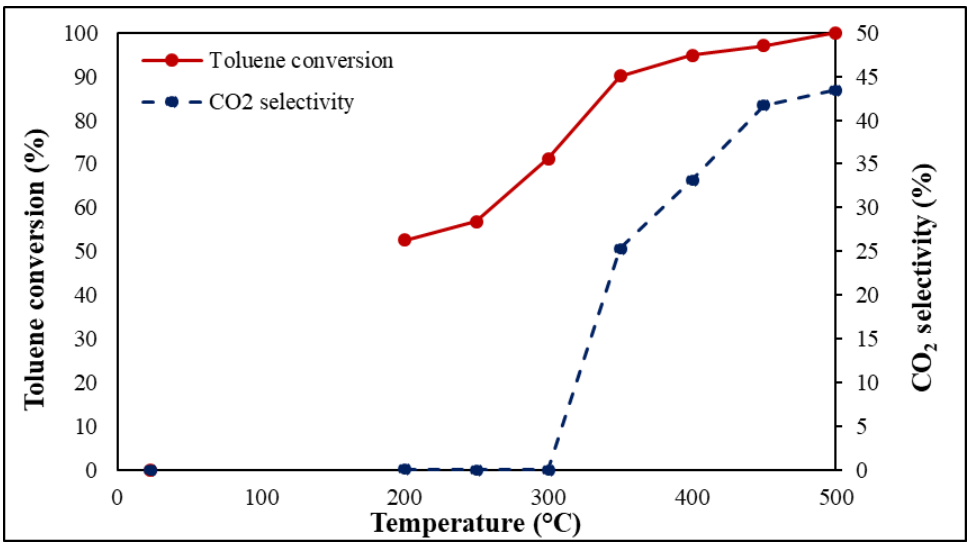

Figure 7.6. Toluene conversion (%) and selectivity towards CO_2 (%) at different temperatures with 2 h reduced $MnFeCrO_4$ as a catalyst

Post catalysis SEM micrograph shown in Figure 7.7 (i) and (ii) revealed that the small amount open pore like structure found in the 2 h reduced sample as shown in Figure 7.2b was no longer seen. After catalysis, there were no pores observed.

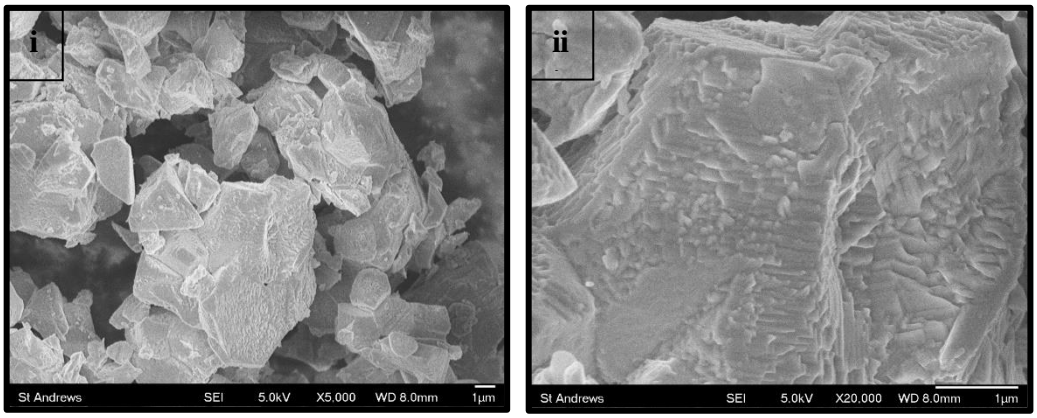

Figure 7.7. SEM micrographs of 2 h reduced $MnFeCrO_4$ sample after being used in catalysis at (i) low and (ii) high magnification

PXRD comparison of the pre- and post- catalysis sample shown in Figure 7.8 showed that the metallic Fe peaks intensity had decreased when the sample was used for catalysis. Small peak at 33° in the post catalysis sample belongs to Fe oxide which meant that under the reaction conditions used, the sample was being oxidised.

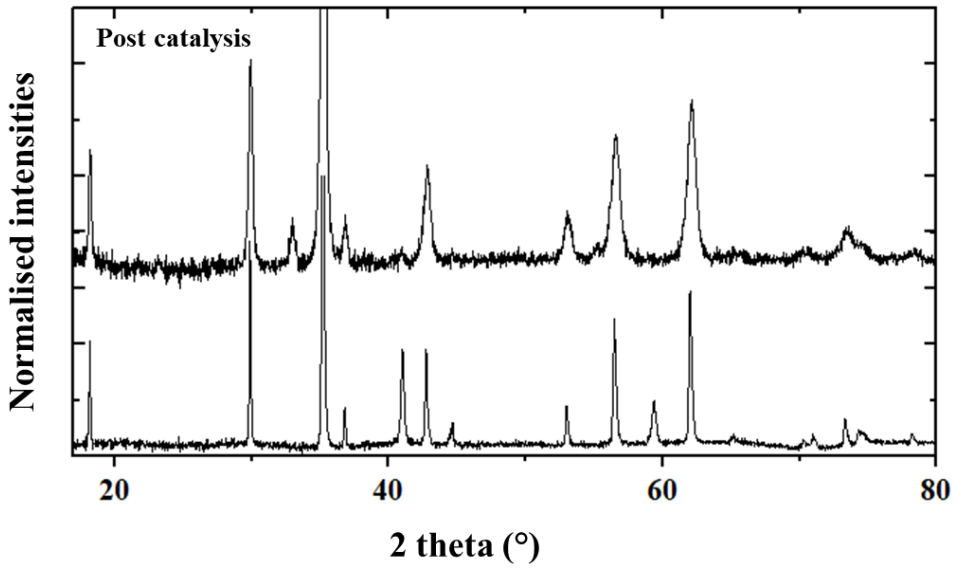

Figure 7.8. PXRD of pre- and post- catalysis of $MnFeCrO_4$ reduced for 2 h

7.3.2 $MnFeCrO_4$ 50 h reduced sample

Figure 7.9 shows that over the 50 h reduced sample, the toluene conversion was similar to that of the 2 h reduced sample at the start. Conversion of 37 % was obtained at 200 °C which slowly increased to 100 % at 450 °C. For temperatures up to 300 °C, toluene was converted in to $C_2H_3^+$ (m/z 27), CH_2OH/OCH_3^+ (m/z 31) and $C_3H_3^+$ (m/z 39). This sample became active towards oxidation at 300 °C, selectivity of 12 % was obtained which very gradually increased to an overall of 45 % at 500 °C. The longer reduced time sample had similar conversion and catalytic trends to that of the 2 h reduced samples.

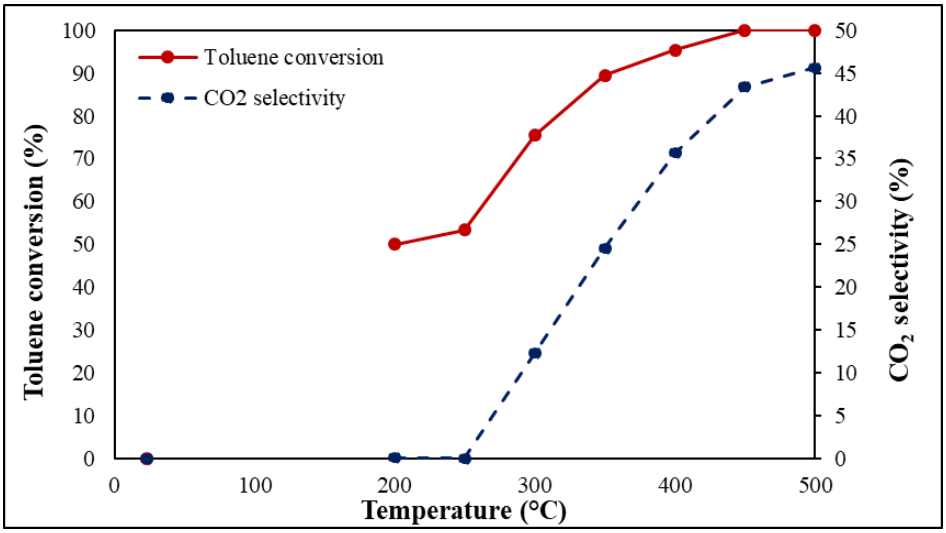

Figure 7.9. Toluene conversion (%) and selectivity towards CO_2 (%) at different temperatures with 50 h reduced MnFeCrO4 as a catalyst

Figure 7.10 (i) and (ii) show that the morphology of the sample after being tested was similar to that prior to being tested. There were a few pores that had been covered but generally, the morphology remained unchanged.

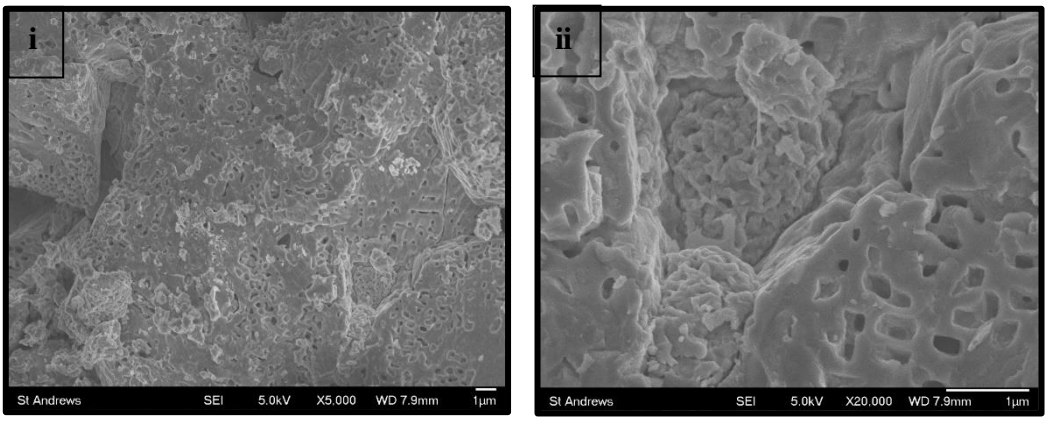

Figure 7.10. SEM micrographs of 50 h reduced $MnFeCrO_4$ sample after being used in catalysis at (i) low and (ii) high magnification

Similar to the previous 2 h reduced sample, PXRD of the pre- and post catalysis shown in Figure 7.11 revealed that after being used, presence of Fe oxide at 33° and general broader peaks indicated that oxidation had occurred.

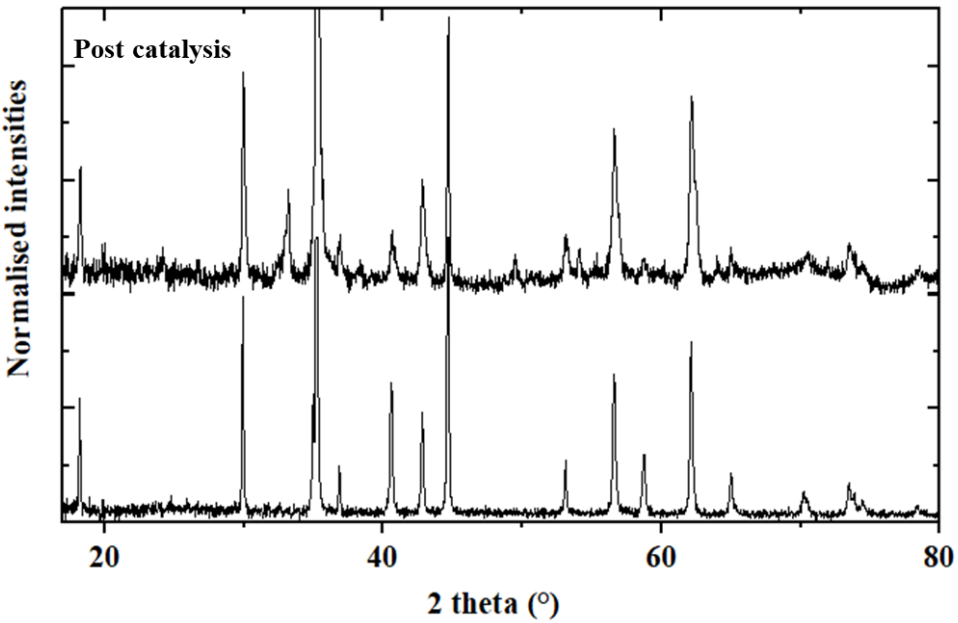

Figure 7.11. PXRD of pre- and post- catalysis of $MnFeCrO_4$ reduced for 50 h

The Fe containing spinels had generally a lower selectivity towards CO_2. The exsolution process had not worked very well in the case of $MnFeCrO_4$.

7.4 $MnNiCrO_4$ spinel oxide

7.4.1 $MnNiCrO_4$ synthesis

To improve the exsolution, a different composition of spinels was synthesised. In this, Ni was used instead of Fe. Previous work in the group had been successful in exsolving Ni nanoparticles on the surface of the spinel oxides [160]. Solution combustion synthesis was method employed to obtain the nano powder. The powders were calcined followed by sintering in muffle furnace. The powders were reduced at 2 and 10 hours in tube furnace under 5 % H_2/Ar. The reduced materials were etched with 1, 2.5 and 5 M of HNO_3 to form a porous scaffold. The porous material was impregnated with Cu oxide as this showed good results with the SS foams. The impregnated spinels were tested for toluene oxidation.

7.4.2 Characterisation of $MnNiCrO_4$

The sintered sample can be seen to have large grains with a smooth surface in Figure 7.12 (a). At the same scale, upon reduction at 2 hours, Ni can be seen to be exsolving on the edges in Figure 7.12 (b). Increasing the reduction dwell time resulted in more exsolution of Ni on the surface which can also be seen in Figure 7.12 (c).

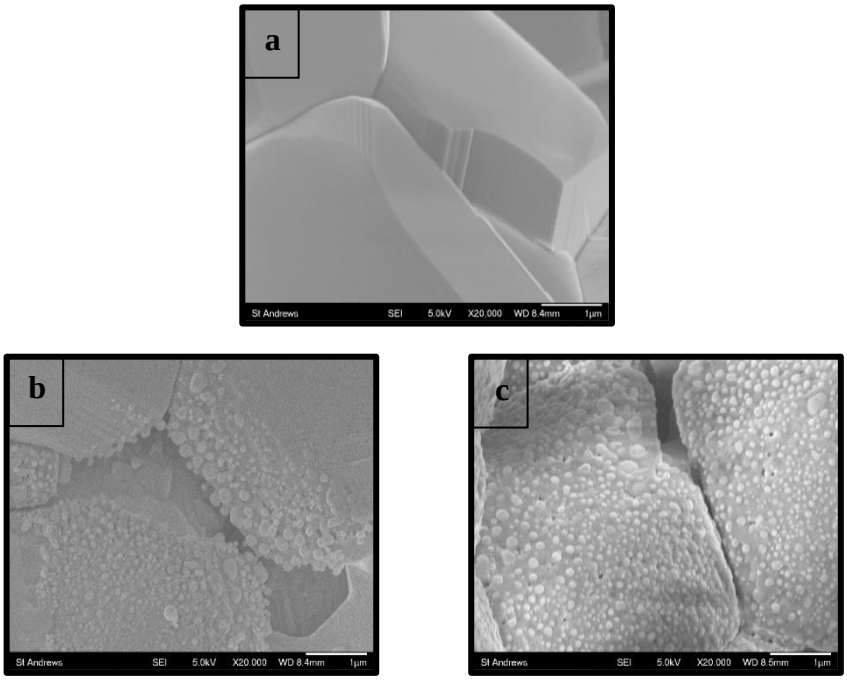

Figure 7.12. SEM micrographs $MnNiCrO_4$ (a) sintered, (b) reduced for 2 h and (c) reduced for 10 h

The 2 h reduced sample was not used further as more exsolved sample was preferred. Figure 7.13 shows the PXRD patterns of sintered and reduced $MnNiCrO_4$ samples. The 10 hours reduced sample showed occurrence of different phases as compared to the sintered sample. The single-phase peaks were seen in the sintered samples however, the presence of high intense peaks for Ni at 44°, 52° and 76° (marked as ■) were observed in the reduced sample.

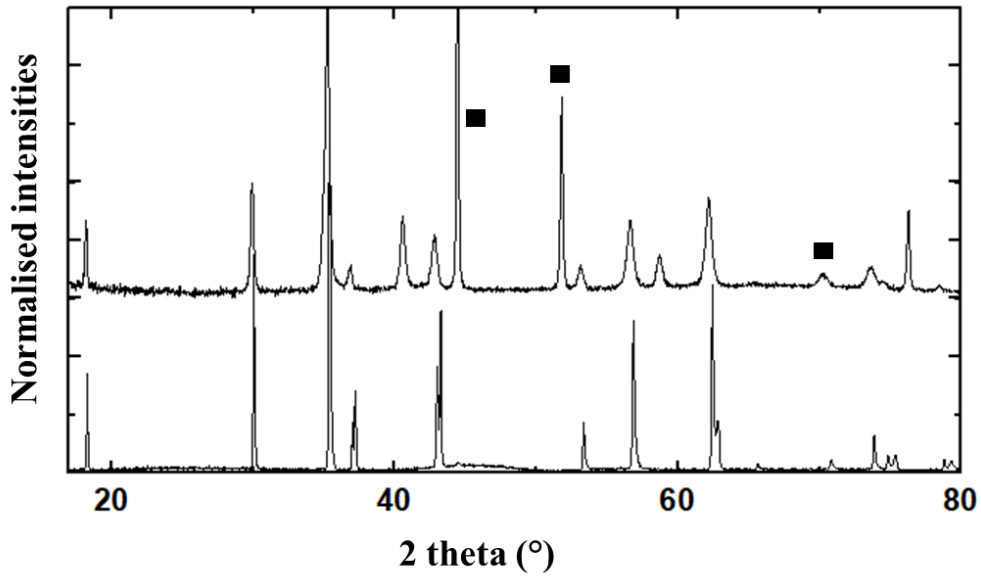

Figure 7.13. PXRD pattern of sintered and reduced $MnNiCrO_4$

As the reduction with Ni showed presence of large Ni metallic particles, this sample was chosen to conduct etching studies.

7.4.1 Ni metallic etching

At first the 1 M concentration of nitric acid was used. SEM micrographs shown in Figure 7.14 (i) and (ii) reveal that at this concentration, a small amount of metal was etched however, it was not enough to etch the metal completely.

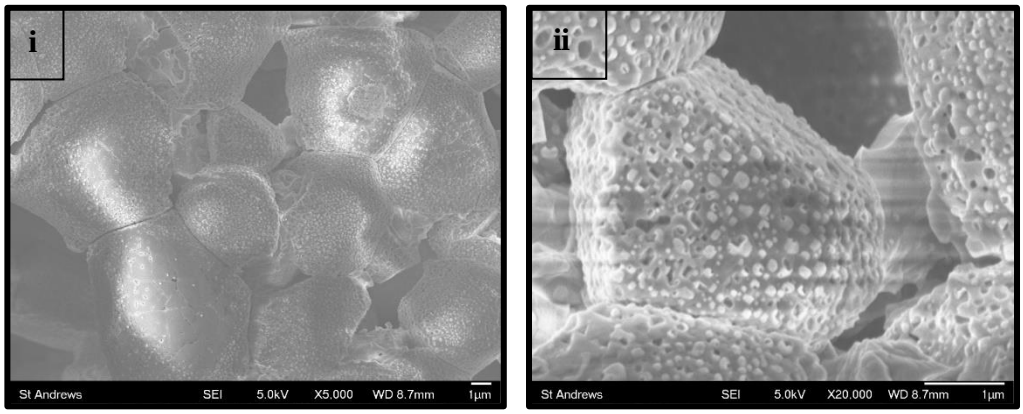

Figure 7.14. SEM micrographs of $MnNiCrO_4$ etched at 1 M at (i) low and (ii) high magnification

The small amount of etching showed that the acid had the potential of being used for etching. The molarity of the nitric acid was increased to 2.5 and 5 M which can be seen in Figure 7.15 (a i and ii, b i and ii) at different magnifications. It can be seen that in both cases, the acid had successfully etched the exsolved particles from the surface and resulted in the formation of pores.

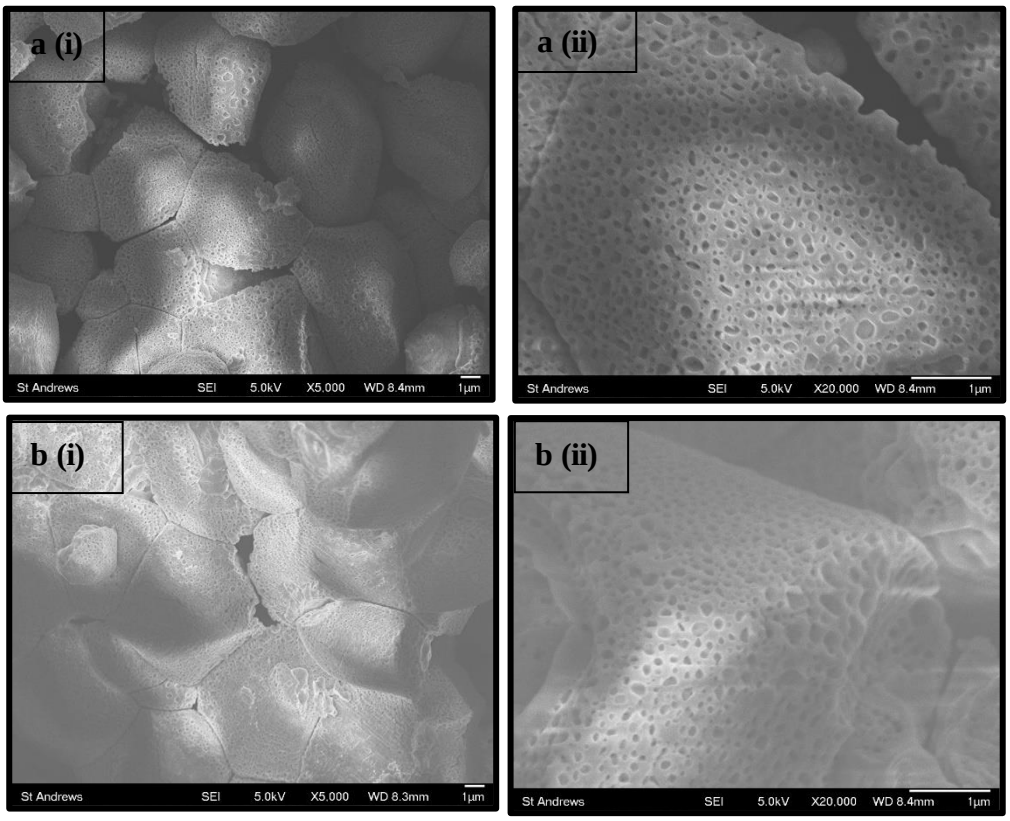

Figure 7.15. SEM micrographs of $MnNiCrO_4$ etched at (a) 2.5 M at (i) low and (ii) high magnification and (b) 5 M at (i) low and (ii) high magnification

7.5 Cu oxide impregnation on $MnNiCrO_4$

As 2.5 M etched sample had resulted in formation of pores, this was used for impregnation of Cu oxide. Solution of 0.5 M copper nitrate was made with de-ionised water. This was impregnated on to the etched powder using incipient wetness. Once all the powder had been covered, the resulting mixture was left at hotplate at 100 °C to evaporate water. Once dried, the powder was calcined at 400 °C for 4 hours. The morphology of the impregnated material can be seen in Figure 7.16. The pores were no longer visible, instead an agglomerated Cu oxide rich layer can be seen. This sample was tested for oxidation of toluene.

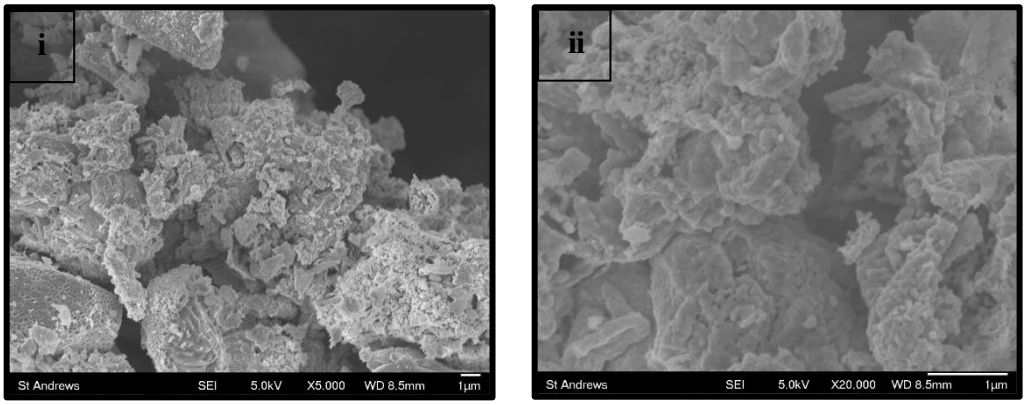

Figure 7.16. SEM micrographs of Cu oxide impregnated $MnNiCrO_4$ etched sample at (i) low and (ii) high magnification

7.6 Catalytic testing of Cu oxide impregnated $MnFeCrO_4$

The impregnated spinel oxide had similar toluene conversion to that seen with the SS 316 Cu oxide impregnated foam. The toluene conversion of 70 % was obtained at 200 °C and full toluene conversion was observed at 250 °C. This sample was more active towards toluene decomposition than the previously MnFeCrO4 reduced samples tested. The selectivity, however, was slightly similar. This sample because active towards oxidation at much lower temperature of 200 °C. 28 % selectivity towards CO_2 at 200 °C which eventually increased to 50 % at 350 °C. The selectivity remained unchanged after this regardless of the temperature.

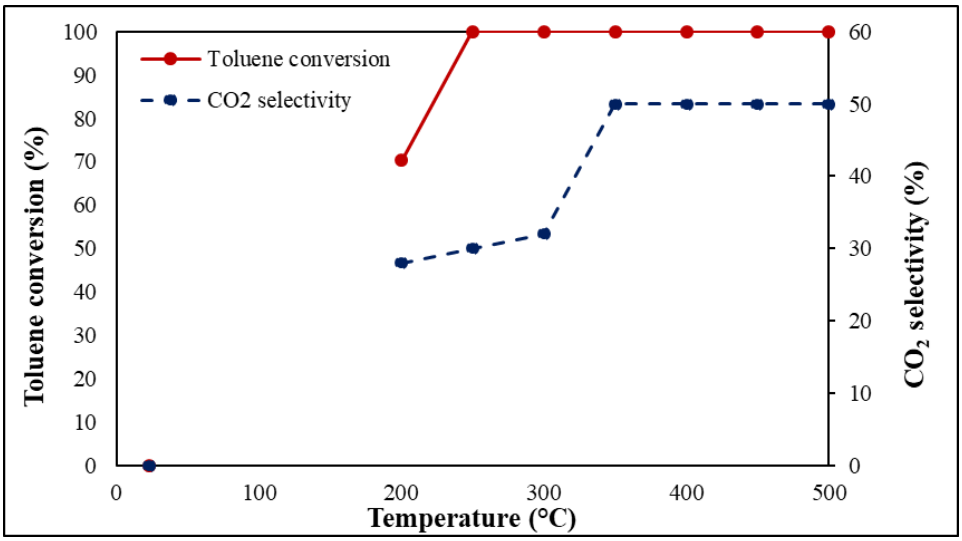

Figure 7.17. Toluene conversion (%) and selectivity towards CO_2 (%) at different temperatures with Cu oxide impregnated $MnNiCrO_4$ as a catalyst

The SEM micrographs of sample post catalysis seen in Figure 7.18 (i) and (ii) at lower and higher magnification that the porous structure had re-appeared after being tested. Agglomeration of the impregnated layer is visible at lower and higher scale. This indicates that the impregnation was not anchored on to the surface very well and upon being in contact with high flow of contaminated air, it failed to stay intact.

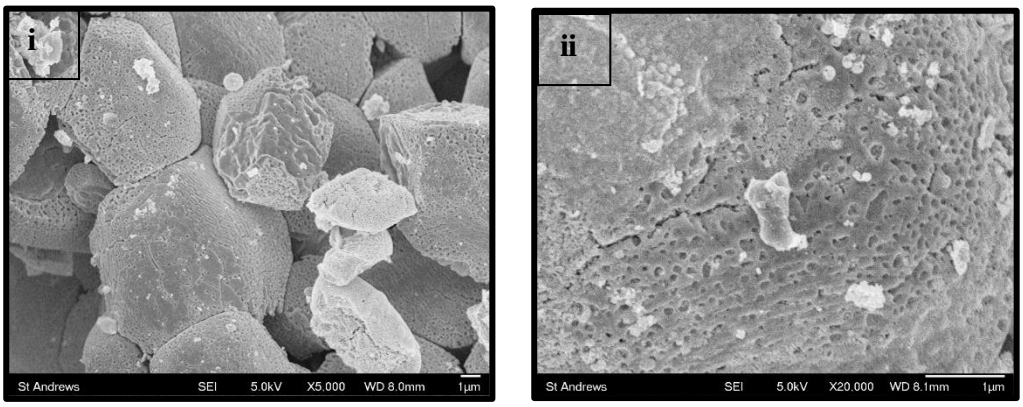

Figure 7.18. SEM micrographs of post catalysis Cu oxide impregnated $MnNiCrO_4$ at (i) low and (ii) high magnification

7.7 Chapter summary

In this chapter, two different compositions; $MnFeCrO_4$ and $MnNiCrO_4$ of spinels were synthesised using solution combustion method. The materials were reduced to obtain metallic Fe at 2, 20 and 50 h and Ni at 2 and 10 h respectively. In the case of $MnFeCrO_4$ the exsolution of Fe had not occurred therefore, the 2 and 50 h reduced samples were tested for oxidation toluene. Both samples had similar toluene conversion and oxidation trends. Toluene conversion of 100 % was obtained at 500 and 450 °C for 2 and 50 h reduced sample respectively. The total oxidation of toluene measured by the amount of CO_2 produced was 43 and 46 % at 500 °C respectively. The $MnNiCrO_4$ was successfully reduced to form Ni nanoparticles on the surface of the $MnCrO_4$ backbone, etching of this resulted in formation of a porous scaffold which was impregnated with Cu oxide. The impregnated material was tested and showed excellent conversion trends for toluene. At 200 °C, 70 % of toluene had decomposed and at 250 °C, all of the toluene had been converted. This sample behaved similarly to that of the Cu oxide impregnated SS 316 foams for conversion trend. The selectivity, however, was lower and different to the SS 316 foam impregnated foam. 28 % of selectivity was observed at 200 °C which increased to 50 % at 350 °C. Though the conversion of toluene had been good, the spinels tested had not been good for oxidation of toluene.

Conclusions and Future work

8.1. Conclusions

This work focused at the use of stainless steel 314/316 foams and spinel oxides as potential catalysts for bleed air contamination. Toluene and ethyl acetate were chosen representatives of the contaminants found in the cabin air.

First, the SS 314 foams were modified and tested for toluene oxidation. The foams were modified *via* oxidation and/or impregnation to obtain a metal oxide rich layer on the surface. The oxidation study revealed that the SS 314 oxidised at 750 °C for 1 h was an ideal candidate for impregnation studies. After varying different experimental parameters, pre-oxidised foam coated with Fe and Mn oxide were tested for oxidation of toluene at temperatures between 200 and 500 °C. In terms of conversions, Mn oxide coated foam gave the highest toluene conversion (100 %) and selectivity towards CO_2 (71 %) at 350 °C. This was the lowest temperature for maximum toluene conversion and selectivity compared to all the other foams tested.

For SS 316 foams, oxidation at 300 °C for 1 h resulted in the formation of a rough layer on the surface of the foam which was used as a substrate for dip coating. Different metal nitrates (Fe, Ni, Cu, Mn and Ce) were coated on the surface of the foam to form respective oxides. The metal oxides were chosen based on their performance as a support and/or oxidation catalyst.

Overall in this chapter, different SS 316 raw/oxidised/impregnated foams were tested for total oxidation of toluene. The first optimisation was carried out in the oxidation step where a rough layer was required to get better metal nitrates impregnation on the surface of the foams. Oxidation at 300 °C for 1 h resulted in a positive outcome and was used as a substrate for impregnation of different metal nitrates to obtain oxides on the surface. The metal oxides (Fe, Ni, Cu, Mn and Ce) were chosen based on their previous good performance as oxidation catalysts. Substrate and solution composition were modified for impregnation studies to find the most optimal surface coverage. From the impregnated foams tested, SS 316 oxidised at 300 °C for 1 h impregnated with 5 wt. % Mn oxide had 100 % toluene conversion and 90 % selectivity towards CO_2 at 300 °C. The conversion and

selectivity with this foam occurred at the lowest temperature compared to the rest of the metal oxides. Finally, the Mn oxide impregnated sample was also tested for an 8-h flight representation at 300 °C which showed that the catalyst remained stable throughout. A good combination of performance and stability was obtained with the pre-oxidised SS 316 Mn oxide coated foam.

After testing toluene, oxidation of ethyl acetate was studied. In this case, Ce oxide impregnated foam was successful in converting ethyl acetate (100 %) at 250 °C. The highest selectivity of 88 % towards CO_2 was obtained with Cu oxide impregnated foam at 300 °C. Alongside CO_2, the main decomposition product of ethyl acetate was of m/z 27 ($C_2H_3^+$). The Mn oxide impregnated foam had not performed as well compared to the performance in oxidation of toluene. This was perhaps due to the Mn being more active towards conjugated system without the presence of oxygen compared to a linear system. Taking both, the conversion and oxidation into account, the Cu oxide foam gave the best results. Ni and Mn oxide impregnated foams had similar composition to that of the spinel oxides therefore, spinels were also tested.

In terms of spinels, two different compositions; $MnFeCrO_4$ and $MnNiCrO_4$ of spinels were synthesised with the solution combustion method. Reduction of $MnFeCrO_4$ was carried out at 2, 20 and 50 h in an attempt to reduce metallic Fe and form Fe nanoparticles. The $MnNiCrO_4$ reduction was carried out at 2 and 10 h in order to obtain Ni nanoparticles on the surface of the spinel backbone. The exsolution of Fe had not been successful, nevertheless, the 2 and 50 h reduced samples were tested for the oxidation of toluene. Toluene conversion of 100 % was obtained at 450 and 500 °C for 50 and 2 h reduced samples respectively. The selectivity towards oxidation of toluene to produce CO_2 was 46 and 43 % for 50 and 2 h reduced samples. The Ni exsolution was successful to be obtained when sample was reduced at 10 h. The formed nanoparticles were then etched to form a porous $MnCrO_4$ which were impregnated with Cu oxide. The impregnated material was tested and showed that 70 % of toluene had been converted at 200 °C which eventually increased to 100 % at 250 °C. The selectivity towards CO_2 of 28 % was observed at 200 °C which increased to 50 % at 350 °C.

Overall, the stainless steel foams particularly the 316 was better candidate for decomposition and oxidation of toluene at lower temperatures. Spinels had good toluene conversion rate, the selectivity towards the oxidation product was rather low. This means that for the application of bleed air contamination, impregnated stainless steel foams would be a better option.

8.2. Future work

This project has the potential to be taken further to develop cheap, effective and easily implemented catalysts. In the case of the stainless steel foams, there is a strong evidence that the foams are a good support and in future, more impregnations could be tested. Combination of Cu and Mn oxide would be interesting to test. The spinels could be impregnated on to the stainless steel foams and tested for toluene and ethyl acetate oxidation. Furthermore, the best performing catalysts for toluene and ethyl acetate conversion and oxidation could be tested for cresol and TCP.

References

1 G. A. Day, *Aircraft Cabin Bleed Air Contaminants: A Review*, 2015.

2 J. De Boer, A. Antelo, Van der Veen, S. Brandsma and N. Lammertse, *Elsevier*, 2015, **119**, 58–61.

3 N. Boschi and F. Haghighat, in *Handbook of Environmental Chemistry*, 2005, vol. 4, pp. 53–83.

4 C. A. . N. M. Dechow, *Aircraft Environmental Control System*, Springer, 2005, p. 8,14,27.

5 E. H. Hunt, D. H. Reid, D. R. Space and F. E. Tilton, *Aerosp. Med. Assoc.*, 1995.

6 C. Van Netten and V. Leung, *Arch. Environ. Heal. An Int. J.*, 2001, **56**, 181–186.

7 B. K. Schindler, T. Weiss, A. Schütze, S. Koslitz, H. C. Broding, J. Bünger and T. Brüning, *Arch. Toxicol.*, 2013, **87**, 645–648.

8 D. Balouet, Christophe-Jean. Megson, *Int. Netw. Environ. Forensics Bull.*, 2016, **1**, 11–15.

9 R. Harrison, J. Murawski, E. McNeely, J. Guerriero and D. Milton, *Exposure to aircraft bleed air contaminants among airline workers, California.*, 2009.

10 G. Denola, P. J. Hanhela and W. Mazurek, *Ann. Occup. Hyg.*, 2011, **55**, 1–13.

11 B. T. Lebele-Alawa, H. Hart, S. O. T. Ogaji and S. D. Probert, *Appl. Energy*, 2008, **85**, 494–505.

12 National Research Council, *The airliner cabin environment and the health of passengers and crew*, *National Academies Press (US)*, 2002, pp. 182–222.

13 C. van Netten, in *Air Quality and Comfort in Airliner Cabins*, ASTM International, 2000, pp. 61–75.

14 S. Michaelis, *J. Biol. Phys. Chem.*, 2011, **11**, 132–145.

15 P. E. Baker, T. B. Cole, M. Cartwright, S. M. Suzuki, K. E. Thummel, Y. S. Lin, A. L. Co, A. E. Rettie, J. H. Kim and C. E. Furlong, *Chem. Biol. Interact.*, 2013, **203**, 257–264.

16 C. Winder and J.-C. Balouet, *Environ. Res.*, 2002, **89**, 146–164.

17 C. Crump, Derrick. Harrison, Paul. Walton, *Aircraft Cabin Air Sampling Study ; Part 1 of the Final Report*, Cranfield, 2011.

18 HSE, *Medical aspects of work-related exposures to organophosphates*, Health and Safety Executive, Norwich, 2000.

19 M. Bagshaw, *Health Effects of Contaminants in Aircraft Cabin Air*, 2013.

20 Senate Commitee, *Air Safety and Cabin Air Quality in the BAe 146 Aircraft, Austrailia*, 2000 (ISBN 0 642 71093 7).

21 V. Harrison and S. J. Mackenzie Ross, *Cortex*, 2016, **74**, 297–302.

22 K. M. Johnson, *Br. J. Ind. Med.*, 1987, **44**, 217–219.

23 M. B. Abou-Donia, *Ann. Rev. PharmacoL ToxicoL.*, 1981, **21**, 11–48.

24 M. A. Hale and J. A. Al-Seffar, *Am. J. Electroneurodiagnostic Technol.*, 2009, **49**, 260–79.

25 L. Karalliedde, S. Feldman, J. Henry and T. Marrs, in *Organophosphates and Health*, *Published by Imperial College Press.*, 2001, pp. 159–160.

26 D. A. Goldstein, M. A. McGuigan and B. D. Ripley, *Hum. Toxicol.*, 1988, **7**, 179–82.

27 C. Wang, X. Yang, J. Guan, K. Gao and Z. Li, *Build. Environ.*, 2014, **78**, 89–94.

28 P. H. Craig and M. L. Barth, *J. Toxicol. Environ. Health. B. Crit. Rev.*,

1999, **2**, 281–300.

29 A. C. Dong, Jun. Migdal, in *Lubricants and Additives*, ed. Leslie R. Rudnick, CRS Press, 2nd edn., 2009, p. 96.

30 E. Carletti, L. M. Schopfer, J.-P. Colletier, M.-T. Froment, F. Nachon, M. Weik, O. Lockridge and P. Masson, *Chem. Res. Toxicol.*, 2011, **24**, 797–808.

31 E. Carletti, L. M. Schopfer, J.-P. Colletier, M.-T. Froment, F. Nachon, M. Weik, O. Lockridge and P. Masson, *Chem. Res. Toxicol.*, 2011, **24**, 797–808.

32 G. Smith, M.I.Elvove, P.J.Frazier, W.H.Mallory, *US Public Heal. Reports*, 1930, **45**, 1703–1716.

33 D. Henschler, *Klin. Wochenschr.*, 1958, **36**, 663–74.

34 C. R. Mackerer, M. L. Barth, A. J. Krueger, B. Chawla and T. A. Roy, *J. Toxicol. Environ. Health. A*, 1999, **57**, 293–328.

35 US Department of Health and Human Services, 1978, 2–6.

36 G. G. Kelso, A.G. Charlesworth, J.M. Mcvea, *Contamination of Environmental Control Systems in Hercules aircraft*, Melbourne, 1988.

37 H. M. Ghose, J. Ferrate, F. C. Honecy, H. M. Ghose, J. Ferrante and F. S. Honecy, *NASA*, 1987.

38 D. Johnson and J. Hils, *Lubricants*, 2013, **1**, 132–148.

39 R. L. Cottington and H. Ravner, *A S L E Trans.*, 1969, **12**, 280–286.

40 H. E. Bieber, E. E. Klaus and E. J. Tewksbury, *A S L E Trans.*, 1968, **11**, 155–161.

41 I. L. Goldblatt and J. K. Appeldoorn, *A S L E Trans.*, 1970, **13**, 203–214.

42 M. Kawamura and K. Fujita, *Wear*, 1981, **72**, 45–53.

43 D. W. Johnson, S. Morrow, N. H. Forster and C. S. Saba, *Chem. Mater.*,

2002, **14**, 3767–3775.

44 In *The airliner cabin environment and the health of passengers and crew*, National Academies Press (US), Washington, DC, 2002, pp. 254–275.

45 T. Dumyahn, J. Spengler, H. Burge and M. Muilenburg, in *Air Quality and Comfort in Airliner Cabins*, ASTM International, West Conshohocken, 2000, pp. 3–23.

46 B. T. Burley and J. et al Harris, Seale, *J. Am. Med. Assoc.*, 1932, **98**, 298.

47 H. V Smith and J. M. Spalding, *Lancet (London, England)*, 1959, **2**, 1019–21.

48 R. P. Travers, *J. R. Soc. Med.*, 1962, **55**, 57–60.

49 S. D. Segalla, *J. North African Stud.*, 2012, **17**, 315–336.

50 A. Bloch, H. Hottinger, *Chem. Cent. II*, 1943, **13**, 197–198.

51 W. N. Aldridge, *Biochem. J.*, 1954, **56**, 185–9.

52 C. Vasilescu and A. Florescu, *Arch. Toxicol.*, 1980, **43**, 305–15.

53 M. Susser and Z. Stein, *Br. J. Ind. Med.*, 1957, **14**, 111–20.

54 N. Senanayake, *J. Neurol. Neurosurg. Psychiatry*, 1981, **44**, 775–80.

55 A. K. Srivastava, M. Das and S. K. Khanna, *Food Chem. Toxicol.*, 1990, **28**, 303–4.

56 W. B. Li, J. X. Wang and H. Gong, *Catal. Today*, 2009, **148**, 81–87.

57 S. Ojala, S. Pitkäaho, T. Laitinen, N. Niskala Koivikko, R. Brahmi, J. Gaálová, L. Matejova, A. Kucherov, S. Päivärinta, C. Hirschmann, T. Nevanperä, M. Riihimäki, M. Pirilä and R. L. Keiski, *Top. Catal.*, 2011, **54**, 1224–1256.

58 E. Olsen and F. Nielsen, *Molecules*, 2001, **6**, 370–389.

59 M. Amann and M. Lutz, *J. Hazard. Mater.*, 2000, **78**, 41–62.

60 B. J. Finlayson-Pitts and J. N. Pitts, *Science*, 1997, **276**, 1045–52.

61 P. W. Park and J. S. Ledford, *Appl. Catal. B Environ.*, 1998, **15**, 221–231.

62 J. Guan, K. Gao, C. Wang, X. Yang, C.-H. Lin, C. Lu and P. Gao, *Build. Environ.*, 2014, **72**, 154–161.

63 K.-J. Kim and H.-G. Ahn, *Microporous Mesoporous Mater.*, 2012, **152**, 78–83.

64 M. Drobek, A. Figoli, S. Santoro, N. Navascués, J. Motuzas, S. Simone, C. Algieri, N. Gaeta, L. Querze, A. Trotta, G. Barbieri, R. Mallada, A. Julbe and E. Drioli, *Microporous Mesoporous Mater.*, 2015, **207**, 126–133.

65 B. Ozturk and D. Yilmaz, *Process Saf. Environ. Prot.*, 2006, **84**, 391–398.

66 S. Scirè and L. F. Liotta, *Appl. Catal. B Environ.*, 2012, **125**, 222–246.

67 T.-T. Win-Shwe and H. Fujimaki, *Toxicol. Lett.*, 2010, **198**, 93–99.

68 D. Beauregard, *Locating and estimating air emissions from sources of toluene., Final Report*, 1993.

69 World Health Organisation, *Air Quality Guidelines for Europe Second Edition*, WHO regional publications, European series; No. 91, 2000 (ISBN 92 890 1358 3).

70 G. R. Christoph, J. F. Hansen and H.-W. Leung, *Neurotoxicology*, 2003, **24**, 861–874.

71 Z. Ye, J.-M. Giraudon, N. De Geyter, R. Morent, J.-F. Lamonier, Z. Ye, J.-M. Giraudon, N. De Geyter, R. Morent and J.-F. Lamonier, *Catalysts*, 2018, **8**, 91.

72 J. Kujawa, S. Cerneaux and W. Kujawski, *J. Memb. Sci.*, 2015, **474**, 11–19.

73 R. K. Shah, B. Thonon and D. M. Benforado, *Appl. Therm. Eng.*, 2000, **20**, 631–650.

74 G. Leson and A. M. Winer, *J. Air Waste Manage. Assoc.*, 1991, **41**, 1045–1054.

75 E. C. Moretti, *Chem. Eng. Prog.*, 2002, **98**, 30–40.

76 P. Ciambelli, V. Palma, P. Russo and S. Vaccaro, *Catal. Today*, 2002, **75**, 471–478.

77 L. F. Liotta, *Appl. Catal. B Environ.*, 2010, **100**, 403–412.

78 P.-O. Larsson and A. Andersson, *J. Catal.*, 1998, **179**, 72–89.

79 J. Peng and S. Wang, *Appl. Catal. B Environ.*, 2007, **73**, 282–291.

80 D. R. van der Vaart, W. M. Vatvuk and A. H. Wehe, *J. Air Waste Manage. Assoc.*, 1991, **41**, 92–98.

81 M. S. Kamal, S. A. Razzak and M. M. Hossain, *Atmos. Environ.*, 2016, **140**, 117–134.

82 J. C. Rooke, T. Barakat, J. Brunet, Y. Li, M. F. Finol, J.-F. Lamonier, J.-M. Giraudon, R. Cousin, S. Siffert and B. L. Su, *Appl. Catal. B Environ.*, 2015, **162**, 300–309.

83 S. A. C. Carabineiro, X. Chen, O. Martynyuk, N. Bogdanchikova, M. Avalos-Borja, A. Pestryakov, P. B. Tavares, J. J. M. Órfão, M. F. R. Pereira and J. L. Figueiredo, *Catal. Today*, 2015, **244**, 103–114.

84 H.-J. Joung, J.-H. Kim, J.-S. Oh, D.-W. You, H.-O. Park and K.-W. Jung, *Appl. Surf. Sci.*, 2014, **290**, 267–273.

85 D. Delimaris and T. Ioannides, *Appl. Catal. B Environ.*, 2008, **84**, 303–312.

86 S. C. Kim, *J. Hazard. Mater.*, 2002, **91**, 285–299.

87 H. Rotter, M. V. Landau, M. Carrera, D. Goldfarb and M. Herskowitz, *Appl. Catal. B Environ.*, 2004, **47**, 111–126.

88 M. Zimowska, A. Michalik-Zym, R. Janik, T. Machej, J. Gurgul, R. P. Socha, J. Podobiński and E. M. Serwicka, *Catal. Today*, 2007, **119**, 321–326.

89 S. A. C. Carabineiro, X. Chen, M. Konsolakis, A. C. Psarras, P. B. Tavares, J. J. M. Órfão, M. F. R. Pereira and J. L. Figueiredo, *Catal. Today*, 2015, **244**, 161–171.

90 W. Tang, X. Wu, G. LIU, S. LI, D. LI, W. LI and Y. Chen, *J. Rare Earths*, 2015, **33**, 62–69.

91 S. C. Kim, Y.-K. Park and J. W. Nah, *Powder Technol.*, 2014, **266**, 292–298.

92 E. D. Banús, M. A. Ulla, E. E. Miró and V. G. Milt, *InTech*, 2013, 118–142.

93 C.-B. Lim, H. Kusaba, H. Einaga and Y. Teraoka, *Catal. Today*, 2011, **175**, 106–111.

94 X.-Y. Zhou, J. Li, B. Long and D.-W. Huo, *Mater. Sci. Eng. A*, 2006, **435**, 40–45.

95 M. Sun, L. Wang, B. Feng, Z. Zhang, G. Lu and Y. Guo, *Catal. Today*, 2011, **175**, 100–105.

96 S.-H. Wei, *Jpn. J. Appl. Phys.*, 2000, **39**, 251.

97 S. Rahim Pouran, A. A. Abdul Raman and W. M. A. Wan Daud, *J. Clean. Prod.*, 2014, **64**, 24–35.

98 K. E. Sickafus, J. M. Wills and N. W. Grimes, *J. Am. Ceram. Soc.*, 2004, **82**, 3279–3292.

99 J. P. Jacobs, A. Maltha, J. G. H. Reintjes, J. Drimal, V. Ponec and H. H. Brongersma, *J. Catal.*, 1994, **147**, 294–300.

100 K. Faungnawakij, N. Shimoda, T. Fukunaga, R. Kikuchi and K. Eguchi, *Appl. Catal. A Gen.*, 2008, **341**, 139–145.

101 G. Meligrana, C. Gerbaldi, A. Tuel, S. Bodoardo and N. Penazzi, *J. Power Sources*, 2006, **160**, 516–522.

102 B. G. Rao, D. Mukherjee and B. M. Reddy, *Nanostructures Nov. Ther.*, 2017, 1–36.

103 T. Athar, in *Emerging Nanotechnologies for Manufacturing*, Elsevier, 2015, pp. 444–538.

104 S. T. Aruna and A. S. Mukasyan, *Curr. Opin. Solid State Mater. Sci.*, **12**, 44–50.

105 J. J. Moore and H. J. Feng, *Prog. Mater. Sci.*, 1995, **39**, 243–273.

106 K. K. Kefeni, B. B. Mamba and T. A. M. Msagati, *Sep. Purif. Technol.*, 2017, **188**, 399–422.

107 V. Meille, *Appl. Catal. A Gen.*, 2006, **315**, 1–17.

108 S. Y. Gómez, J. A. Escobar, O. A. Alvarez, C. R. Rambo, A. P. N. de Oliveira and D. Hotza, *J. Mater. Sci.*, 2009, **44**, 3466–3471.

109 M. M. O. SANZ, F. J. ECHAVE, M. SÁNCHEZ, A. MONZÓN, *Appl. Catal.*, 2008, **340**, 125–132.

110 S. Dhara and P. Bhargava, *J. Am. Ceram. Soc.*, 2003, **86**, 1645–1650.

111 L. Giani, G. Groppi and E. Tronconi, *Ind. Eng. Chem. Res.*, 2005, **44**, 4993–5002.

112 C. Y. Zhao, T. J. Lu, H. P. Hodson and J. D. Jackson, *Mater. Sci. Eng. A*, 2004, **367**, 123–131.

113 D. K. Balch, J. G. O 'dwyer, G. R. Davis, C. M. Cady, G. T. Gray Iii and D. C. Dunand, *Mater. Sci. Eng. A*, 2005, **391**, 408–417.

114 C. Park and S. . Nutt, *Mater. Sci. Eng. A*, 2001, **297**, 62–68.

115 A. E. Markaki and T. W. Clyne, *Acta Mater.*, 2003, **51**, 1341–1350.

116 S. Zhao, J. Zhang, D. Weng and X. Wu, *Surf. Coatings Technol.*, 2003, **167**, 97–105.

117 T. Miyoshi, M. Itoh, S. Akiyama and A. Kitahara, *Adv. Eng. Mater.*, 2000, **2**, 179–183.

118 K. Boomsma, D. Poulikakos and F. Zwick, *Mech. Mater.*, 2003, **35**, 1161–1176.

119 K. Boomsma and D. Poulikakos, *J. Fluids Eng.*, 2001, **124**, 263–272.

120 K. Boomsma, A. Member and D. Poulikakos, *J. Fluids Eng.*, 2002, **124**, 239–272.

121 J. P. Bortolozzi, E. D. Banús, V. G. Milt, L. B. Gutierrez and M. A. Ulla, *Appl. Surf. Sci.*, 2010, **257**, 495–502.

122 S. Joshi, G. Gupta, M. Sharma, A. Telang and T. Mahra, *Mater. Sci. Res. India*, 2015, **12**, 43–49.

123 H. I. Bakan and K. Korkmaz, *Mater. Des.*, 2015, **83**, 154–158.

124 J. Banhart, *Prog. Mater. Sci.*, 2001, **46**, 559–632.

125 P. Quadbeck, G. Stephani, K. Kümmel, J. Adler and G. Standke, *Mater. Sci. Forum*, 2007, **534**–**536**, 1005–1008.

126 K. Kenneth Kremer, A. Anthony Liszkiewicz and J. James Adkins, *Development of Steel Foam Materials and Structures*, Golden, Co, **2**, 2004.

127 W. Kaltner, M. Veprek-Heijman, A. Jentys and J. A. Lercher, *Appl. Catal. B Environ.*, 2009, **89**, 123–127.

128 M. Ferrandon, M. Berg and E. Björnbom, *Catal. Today*, 1999, **53**, 647–659.

129 E. D. Banús, M. A. Ulla, E. E. Miró and V. G. Milt, *Appl. Catal. A Gen.*, 2011, **393**, 9–16.

130 D. Fino, P. Fino, G. Saracco and V. Specchia, *Chem. Eng. Sci.*, 2003, **58**, 951–958.

131 A. N. Pestryakov, N. E. Bogdanchikova and A. Knop-Gericke, *Catal. Today*, 2004, **91**, 49–52.

132 E. D. Bans, M. A. Ulla, E. E. Mir and V. G. Milt, in *Diesel Engine - Combustion, Emissions and Condition Monitoring*, InTech, 2013.

133 A. N. Pestryakov, E. V Smolentseva, A. N. Kryazhov, V. V Lunin, N. E. Bogdanchikova and V. P. Petranovskii, *Catal. Today*, 1996, **29**, 67–70.

134 M. V. Twigg and J. T. Richardson, *Chem. Eng. Res. Des.*, 2002, **80**, 183–

189.

135 U. Schubert, in *The Sol-Gel Handbook*, Wiley-VCH Verlag GmbH & Co. KGaA, Weinheim, Germany, 2015, pp. 1–28.

136 J. Ružić, M. Vilotijević, D. Božić and K. Raić, *AMES*, 2012, **18**, 2733–282

137 C.-L. Lin, F.-S. Chen, L.-J. Twu and M.-J. J. Wang, *Hum. Factors Ergon. Manuf. Serv. Ind.*, 2014, **24**, 124–129.

138 J.Gavrilenko and S.Fernandez, *in Raman, IR, optical and SEM/EDX microscopy of prehistoric rock paintings, Rock Chemistry. 81-102,* 2010.

139 S. J. B. Reed, *Electron Microprobe Analysis and Scanning Electron Microscopy in Geology*, Cambridge University Press, Cambridge, 2005.

140 M. Henini, *III-Vs Rev.*, 2000, **13**, 40–44.

141 A.Chauhan and P. Chauhan, *J Anal Bioanal Tech*, 2014, 5–15.

142 J. C. Lindon, G. E. Tranter and J. L. (John L. Holmes, *Encyclopedia of spectroscopy and spectrometry*, Academic Press, 2000.

143 H. Stanjek and W. Häusler, *Hyperfine Interact.*, 2004, **154**, 107–119.

144 A.Ashcroft, *An Introduction to Mass Spectrometry. Available at: http://www.cerm.unifi.it/static/piccioli/MS1.pdf* (Accessed April 2020).

145 A. M. Barbara Małecka, Agnieszka Lacz, Ewa Drozd, *Therm Anal Calorim*, 2015, **119**, 1053–1061.

146 E. Stefan, G. Tsekouras and J. T. S. Irvine, *Adv. Energy Mater.*, 2013, **3**, 1454–1462.

147 R. D. Goodwin, *J. Phys. Chem. Ref. Data*, 1989, **18**, 1565–1636.

148 Y. Kim, S. Kim and B. Choe, *Metals (Basel).*, 2019, **9**, 406.

149 M. S. Kamal, S. A. Razzak and M. M. Hossain, *Atmos. Environ.*, 2016, **140**, 117–134.

150 E. N. Kolentsova, D. Y. Dimitrov, P. C. Petrova, G. V Avdeev, D. D.

Nihtianova, I. Krasimir and T. T. Tabakova, 2016.

151 X. Li, L. Wang, Q. Xia, Z. Liu and Z. Li, *Catal. Commun.*, 2011, **14**, 15–19.

152 Toluene, *https://webbook.nist.gov/cgi/cbook.Mass-Spec*.Date accessed: 07/04/2020.

153 K. Everaert and J. Baeyens, *J. Hazard. Mater.*, 2004, **109**, 113–139.

154 A. J. Burn, *Tetrahedron*, 1966, **22**, 2153–2161.

155 C. Doroftei, in *Nanostructures in Energy Generation, Transmission and Storage*, IntechOpen, 2019.

156 S. M. Saqer, D. I. Kondarides and X. E. Verykios, *Appl. Catal. B Environ.*, 2011, **103**, 275–286.

157 Y. Guo, X. Liao, M. Fu, H. Huang and D. Ye, *JES*, 2015, **28**, 187–194.

158 R. Furushima, S. Tanaka, Z. Kato, T. Shiomi and K. Uematsu, *J. Am. Ceram. Soc.*, 2011, **94**, 2819–2824.

159 A. Jodaei, D. Salari, A. Niaei, M. Khatamian, & Seyed, A. Hosseini and S. A. Hosseini, *J. Environ. Sci. Heal. Part A*, 2011, **46**, 50–62.

160 D. Neagu, G. Tsekouras, D. N. Miller, H. Ménard and J. T. S. Irvine, *Nat. Chem.*, 2013, **5**, 916–923.